

DEVELOPMENT OF POLY(PROPYLENE FUMARATE) (PPF), VINYL
PHOSPHONIC ACID (VPA) AND VINYL PHOSPHONIC ACID DI-ETHYL ESTER
(VPES) BASED SCAFFOLDS FOR BONE TISSUE ENGINEERING



by
Görkem Özdemirli

Submitted to Graduate School of Natural and Applied Sciences
in Partial Fulfillment of the Requirements
for the Degree of Doctor of Philosophy in
Biotechnology

Yeditepe University

2019

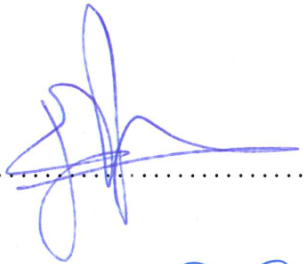
DEVELOPMENT OF POLY(PROPYLENE FUMARATE) (PPF), VINYL PHOSPHONIC
ACID (VPA) AND VINYL PHOSPHONIC ACID DI-ETHYL ESTER (VPES) BASED
SCAFFOLDS FOR BONE TISSUE ENGINEERING

APPROVED BY:

Prof. Dr. Gamze Torun Köse
(Thesis Supervisor)
(Yeditepe University)



Assoc. Prof. Dr. Erde Can
(Thesis Co-Supervisor)
(Yeditepe University)



Prof. Dr. Ebru Toksoy Öner
(Marmara University)



Assoc. Prof. Dr. Fatma Neşe Kök
(İstanbul Technical University)



Assist. Prof. Dr. Andrew Harvey
(Yeditepe University)



Assist. Prof. Dr. Cem Levent Altan
(Yeditepe University)

DATE OF APPROVAL:/...../2019

ACKNOWLEDGEMENTS

Before anything else, I would like to thank to my supervisor Prof. Dr. Gamze Torun Köse and my co-advisor Assoc. Prof. Dr. Erde Can for their support, heartening, contributions of time, idea and funding to make my Ph.D. experience productive and inspiring. They and their supports were my luck in this journey. I also would like to thank for the great example they had provided as successful women scientists.

I am also deeply thankful to Prof. Dr. Seyda Bucak, Assoc. Prof. Dr. Andrew Harvey, and Assoc. Prof. Dr. Fatma Neşe Kök for generously sharing their time and their detailed critique on this thesis as committee members of my thesis. They guided me through all these years. I also would like to acknowledge Prof. Dr. Fikretin Şahin for his help and support through hard times.

The members of YUTEG group have contributed extremely to my professional time at Yeditepe University. The group has been a full of friendships, helpful, advice and collaboration. I gratefully thank to the funding received from TÜBİTAK Domestic Ph.D. Scholarship that made my Ph.D. work possible.

I am heartily thankful to my dearest friends Dr. Başak Kandemir, Dr. Ezgi Avşar Abdik, Dr. Hüseyin Abdik and Dr. Merve Seven for their friendship, support, willingness to share everything, and for all the fun and memories through these years.

Last, but not least, I would like to thank to my parents Güzide Özlem Cemali and Yahya Cemali, also my sisters Elif Orpak Metin and Elif Kübra Alcaz for their encouragement and love. My parents raised me with the unconditional love of science and supported me in all my research.

I also would like to thank to my husband, Anıl Özdemirli, who taught me that I can be flawed enough but perfect for a person; for someone who will be there for me when I fall apart. Without him, it would have been impossible for me to finish this study.

This project was funded by TÜBİTAK-MAG (Project no: 114M195).

ABSTRACT

DEVELOPMENT OF POLY(PROPYLENE FUMARATE) (PPF), VINYL PHOSPHONIC ACID (VPA) AND VINYL PHOSPHONIC ACID DI-ETHYL ESTER (VPES) BASED SCAFFOLDS FOR BONE TISSUE ENGINEERING

Autologous and allogeneous bone grafts or permanent prosthetic implants are used in treatment of bone damages. The limitations and disadvantages of these techniques led to find other ways of healing the damaged bones. A biodegradable material which acts as a structural support to the damaged area and as a scaffold that guides bone formation is one desirable solution. Biodegradable materials have the advantage of enhancing the regeneration of the damaged area.

Poly(propylene) fumarate (PPF) is an unsaturated polyester. PPF can be copolymerized with a vinyl monomer to give a biocompatible and biodegradable thermoset. Recently, N-vinyl pyrrolidone (VP) is widely used as a co-monomer with PPF in different weight ratios in order to support the damaged area of a bone. In addition, it is observed that the resulting biomaterial also acts as a scaffold that guides the bone formation. Moreover, composites of PPF/VP biomaterial (containing inorganic additives) gave promising results as bone tissue engineering scaffolds.

In this study, the PPF polymer was synthesized via polycondensation of excess propylene glycol and fumaric acid. The PPF pre-polymer was then thermally cured with vinylphosphonic acid (VPA) and diethyl vinylphosphonate (VPES) in the presence of benzoyl peroxide initiator, via radical polymerization at changing co-monomer and initiator weight ratios. Additionally synthesized PPF was cured via UV light in the presence of phenylbis(2,4,6-trimethylbenzoyl)phosphine oxide with the same co-monomers.

Effect of co-monomer contents on thermal transitions, thermomechanical properties, compressive properties, biodegradability and hydrophilicity of the resulting biomaterials were evaluated. Biocompatibility of the resulting materials with the use of VPA and VPES was analysed by the MTS assay. Results of von Kossa, alkaline phosphatase and osteocalcin activities were evaluated in order to observe the osteoblast activity.

ÖZET

POLİ(PROPİLEN FUMARAT), VİNİL FOSFONİK ASİT VE VİNİL FOSFONİK ASİT Dİ-ETİL ESTERİ BAZLI KEMİK DOKU MÜHENDİSLİĞİ İSKELELERİNİN GELİŞTİRİLMESİ

Kemik hasarlarının tedavisinde, otolog ve allojenik kemik nakilleri veya kalıcı protez implantlar kullanılmaktadır. Bu tekniklerdeki kısıtlamalar ve dezavantajlar, hasarlı kemik dokuları iyileştirmek için başka yollar bulmaya yol açmıştır. Hasarlı bölgeye yapısal destek olan ve kemik oluşumunu destekleyen, bir iskelet olarak işlev gören, biyolojik olarak parçalanabilen bir materyal arzu edilen bir çözümdür.

Poli(propilen fumarat) (PPF) doymamış bir poliesterdir. PPF biyo-uyumlu ve biyo-bozunur bir termoset vermek üzere bir vinil monomer ile kopolimerleştirilebilir. Son zamanlarda, N-vinil piroolidon (VP) komonomer olarak, kemiğin hasarlı alanını desteklemek için PPF ile farklı ağırlık oranlarında yaygın olarak kullanılmaktadır. Buna ek olarak, ortaya çıkan biyomalzemenin ayrıca kemik oluşumunu yönlendiren bir iskelet işlevi gördüğü gözlenmiştir. Ayrıca, PPF/VP biyomalzemesinin (inorganik katkı maddeleri içeren) kompozitleri, kemik doku mühendisliğinde iskeleler olarak kullanılmak üzere ümit vaat eden sonuçlar vermiştir.

Bu çalışmada, PPF polimeri propilen glikol fazlası ve fumarik asidin polikondenzasyonu ile sentezlenmiştir. PPF ön-polimeri daha sonra benzoil peroksit başlatıcısı varlığında vinilfosfonik asit (VPA) ve dietil vinilfosfonat (VPES) ile termal olarak, ko-monomer ve başlatıcı ağırlık oranları değiştirilerek radikal polimerizasyon yoluyla kür edilmiştir. Ek olarak sentezlenmiş PPF, aynı ko-monomerlerle, fenilbis (2,4,6-trimetilbenzoil) fosfin oksit varlığında UV ışınıyla kür edilmiştir.

Ko-monomer içeriğinin, elde edilen biyomalzemelerin termal özellikleri, mekanik özellikleri, biyolojik bozunabilirlikleri ve hidrofiliteleri üzerindeki etkileri değerlendirilmiştir. VPA ve VPES kullanımı ile elde edilen malzemelerin biyo-uyumluluğu ise MTS deneyi ile analiz edilmiştir. Ayrıca osteoblast aktivitesini gözlemek için von Kossa, alkalen fosfataz ve osteokalsin aktiviteleri değerlendirilmiştir.

TABLE OF CONTENTS

ACKNOWLEDGEMENTS.....	iii
ABSTRACT.....	iv
ÖZET	v
LIST OF FIGURES	xi
LIST OF TABLES.....	xvi
LIST OF SYMBOLS/ABBREVIATIONS.....	xvii
1. INTRODUCTION.....	1
2. THEORY.....	2
2.1. INTRODUCTION TO POLYMER SCIENCE	2
2.2. CLASSIFICATION OF POLYMERS	3
2.2.1. Thermoplastics and Thermosets	3
2.2.2. Polymer Structure.....	4
2.2.2.1. Linear, Branched, Cross Linked and Network Polymers	4
2.2.2.2. Cis-Trans Isomerism.....	5
2.2.2.3. Homopolymers and Copolymers	5
2.3. POLYMER SYNTHESIS	5
2.3.1. Addition (Chain Growth) Polymerization.....	6
2.3.2. Condensation (Step Growth) Polymerization.....	7
2.4. SOLID STATE PROPERTIES	8
2.4.1. The Amorphous State	8
2.4.1.1. Chain Entanglements	8
2.4.1.2. Glass Transition Temperature (T_g)	8
2.4.2. The Crystalline State	9
2.4.2.1. Ordering of Polymer Chains	10
2.4.2.2. Crystalline Melting Temperature.....	11

2.4.3. Mechanical Properties of Polymers	11
2.4.3.1. Tensile Strength (TS).....	13
2.4.3.2. Percent Elongation at Break (Ductility).....	14
2.4.3.3. Young's Modulus	15
2.4.3.4. Toughness	16
2.4.3.5. Compressive Properties	16
2.5. BONE TISSUE ENGINEERING	17
2.5.1. Polymers Used as Scaffolds in Bone Tissue Engineering.....	18
2.5.2. Polypropylene fumarate (PPF)	19
2.5.3. Vinylphosphonic Acid and Derivatives.....	20
2.6. AIM.....	21
3. MATERIALS AND METHODS	22
3.1. SYNTHESIS OF POLY(PROPYLENE FUMARATE) (PPF).....	22
3.1.1. Chemicals	22
3.1.2. PPF Synthesis	22
3.1.3. Purification of the PPF Resin	24
3.1.4. Proton NMR (¹ H-NMR) Spectroscopy and Gel Permeation Chromatography (GPC) Analysis of PPF Resin.....	25
3.1.5. FT-IR Spectroscopy Analysis of PPF.....	25
3.2. PREPARATION OF THERMALLY CURED COPOLYMERS	25
3.2.1. Crosslinking of PPF with VPA or VPES via Thermal Cure	26
3.2.2. FT-IR Spectroscopy Analysis of Thermally Cured Copolymers	27
3.3. PREPARATION OF UV CURED COPOLYMERS	27
3.3.1. Crosslinking of PPF with VPA or VPES <i>via</i> UV Cure	28
3.4. PPF BASED END PRODUCTS	28
3.5. CROSS-LINK DENSITY ANALYSIS OF PPF/VPA AND PPF/VPES POLYMERS	29

3.6. SCANNING ELECTRON MICROSCOPY (SEM) ANALYSIS.....	30
3.7. DIFFERENTIAL SCANNING CALORIMETRY (DSC) AND THERMAL GRAVIMETRIC ANALYSIS (TGA)	31
3.8. DETERMINATION OF EQUILIBRIUM WATER CONTENT AND DYNAMIC CONTACT ANGLE WITH WATER.....	32
3.9. DYNAMIC MECHANICAL ANALYSIS (DMA)	33
3.10. MECHANICAL TESTING	33
3.11. <i>IN VITRO</i> DEGRADATION	33
3.12. <i>IN VITRO</i> CELL INTERACTION STUDIES OF THERMALLY CURED PPF/VPA AND PPF/VPES POLYMERS	34
3.12.1. Cell Viability and Proliferation (MTS) Studies.....	35
3.12.2. Scanning Electron Microscopy of Cell Seeded Polymers	36
3.12.3. Determination of Mineralization by Von Kossa Staining	36
3.12.4. Alkaline Phosphatase Assay (ALP).....	37
3.12.5. Osteocalcin Assay (OST)	37
4. RESULTS AND DISCUSSION.....	38
4.1. CHARACTERIZATION OF PPF BY FT-IR AND ¹ H-NMR SPECTROSCOPY AND MOLECULAR WEIGHT ANALYSIS VIA GPC.....	38
4.2. FT-IR ANALYSIS OF THE CURED PPF/VPA AND PPF/VPES POLYMERS ...	40
4.2.1. PPF/VPA Products	40
4.2.2. PPF/VPES Products.....	42
4.3. CROSS-LINK DENSITY ANALYSIS OF THERMAL CURED PPF/VPA AND PPF/VPES POLYMERS	43
4.4. SCANNING ELECTRON MICROSCOPY (SEM) ANALYSIS.....	47
4.4.1. Scanning Electron Microscopy Analysis of Thermal Cured Polymers.....	47
4.4.2. Scanning Electron Microscopy Analysis of UV Cured Polymers.....	50
4.5. DIFFERENTIAL SCANNING CALORIMETRY (DSC) AND THERMAL GRAVIMETRIC ANALYSIS (TGA)	52

4.5.1. DSC Analysis of Thermal Cured Polymers.....	53
4.5.1.1. Effect of Change in Comonomer Content	53
4.5.1.2. Effect of Comonomer	55
4.5.2. DSC Analysis of UV Cured Polymers	56
4.5.3. Thermogravimetric Analysis of Thermal Cured PPF/VPA and PPF/VPES Polymers	58
4.5.3.1. Effect of Change in Comonomer Content	58
4.5.3.2. Effect of Initiator Amount	61
4.5.3.3. Effect of Comonomer	62
4.5.4. Thermogravimetric Analysis of UV Cured Polymers	64
4.6. EQUILIBRIUM WATER CONTENT AND DYNAMIC CONTACT ANGLE WITH WATER	66
4.6.1. EWC Analysis of Thermal Cured PPF/VPES and PPF/VPA Polymers	66
4.6.2. EWC Analysis of UV Cured PPF/VPA and PPF/VPES Polymers	68
4.6.3. Dynamic Contact Angle With Water	69
4.7. DYNAMIC MECHANICAL ANALYSIS (DMA)	71
4.7.1. Dynamic Mechanical Analysis of Thermal Cured PPF/VPA and PPF/VPES Polymers	71
4.8. MECHANICAL TESTING	86
4.8.1. Compressive Properties of Thermal Cured Polymers	86
4.9. <i>IN VITRO</i> DEGRADATION	89
4.9.1. <i>In Vitro</i> Degradation of Thermal Cured Polymers	89
4.9.1.1. Analysis of Biodegradation via Weight Loss Measurements	89
4.9.1.2. Analysis of Biodegradation via pH Track	95
4.9.2. <i>In Vitro</i> Degradation of UV Cured Polymers.....	101
4.9.2.1. Analysis of Biodegradation via Weight Loss Studies	101
4.9.2.2. Analysis of Biodegradation via pH Track	102

4.10. <i>IN VITRO</i> CELL INTERACTION STUDIES OF THERMAL CURED SAMPLES	104
4.10.1. MTS Assay of Thermal Cured Polymers	105
4.10.2. Scanning Electron Microscopy of Thermal Cured Cell Seeded Polymers.....	106
4.10.3. Determination of Mineralization by von Kossa Staining of Thermal Cured Polymers	108
4.10.4. Determination of ALP Activity of Thermal Cured Polymers	112
4.10.5. Determination of OST Activity of Thermal Cured Polymers	113
5. CONCLUSIONS	115
6. FUTURE PROSPECTS.....	117
REFERENCES	118
APPENDIX A.....	126
APPENDIX B	127

LIST OF FIGURES

Figure 2.1. The stress–strain behaviour for brittle (curve A), plastic (curve B), and highly elastic (elastomeric) (curve C) polymers	12
Figure 2.2. The effect of temperature on the stress–strain curve of polymers	13
Figure 2.3. Characteristic stress-strain curves for plastics with different levels of ductility	14
Figure 2.4. Stress-strain curves for polymers at room temperature: a low ductility polymer, a ductile polymer, a ductile polymer capable of cold drawing, and a polymer with long-range elasticity	15
Figure 2.5. Relationship between stress-strain curve and Young’s Modulus.....	15
Figure 2.6. Relationship between stress-strain curve and Toughness	16
Figure 3.1. Reaction scheme of PPF synthesis	23
Figure 3.2. Set-up of the PPF synthesis	24
Figure 3.3. Radical polymerization scheme of PPF with comonomers.....	27
Figure 4.1. FT-IR spectrum of the synthesized PPF pre-polymer.....	38
Figure 4.2. ¹ H-NMR spectrum of the synthesized PPF pre-polymer	39
Figure 4.3. The FT-IR spectrum of the PPF/VPA (70/30) product cured with 2 and 3 weight percent initiator	41
Figure 4.4. The FT-IR spectrum of the PPF/VPES (70/30) product cured with 2 and 3 weight percent initiator	43
Figure 4.5. Bar graphs of crosslink density and number average molecular weight between cross-links (Mc) values of thermally cured PPF/VPA and PPF/VPES polymers	46
Figure 4.6. Scanning electron micrographs of PPF/VPA (70/30) sample cured with 2 weight percent BP at 1500x and 3000x magnification.....	48
Figure 4.7. Scanning electron micrographs of PPF/VPA (70/30) sample cured with 3 percent BP at 1000x and 2000x magnification.....	48

Figure 4.8. Scanning electron micrographs of PPF/VPA (60/40) sample cured with 2 percent BP at 100x and 1500x magnification.....	49
Figure 4.9. Scanning electron micrographs of PPF/VPA (80/20) sample cured with 2 and 3 weight percent BP at 2000x magnification.....	49
Figure 4.10. Scanning electron micrographs of PPF/VPES (70/30) sample cured with 2 weight percent and 3 weight percent BP at 3000x and 2000x magnification.....	50
Figure 4.11. Scanning electron micrographs of UV cured PPF/VPA (70/30) samples containing 2 percent BAPO and 3 percent BAPO at 2000X magnification.....	51
Figure 4.12. Scanning electron micrographs of UV cured PPF/VPES (70/30) samples containing 2 percent BAPO and 3 percent BAPO at 2000X magnification.....	52
Figure 4.13. DSC plots of PPF/VPA samples cured with 2 and 3 weight percent initiator	54
Figure 4.14. DSC plots of PPF/VPES samples cured with (a) 2 and (b) 3 weight percent initiator.....	55
Figure 4.15. DSC plots of PPF/VPA and PPF/VPES (70/30) polymers cured with 2 and 3 weight percent initiator	56
Figure 4.16. DSC thermograms of UV cured PPF/VPA and PPF/VPES samples	57
Figure 4.17. Weight percentage vs temperature plots of PPF/VPES polymers at changing VPES contents, cured with 2 3 percent initiator	59
Figure 4.18. Weight percentage vs temperature plots of PPF/VPA polymers at changing VPA contents,cured with 2 and 3 percent initiator	60
Figure 4.19. Weight percentage vs temperature plots of PPF/VPES (70/30) and PPF/VPA (70/30) polymers at changing initiator amounts	62
Figure 4.20. Weight percentage vs temperature plots of PPF/VPA (70/30) and PPF/VPES (70/30) polymers cured with 2 and 3 percent initiator amount.....	63
Figure 4.21. Weight percent versus temperature graphs of UV cured PPF/VPA (70/30) and PPF/VPES (70/30) samples cured with varying amounts of UV initiator (BAPO)	65
Figure 4.22. Column plots for the equilibrium water content (weight percent) data of the PPF/VPES and PPF/VPA polymers.	67

Figure 4.23. Equilibrium water content values of UV cured PPF/VPA and PPF/VPES samples.....	68
Figure 4.24. Dynamic contact angle with water values at the 30 th second of measurements for all thermal cured samples.....	70
Figure 4.25. Storage modulus, loss modulus and tan delta versus temperature graphs of 3 percent BP containing PPF/VPES samples	75
Figure 4.26. Storage modulus, loss modulus and tan delta versus temperature graphs of 2 percent BP containing PPF/VPES samples	77
Figure 4.27. Storage modulus , loss modulus and tan delta versus temperature graphs of 3 percent BP containing PPF/VPA samples	79
Figure 4.28. Storage modulus, loss modulus and tan delta versus temperature graphs of 2 percent BP containing PPF/VPA samples	81
Figure 4.29. Comparison graphs of 3 and 2 percent BP containing PPF/VPA (70/30) samples in terms of storage and loss modulus.....	82
Figure 4.30. Comparison graphs of 3 and 2 percent BP containing PPF/VPES (70/30) samples in terms of storage and loss modulus.....	83
Figure 4.31. Comparison graphs of PPF/VPA and PPF/VPES (70/30) samples with 3 percent BP in terms of storage and loss modulus	85
Figure 4.32. Comparison graphs of PPF/VPA and PPF/VPES (70/30) samples with 2% BP in terms of storage and loss modulus.....	86
Figure 4.33. Compressive modulus and compressive strength bar graphs.....	88
Figure 4.34. Weight loss versus time graphs of 2 percent BP and 3 percent BP containing PPF/VPA samples.....	90
Figure 4.35. Weight loss versus time graphs of 2 percent BP and 3 percent BP containing PPF/VPES samples.....	92
Figure 4.36. Comparison of weight loss profiles of 2 and 3 percent BP containing PPF/VPA (70/30) samples	93
Figure 4.37. Comparison of weight loss profiles of 2 and 3 percent BP containing PPF/VPES (70/30) samples	93

Figure 4.38. Comparison of weight loss profiles of 2 and 3 percent BP containing PPF/VPA and PPF/VPES (70/30) samples.....	94
Figure 4.39. pH versus time graphs of 3 percent BP containing PPF/VPA samples.....	96
Figure 4.40. pH versus time graphs of 2 percent initiator containing PPF/VPA samples...	96
Figure 4.41. pH data of 3 percent initiator containing PPF/VPES samples	97
Figure 4.42. pH data of 2 percent initiator containing PPF/VPES samples	98
Figure 4.43. Comparison of pH data of 2 and 3 percent initiator containing PPF/VPA samples.....	98
Figure 4.44. Comparison of pH data of 2 and 3 percent initiator containing PPF/VPES samples.....	99
Figure 4.46. Comparison of pH data of 2 percent initiator containing PPF/VPA and PPF/VPES samples	100
Figure 4.47. Comparison of pH data of 3 percent initiator containing PPF/VPA and PPF/VPES samples	100
Figure 4.48. Weight loss profiles of all UV cured polymer compositions	102
Figure 4.49. pH track of UV cured PPF/VPA polymers	103
Figure 4.50. pH track of UV cured PPF/VPES polymers.....	104
Figure 4.51. Cell proliferation on the thermal cured polymers	105
Figure 4.52. Scanning electron micrographs of cell seeded thermal cured polymers after 7, 14, 21 and 28 days of incubation	107
Figure 4.53. Von kossa staining of all thermal cured polymers at day 7.....	109
Figure 4.54. Von kossa staining of all thermal cured polymers at day 14.....	110
Figure 4.55. Von Kossa staining images of thermal cured PPF/VPA and PPF/VPES polymers at day 21	111
Figure 4.56. Von Kossa staining images of thermal cured PPF/VPA and PPF/VPES polymers at day 28.....	112
Figure 4.57. Alkaline phosphatase activity of HOb cells throughout 28 days of incubation on thermal cured samples	113

Figure 4.58. Osteocalcin activity of HOb cells throughout 28 days on thermal cured samples..... 114



LIST OF TABLES

Table 3.1. Chemicals used for PPF synthesis and purification.....	22
Table 3.2. Chemicals used for preparation of thermally cured copolymers.....	25
Table 3.3. Chemicals used for preparation of UV cured copolymers.....	28
Table 3.4. Cured PPF based copolymers	29
Table 3.5. Chemicals, reagents and kits used for cell culture studies.....	34
Table 4.1. Crosslink density and number average molecular weight between cross-links (Mc) values of thermally cured PPF/VPA and PPF/VPES polymers.....	46
Table 4.2. Equilibrium water content (wt%) values of the PPF/VPES and PPF/VPA polymers.....	67
Table 4.3. Equilibrium water content results of UV cured PPF/VPA and PPF/VPES samples.....	69
Table 4.4. Average dynamic contact angle with water values at the 30 th second of measurements for all thermal cured samples	70
Table 4.6. Storage and loss modulus values at 37°C and Tg values which are determined from loss modulus and tan delta maxima of all thermal cured polymer compositions	72
Table 4.7. Compressive modulus and strength of all thermal cured materials	87

LIST OF SYMBOLS/ABBREVIATIONS

E'	Storage modulus
E''	Loss modulus
M_c	Number average molecular weight between cross-links
pH	Negative log of hydrogen ion concentration
Q	Swelling coefficient
T_g	Glass transition temperature
T_m	Melting temperature
wt%	Weight percent
3D	Three dimensional
ABS	Acrylonitrile butadiene styrene
ALP	Alkaline phosphatase
BAPO	Phenylbis (2,4,6-trimethylbenzoyl) phosphine oxide
BP	Benzoyl peroxide
BTE	Bone tissue engineering
$CaCl_2$	Calcium chloride
$CDCl_3$	Deuterated chloroform
CH_2Cl_2	Dichloromethane
cm	Centimeter
cm^3	Centimeter cube
CO_2	Carbon dioxide
DA	Diacrylate
dH_2O	Distilled water
DMA	Dynamic mechanical analysis
DMEM	Dulbecco's modified Eagle's medium
DMSO	Dimethyl sulfoxide
DMT	N,N-dimethyl p-toluidine
DPBS	Dulbecco's phosphate buffer saline
DSC	Differential scanning calorimetry
ECM	Extracellular matrix

EDTA	Ethylenediaminetetraacetic acid
EL%	Percentage elongation
ELISA	Enzyme-linked immune-sorbent assay
EWC	Equilibrium water content
FBS	Fetal bovine serum
FTIR	Fourier-transform infrared spectroscopy
g	Gram
GPC	Gel permeation chromatography
HOb	Human osteoblast
hOST	Osteocalcin (human)
Hz	Hertz
IR	Infrared spectroscopy
K	Kelvin
KBr	Potassium bromide
kN	Kilonewton
kV	Kilovolt
M	Molar
μg	Microgram
μl	Microliters
mm	Milimeter
mM	Milimolar
M _n	Number average molecular weight
MPa	Megapascal
MTS	3-(4,5-dimethylthiazol-2-yl)-5-(3-carboxymethoxyphenyl)-2-(4-sulfophenyl)-2H-tetrazolium, inner salt
mW	Miliwatts
M _w	Weight average molecular weight
nm	Nanometer
NMR	Nuclear magnetic resonance
NVP	N-Vinylpyrrolidone
OC	Only cells
OCN	Osteocalcin
OM	Osteogenic media

PBS	Phosphate buffered saline
PC	Polycarbonate
PCL	Poly(ϵ -caprolactone)
PDI	Polydispersity index
Pen/Strep	Penicillin/Streptomycin solution
PET	Poly(ethylene terephthalate)
PGA	Poly(glycolic acid)
PLGA	Poly lactic-co-glycolic acid (PLGA)
PLLA	PLLA (poly-L-lactic acid)
PMMA	Poly(methyl methacrylate)
PPF	Poly(propylene fumarate)
ppm	Chemical shift (parts per million)
PS	Polystyrene
psi	Pounds per square inch
RA%	Percentage reduction in area
RIPA	Radio immunoprecipitation assay
rpm	Roots per minute
RT	Room temperature
SEM	Scanning electron microscopy
TG	Thermogravimetry
TGA	Thermogravimetric analysis
THF	Tetrahydrofuran
TS	Tensile strength
UV	Ultraviolet
VP	N-Vinylpyrrolidone
VPA	Vinylphosphonic acid
VPES	Diethyl vinylphosphonate (Vinylphosphonic acid diethyl ester)

1. INTRODUCTION

Biomaterials can be synthetic or natural materials that can be used in medical applications to perform a body function to replace a body part or a tissue. Since the polymeric biomaterials are easy to manufacture, compared to metal or ceramic materials this gives them a remarkable advantage to produce various shapes.

Polymeric biomaterials can be used in bone replacements as a part of tissue engineering. In case of fracture, it takes a quite long time for bone to heal itself and during the recovery period bone cannot bear weight. Polymers have much superior properties compared to conventional materials which cannot degrade in human body. Also they have to be removed from body after recovery. Polymeric materials have a better combination of features which are microstructure, biocompatibility, degradation rate and mechanical properties. However, biocompatible and biodegradable polymers can stay longer in the body compared to other materials such as steel pins and rods and they degrade slowly over time. In addition, studies showed that using these materials have several disadvantages such as decreasing the strength of bone and decreasing the durability of bone. When bone is broken, the ability of bearing weight decreases and it takes time for full recovery. As a result, bone can strengthen itself gradually with increasing weight bearing. These properties of polymers make them most preferable materials as a bone replacement.

Polypropylene fumarate (PPF) is a synthetic, unsaturated, biodegradable, biocompatible and linear polyester which can be cross-linked through its fumarate double bonds and degraded by random hydrolytic separation of its ester groups. When PPF deteriorates, propylene glycol and fumaric acid are produced at the end of the reaction. These products are biocompatible and quite easily removed from the body. When cross-linked, the tight network structure of PPF imparts mechanical strength sufficient for its use in bone replacement scaffolds.

Furthermore, porous PPF scaffolds can provide osteoconductive surface for bone in-growth, making it an attractive biomaterial for orthopaedic and dental use.

2. THEORY

2.1. INTRODUCTION TO POLYMER SCIENCE

Polymers are macromolecules, formed by repeated units. In other words, natural and synthetic polymers consist of many small units which are monomers [1]. Their resulting molecular weight relative to smaller molecules provides incomparable physical features, containing toughness, viscoelasticity, and a tendency to form glasses and semi-crystalline structures.

Poly means “many” and meres means “parts” in the classical Greek words that are combining and the word polymer is formed. Specific polymers, like proteins, cellulose, and silk, are natural polymers, while some polymers such as nylon, polystyrene and polyethylene are synthetic. Polymers that occur in natural ways may be produced synthetically in some cases [2].

In the mid-nineteenth century, polymer science was born. Charles Goodyear developed the vulcanization process which converted the sticky latex of natural rubber into a beneficial elastomer for tire use in the 1830s. Cellulose was reacted with nitric acid by Christian F. Schönbein to produce cellulose nitrate in 1847. In the 1860s, this material that is celluloid was used as the first man-made thermoplastic. Phenol-formaldehyde resin that is known as Bakelite was produced by Leo Hendrik Baekeland in 1907. In 1912, General Electric developed unsaturated- polyester resin (Glyptal) as a protective coating resin [3].

Polymer science is an interdisciplinary field consisting of chemical, physical, engineering, processing and theoretical aspects. Also, on contemporary materials science, it has tremendous effect. Its aim is to provide the ground for the formation and characterization of polymeric materials and an understanding for structure/property relationships. Polymeric materials are resistant against corrosion, can be produced into complex shapes, which usually leads to a large decrease in product costs [4].

2.2. CLASSIFICATION OF POLYMERS

Polymers can be categorized into various categories such as polymer structure basis, processing type, thermal properties and configuration. In order to comprehend polymer characteristics, these property classifications are used.

2.2.1. Thermoplastics and Thermosets

Thermoplastics have weaker crosslinking of the molecular chains, and these links are less effective than in the case of thermosetting plastics. The long polymeric chains are seized together by relatively weak connection, either by 'Van der Waals' forces or by hydrogen bridges, that are reversible bonds. These ingredients can be softened by heat and then regain their unique features upon cooling. The feasibility of heating and cooling thermoplastics is a fundamental advantage, which is the principle of most processing technique for these polymers. It has its interests, but, on the other hand thermoplastic polymers are sensitive to heat. Polyethylene, polystyrene, polyvinyl chloride, polyamides, cellulose acetate, polypropylene and poly methyl methacrylate (PMMA) are some examples of thermoplastic polymers [5].

Thermosets have stronger and more effective crosslinking of the molecular chains. They are produced with a chemical reaction which has two steps. In the first step, formation of long molecule chains occur, similar to those present in thermoplastics. In the second step, very strong covalent bonds among polymeric chains are formed, supplying a tri-dimensional network deeply rigid that is practically irreversible (crosslinking of chains). These materials cannot be re-melted by heating. In fact, heating operation can result in a rigid material because of the formation of excellent amounts of crosslinks among polymeric chains. But, when an excess of heat is applied to these materials, they will burn down. Since the crosslinking of molecules results in strong chemical bonds, thermosets are rigid materials and their mechanical features are less heat sensitive (within a certain temperature range) than thermoplastic materials. Epoxy resin systems, unsaturated polyesters, furan, vinyl ester and phenol resins are included in this group of polymers [5].

2.2.2. Polymer Structure

Characteristics of the polymer chains are directly affected by structure. These properties are the general structure of polymer chains, stereochemistry of the chain, and the geometric isomerization for diene-type polymers [2].

2.2.2.1. Linear, Branched, Cross Linked and Network Polymers

The basic units coming about because of the response of monomers may on a basic level be linked together in any possible example. Binary functional building units can go into two and just two linkages with other structural units. This implies that the succession of linkages between bi-functional units is fundamentally linear. The aroused polymer is said to be linear. Nonetheless, the reaction among multifunctional molecules brings about basic units that might be connected to from nonlinear structures [6].

Polymers formed by condensation polymerisation of absolutely bi-functional monomers must be linear. The chains created in addition polymerisations may have various short or long branches connected indiscriminately along their axes. Particularly in radical polymerisation, branching is plausible and can't be effectively controlled. Branching influences the features of a polymer in the molten condition and in a solution. Viscometric, nuclear magnetic resonance (NMR) and infrared adsorption (IR) techniques are the most encouraging techniques for measuring of the branching features of a polymer in the molten condition and in solution [7].

A cross-link is a chemical bond between polymer chains other than at the end points. Cross-links are critical in deciding physical properties since they increment the molecular weight and limit the translational motions of the chains as for each other [8].

Network polymers are achieved when linear or branched polymer chains are combined by covalent bonds, a procedure called crosslinking. Vulcanization of elastic is a case of a crosslinking procedure. Network polymers are additionally obtained from poly-functional monomers. By means of crosslinking, the polymer chains of network polymers lose their capability to flow. Thus the polymer will not soften or flow and can't, hence, be combined [9].

2.2.2.2. Cis-Trans Isomerism

Cis and trans configurations depict the disposition of indistinguishable atoms or set of atoms which surrounds a double bond in a repeating unit. These configurational isomers are spatially stationary and, cannot be changed from one to the next by rotation about covalent bonds [4].

2.2.2.3. Homopolymers and Copolymers

Polymers might be either homopolymers or copolymers relying upon the combination of monomers. Homopolymers are known as the polymers made out of just a single repeating unit in the polymer chain [7].

A random copolymer is a copolymer when two different monomers are distributed on the chain irregularly. An alternating copolymer, whose name contains a hint, is a copolymer when two different monomers are distributed on polymer chain back-to-back. A block copolymer consists of inseparable repeating units like blocks are located in the chain. Lastly, one type of homopolymer side branch can be bonded to homopolymer main chain which is composed of a distinct repeat unit; which is called as a graft copolymer [10].

2.3. POLYMER SYNTHESIS

Polymerization occurs when many monomers are covalently bonded to produce a chain or network. Some atoms or molecules are excluded from each monomer, during the polymerization process [11].

Some dominating industries as textile, automotive, house goods and medical devices utilize both biological and synthetic polymers. They can be produced as purpose-oriented, hard or soft, elastomeric or fibrous, sponge like or crystalline. Synthetic polymers can be synthesized via miscellaneous polymerization routes to generate different products in terms of molecular mass, component assembly, stereoregularity and crystallinity. All of the variations results in polymers with unique mechanical and physical properties. As the usable monomers are rich in numbers, the miscellany of possible polymeric products is

also considerable. Polymers can be viscoelastic or plastic. Polymers do not always have linear structures. However they can be branched with the same monomer or different monomers which cause changes in the chemistry and the crystallinity of the resulting polymer. The polymer may also be cross-linked which makes it insoluble and swell in some solvents. More than one monomer can be used at once to produce polymers to respond the need. The needs play a determinative role if a polymer should be load-bearing or should be a soft tissue replacement in the human body [12].

Step-growth and chain-growth polymerization are the ways of synthetic methods. The main difference between the two is that monomers are linked to the chain one at a time, controversially in chain-growth polymerization, monomer chains can combine with each other straight away in step-growth polymerization [11].

2.3.1. Addition (Chain Growth) Polymerization

Addition polymerization is a process by which unsaturated monomers are converted to polymers with high molecular weight, exhibiting the characteristics of a typical chain reaction [7]. Polyethylene, polypropylene, poly(vinyl chloride), poly(vinylidene chloride), polystyrene, polyacrylonitrile, polytetrafluoroethylene, poly(methyl methacrylate), poly(vinyl acetate), cis-polyisoprene, polychloroprene are given as examples of addition polymers. Initiation, propagation and termination are three stages of addition polymerization. At first phase, a substance is divided into two identical units which possess an unpaired electron. They are called as free radicals. The free radical subsequently inducts the reaction by forming a bond with one of the carbon atoms in the double bond of the monomer [13].

A reactive species and a monomer react in order to form an active site while chain growth polymerization starting. Free radical, anionic, cationic, and coordination polymerization are four principal mechanisms of chain growth polymerization. The first three refer to the chemical nature of the active group at the growing end of the monomer. Coordination polymerization, on the other hand, involves reactions where the polymers are produced with a company of a catalyst. Coordination polymerization can happen via a free radical, anionic, or cationic reaction. The catalyst performs as a reaction rate accelerant and

provides better control of the process. The choice of one polymerization method over another is defined by the type of monomer and the desired properties of the polymer [14].

2.3.2. Condensation (Step Growth) Polymerization

A step-growth polymerization is a stepwise reaction between bi-functional or multifunctional monomers in which a polymer with high-molecular-weight is produced after several steps. The step-growth polymerization produces many natural and synthetic polymers such as polyesters, polyethers, urethanes, epoxies, and polyamides [15]. Polyester, polyanhydride, polyacetal, polyamide, polyurethane, polyuria, silk fibrion, cellulose, phenol-aldehyde, urea-aldehyde, polysulfide, polysiloxane are given as examples of step-reaction polymers [16].

Step-growth polymers have been identified with the discovery of functional synthetic polymers in tremendous application areas. It started in 1907 with the Belgian chemist Baekeland, who discovered bakelite which is a product of the condensation reaction of phenol and formaldehyde. It was the innovating study of Wallace Carothers and his research group at DuPont that guide to the discovery of the 20th century's most widely used synthetic polymers, which are nylon and polyester. He clarified the keystone laws of step-growth polymers and open the door for the later work of Whinfield and Dickson in which they discovered poly(ethylene terephthalate) (PET) [15].

In step-growth polymerizations, any species (monomers, dimers, trimers, etc.) may give reaction at any time, resulting in increase in terms of molecular weight. Generally, polycondensations and polyadditions are count as two types of step-growth polymerization. Polycondensation reactions, containing polyesters and polyamides formation, are occured by a small molecule ejection (e.g. water, methanol) as a by-product. The formation of polyurethanes and polyurea are typical examples of polyaddition type of step-growth polymerizations, in which monomers react without any small molecule ejection [15].

2.4. SOLID STATE PROPERTIES

There are two distinct forms in which a polymer can display the mechanical features that can be associated with solids; as a crystal or as a glass.

2.4.1. The Amorphous State

They are generally clear and have diffused melting point. The molecules are ordered randomly and results in molding difficulties compared to crystalline polymers. After curing they shrink less as dissimilar with crystalline thermoplastics. Polycarbonate (PC), poly methyl methacrylate (PMMA), polystyrene (PS), poly phenylene oxide (PPO), acrylonitrile butadiene styrene (ABS) are some examples of them [17].

2.4.1.1. Chain Entanglements

Entanglement means that the molecular mobility of other chains is topologically limited [24]. Entanglements happen if there are two chains in a loop over one another, or when, intermolecular relationship through hydrogen bonding or some other particular chemical interaction occurs. It is important to realize how the chain entanglements concentration is influenced by the length of chain, loop dimensions, stereo chemical configuration and temperature, and to characterize and decide individually from these agents a parameter measuring the essential tendency for a repeating unit of a given chemical structure to frame entanglements [18].

The polymer chain movements are influenced by chain entanglements. For this reason, this must be recognized by slowdown of polymer progression and must be visible in a few viscoelastic features [19].

2.4.1.2. Glass Transition Temperature (T_g)

The glass transition temperature (T_g) is a parameter certain interest in fabricating of synthetical polymer. T_g tells of the temperature at which amorphous polymers change over

to a rubbery, viscous amorphous polymer. The glass transition temperature might be changed by modifying the branching or crosslinking amount in the polymer or by the use of plasticizer [20].

On the other hand, the temperature when amorphous parts of a polymer present the distinguishing features of the glassy state -brittleness, stiffness, and rigidity- is called glass transition temperature [21].

The ingredients of the chemical structures associated with the polymer glass transition behaviour could be divided into two categories corresponding to the intrinsic and extrinsic levels separately [22].

The first category is the predominant agent of glass transition temperatures:

- i. The polymer chains are more rigid, the glass transition temperatures are higher;
- ii. The inter-chain interactions are stronger, glass transition temperatures are again higher [22].

The second category includes the auxiliary factor for the glass transition temperatures:

- i. For the high molar mass region, the glass transition becomes insensible to the molecular weight of polymers. However for the low molar mass region, the chain ends include elevated mobility; then having extra free volume.
- ii. The cross-links limit the mobility of network chains. That is why, T_g increases with the crosslink density [22].

2.4.2. The Crystalline State

In crystalline state, atoms stay immobile, even though there are lots of vibrations around lattice place. A phase change takes place from the ordered structure to the disordered liquid phase, while heating at any upper level of the melting temperature, T_m . Atoms and molecules are in random motion in the liquid phase [23].

When a polymer is stereoregular with particle or any chain branching, or when it contains highly polar groups that produces dipole-dipole interactions, it may exist as crystalline [23].

There are three factors to determine crystallization tendency;

- Structural regularity - For the efficient usage of the secondary intermolecular bonding forces through the generation of a crystalline structure, intimate coalition of polymer molecules is essential. Any structural property of a polymer chain that inhibits this phenomenon must inevitably reduce crystallinity [7].
- Chain flexibility - Aggregation, which results in crystalline solid, polymer molecules are in conflict with thermal agitation, which stimulates metameric rotational and vibrational motion. Elastic chained polymers are more sensitive to that stimulation than stiff backboned polymers. As a result, chain flexibility decreases the crystallization [7].
- Intermolecular bonding - Since intermolecular bonding is the result of secondary bonding forces, polymer particles with certain groups that encourage increased intermolecular interaction and due to structural properties they are more crystallisable [7].

2.4.2.1. Ordering of Polymer Chains

The tendency of a polymer to crystallize, the crystallinity magnitude and crystallization stability are specified by several factors. These are the grade of close packing and the presence of intermolecular forces. The cooling rate of the melt for solidification also affects the degree of crystallinity; during crystallization, upon cooling through melting point, polymers become deeply viscous. Time is necessary for random and entangled chains to become ordered, slow cooling lets time for molecules to align themselves into an orderly structure [4].

The crystallinity amount also depends on the tacticity of the polymer. The larger the order in a macromolecule, the larger the possibility of the molecule to crystallize. For instance, isotactic polypropylene is generally more crystalline than syndiotactic polypropylene, and atactic polypropylene counts as uncrystallizable while the polymer chain is irregular. Actually, nearly all atactic polymers cannot be crystallized [24].

Strong intermolecular forces and a rigid chain backbone support the crystallization because the molecules tend to maximize number of secondary bond by maximizing packing. Therefore, the molecules are disposed to distribute together to form a crystalline structure [24].

Bulky side groups have just opposite effects in terms of crystallinity. With rising size of the side groups it gets more challenging for the polymer to fold and align itself throughout the crystallization. Thus, bulky side groups and branching decrease the capability and possibility of a polymer to crystallize. Most network polymers do not crystallize since the polymer subchains do not have the space for motion [24].

2.4.2.2. Crystalline Melting Temperature

Melting is a true first-order thermodynamic transition which includes a phase change. In theory, any feature whose values are different for the crystalline and amorphous states ensure a suitable way in order to measure the crystalline melting point. The expression melting point, when administered to polymers, proposes not a solid-liquid phase transition but a transition from a crystalline or semi-crystalline phase to a solid amorphous phase. In synthetic polymers family, crystalline melting is observed for thermoplastics, while thermosetting polymers will disintegrate at high temperatures but do not melt [7].

Techniques for quantifying the crystalline melting point contain dilatometry, calorimetry, and thermal analysis; dynamic techniques; stress relaxation; and creep [7].

2.4.3. Mechanical Properties of Polymers

The mechanical properties of polymers are defined as modulus of elasticity, yield and tensile strengths. For numerous polymeric substances, the easy stress–strain test is used for the identification of many of these mechanical quantities. The mechanical properties of polymers, are deeply responsive to the rate of deformation (strain rate), the temperature, and the chemical character of the environment (the presence/absence of water, oxygen, organic solvents, etc.) [11].

All polymers have several mechanical manners, from brittle-elastic at low temperatures, through plastic to viscoelastic / leathery, to rubbery and viscous at high temperatures. The mechanical state of a polymer is influenced by its molecular mass and by the temperature; or, more implicitly, by how close the temperature is to its glass transition temperature [25].

There are three distinctive categories of stress–strain attitude for polymeric materials, as described in Figure 2.1. Curve A describe the stress–strain nature for brittle polymers, in as much as it breaks meanwhile in the elastic linear region. The behaviour for a plastic material, curve B, is valid for plenty of polymeric materials; the primary degradation is elastic, that is chased by yielding and a field of plastic deformation. Lastly, the degradation represented by curve C is completely elastic; this rubber-like elasticity (generous restorable strains generated at small amounts of stress points) is exhibited by a group of polymers refer to the elastomers [11].

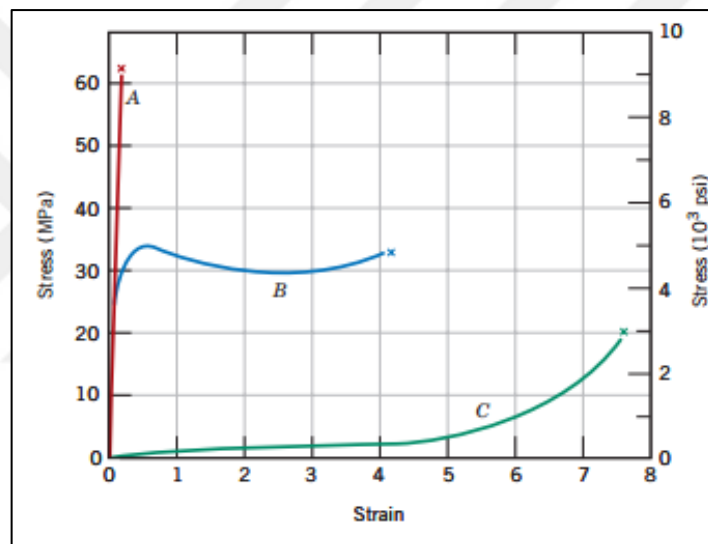


Figure 2.1. The stress–strain behaviour for brittle (curve A), plastic (curve B), and highly elastic (elastomeric) (curve C) polymers [11]

Mechanical properties of polymers vary impressively with material temperature, going from glass-like brittle manner at low temperatures to a rubber-like manner at high temperatures [26]. The effect of temperature on stress–strain curve of polymers is illustrated on Figure 2.2.

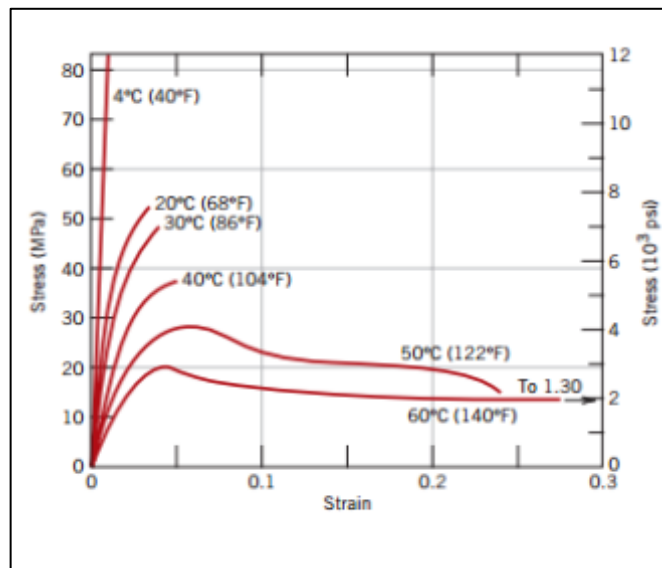


Figure 2.2. The effect of temperature on the stress–strain curve of polymers [11]

The effect of strain rate on the mechanical behaviour may also be significant. Generally, reducing the speed of deformation has the similar effect on the stress–strain features as raising the temperature; as the material evolves softer and more ductile [11].

The stiffness and the strength of a polymer are different terms. The stiffness defines the strength to elastic deformation; the strength defines the resistivity to crumble by plastic yielding or by breaking [25].

2.4.3.1. Tensile Strength (TS)

Tensile strength is described as the power necessary to fracture the sample or result in complete separation of component in a linear way. To put differently, tensile strength is a measurement of the mechanical features of a material. It represents the standing capacity for breaking under tensile stress. This feature is one of the most critical and widely measured characteristic of materials used in structural effectuation. The required force per area (MPa or psi) to rupture a material in this way is the maximum tensile strength. Generally, tensile strength measures required amount of stress the material resists before experiencing continuous damages [27].

2.4.3.2. Percent Elongation at Break (Ductility)

Elongation to break means the strain in the material on its breakage, which quantifies the relative change in the material length before break down. It is a quantification of ductility [28].

Ductility is an assessment of the capability of a material to subject plastic deformation sooner than breaking. It can be verbalized as percentage elongation (% EL) or percentage decrease in area (% RA) from the tensile test [11]. An example of stress-strain curves for plastics with various amounts of ductility is illustrated on Figure 2.3. [29].

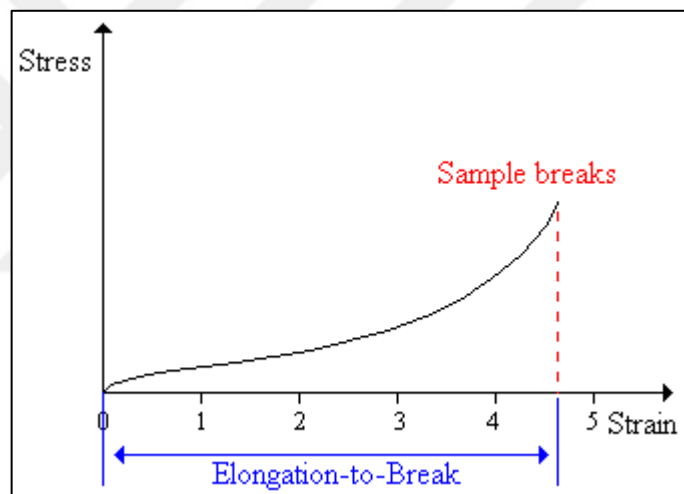


Figure 2.3. Characteristic stress-strain curves for plastics with different levels of ductility

Elongation at break is the strain at which a polymer fractures during tension test at a fixed temperature. Raising practices are being improved for thermoplastics in which a constructed article is faced to an extended uninterrupted stress. Under such environment, materials display (to varying extents) continuous deformation as time. This occasion is called 'creep'. Under suitable conditions of stress and temperature, a wide diversity of materials will indicate a typical type of creep behaviour [29]. An example of stress-strain curves for polymers at room temperature is presented in Figure 2.4. [4].

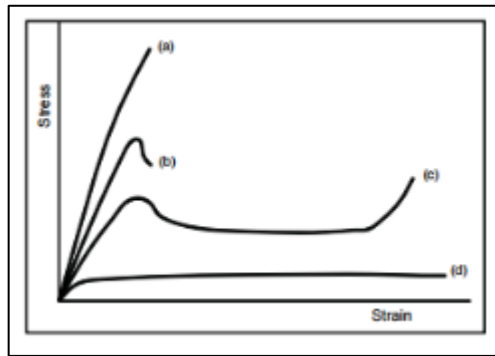


Figure 2.4. Stress-strain curves for polymers at room temperature: (a) a low ductility polymer, (b) a ductile polymer, (c) a ductile polymer capable of cold drawing, and (d) a polymer with long-range elasticity

2.4.3.3. Young's Modulus

Young's modulus means the proportion of stress to strain in the linearly elastic region. This ratio is also named the modulus of elasticity or tensile modulus. Relationship between stress-strain curve and Young's Modulus is illustrated in Figure 2.5. It can be evaluated by dividing the stress by the strain [30]:

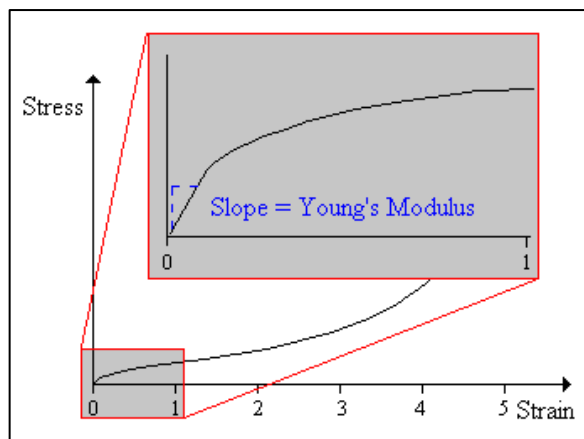


Figure 2.5. Relationship between stress-strain curve and Young's Modulus

High Young's modulus values point out that the substance is stiff and repellent to elongation and stretching [30].

Commonly, fibers possess high Young's modulus amounts, elastomers possess low Young's modulus amounts, and plastics are between them [31].

2.4.3.4. Toughness

Toughness is a measure of the absorbed energy amount during braking. Toughness is represented by the total area under the curve of stress-strain [7]. Relationship between stress-strain curve and toughness is illustrated on Figure 2.6.

Strength says how much force is needed to break the sample. Strong polymer sample does not mean that it is also tough [32].

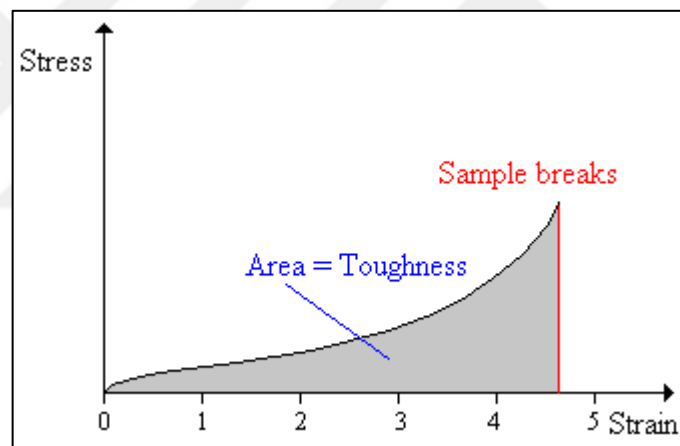


Figure 2.6. Relationship between stress-strain curve and Toughness

2.4.3.5. Compressive Properties

Compressive characteristics contain modulus of elasticity, yield stress, deformation beyond yield point, and compressive strength (if the substance solely smooth but does not brake). Materials having a low order of ductility not always indicate a yield point. In the case of a material which yields in pressing by a smashing fracture, the compressive strength possesses a much specific respect. If a material which does not yield in compression by a smashing fracture, the compressive strength is an unpredictable one attaching upon

disturbance amount which is taken into account as representing whole collapse of the material. Several plastics will keep going to change shape in compression till a straight disk is manufactured. During this process, the compressive stress (nominal) is increasing steadily, without any well-described break down happening. Compressive strength is insignificant in such situation.

2.5. BONE TISSUE ENGINEERING

Tissue engineering and regenerative medicine are popular nowadays with novel advances for de novo skeletal tissue formation in an effort to point the need for bone augmentation and skeletal renewal [33].

Keystones of bone tissue engineering (BTE) are the perceiving the structure of bone and its mechanics, development of tissue while influencing new functional bone tissues. Alias, to achieve bone repair or regeneration, background of the bone biology and its development is vital. Bone can respond a wide range of functions, and bone answers to various metabolic, physical and endocrine input.

Bones symbolize a basement for our bodily locomotion, which bears load for our skeleton and protect internal organs, contains the biological elements compulsory for hematopoiesis, trap heavy metals (i.e., lead), and preserves the essential electrolytes to provide homeostasis via calcium and phosphate depot. Effective bone tissue engineering needs the newly constructed bone to be completely incorporated with the neighboring host bone, and noteworthy, to perform the previously indicated functions of native bone [34].

Dealing with a complex biological and sensitive system like human body, the qualifications of materials for tissue engineering scaffolds are numerous and exceedingly challenging. Foremost, biocompatibility of the substrate materials is mandatory; which means the material must not arouse a problematic inflammation or show immunogenicity or cytotoxicity. Also, the mechanical features of the scaffold must be suitable to the application and not break down during treatment and during the patient's daily routine [35].

Materials stimulating bone regeneration have an impact in clinical applications such as the treatment of nonunion fractures and spinal fusion. The utilization of porous scaffolds such as bioceramic and polymers to reinforce bone cell and tissue growth is not a very recent research field. Contemporary troubles contain the engineering of materials that can suit both the mechanical and biological structure of bone matrix and reinforce the vascularization of large tissue assemblies. Scaffolds with novel functions that try to reanimate nanoscale topographical and biofactor signals from the extracellular environment are apparently attractive possible biomimetic materials [36].

The ideal orthopedic prostheses should have 3D bone-like interconnected porous structures with an appropriate organization, porosity and scale to favor tissue integration and vascularization, likewise support flow for the transportation of nutrients and metabolic waste. Contemporary, researchers are seeking for the optimum pore size and shape for several bone tissue engineering operations. It is also vital to arrange the suitable porosity of scaffolds by varying possible production techniques to unite the porosity of true bone. It is very important that the porosity, pore shapes, and pore size have an impact on mechanical and biological features of scaffolds [37].

2.5.1. Polymers Used as Scaffolds in Bone Tissue Engineering

Musculoskeletal, bone and cartilage tissues are major research areas of tissue engineering. Tremendous biodegradable and bioresorbable materials as scaffolds and their designs, have been experimentally and/or clinically investigated. An ideal scaffold should have the following properties:

- i. three-dimensional and interporous network for cell adhesion growth and flow for the transport of nutrients and metabolic waste;
- ii. biocompatible and bioresorbable with an adjustable degradation rate and resorption rate to couple cell-tissue growth *in vitro* and/or *in vivo*;
- iii. proper surface hydrophilicity for cell attachment, proliferation, and differentiation and
- iv. mechanical properties to bear tissues at the implantation area [38].

Various scaffolds have been produced for tissue engineering with polymers, ceramics and their composites. Biomimicry has been accepted as preponderance of the 3D scaffold fabrication both in terms of physicochemical features and bioactivity for master tissue regeneration. Scaffolds produced using salt leaching, particle sintering, and lithography techniques have been profitable in enhancing *in vitro* cell proliferation and *in vivo* tissue regeneration. Scaffold produced by decellularization has been in demand because of their certain biocompatibility and bioactivity. Conventional scaffold production methods usually failed to produce complicated structures with extensive purpose, not consistent and require multiple steps [39].

To fulfil these scaffolds, both synthetic and natural polymers have been preferred biomaterials because of their unlimited variety of features and bioactivity [40]. Natural polymers were among the first biodegradable scaffold materials in clinical usage, because of their advance entire interactions with different cell types, and they do not have any immune response. Nevertheless, synthetic polymers were subsequently understood to be inexpensive and permit better functions than natural polymers, regardless of the potency for an immune response or toxicity primarily with the use of certain polymer associations. Among the synthetic polymers, poly(L-lactic acid) (PLLA), poly(glycolic acid) (PGA), poly(caprolactone) (PCL) and poly(lactic-co-glycolic) acid (PLGA) are nowadays the most preferred for the generation of 3D scaffold structures. These polymers are also combined with natural polymers to enhance adverse proclaims ally with hydrophilicity, cell attachment, and biodegradability. Additionally, surfaces of the scaffolds are functionalized by usage of specific ligands such as protein molecules increasing cellular responses [41].

2.5.2. Poly(propylene fumarate) (PPF)

Poly(propylene fumarate) (PPF) is a biodegradable and injectable polymer. It has been used for producing preformed tissue engineering scaffolds due to *in situ* crosslinking features. PPF is an unsaturated linear polyester which may be cross-linked through carbon double bonds along its backbone and degraded by simple hydrolysis of the ester bonds into nontoxic units of propylene glycol, poly(acrylic acid-co-fumaric acid), and fumaric acid. PPF is a favourable material for tissue engineering operations, remarkably for bone formation. Earlier studies have demonstrated that the introduction of ceramic compounds,

such as β -tricalcium phosphate, to PPF improved both mechanical strength and osteoconductive features of the scaffold [42].

Purified PPF can be crosslinked via covalent bonds to produce degradable polymer networks, which have been extensively investigated for biomedical applications. The characteristics of crosslinked PPF networks related to the molecular features of the polymer, such as the molecular mass. The virginity of the reactants and the elimination of water from the reaction system have the maximum significance in the production of high-molecular-weight PPF products. Moreover, the duration of the reaction and temperature affect the molecular weight of the PPF product [43].

Poly(propylene fumarate) is a linear fumaric acid-based polyester. The primary advantages of PPF are (i) the unsaturated carbon carbon double bonds of the fumaric acid that permit cross-linking of the resin into a polymeric network, and (ii) the production of biocompatible and avoidable degradation products, mostly fumaric acid and propylene glycol, during hydrolysis of its ester bonds. The major weakness of PPF is that it is viscous at room temperature (25°C), making handling of the polymer challenging [43].

2.5.3. Vinylphosphonic Acid and Derivatives

In this project, biodegradable polymers, which have been produced by crosslinking PPF with vinylphosphonic acid (VPA) and vinylphosphonic acid di-ethyl ester (VPES) , are expected to enhance biocompatibility compared to current PPF systems (PPF-VP) via phosphonic acid and ester structures. Meanwhile, it is also expected that the polyvinyl phosphonic acid or ester incorporated into the PPF-based network structure will promote bone formation by enhancing osteoblast activity and reducing osteoclast activity [44].

A recent polymer which is containing phosphonate, poly- (vinylphosphonic acid-co-acrylic acid) (PVPA-co-AA) has been categorized as a possible candidate for scaffolds used in bone tissue engineering [45,46]. It is suggested that this material imitates the duty of bisphosphonates, which are used in osteoporosis treatment [47]. Bisphosphonates are counted as synthetic analogues of inorganic pyrophosphate, a physiological regulator of calcification and bone resorption. Present acid groups and the strong environmental negative charge of PVPA-co-AA are supposed to imitate the structure of bisphosphonates.

Structure of the backbone allows bisphosphonates to bind to divalent metal cations, consequently bisphosphonates can bind to bone mineral surfaces *in vivo* [48].

Gemeinhart et al. [49] have synthesized copolymers of poly- (vinylphosphonic acid-co-acrylamide) discovered that 30 mol percent was the ideal VPA concentration for maximum mineralization of the matrix of the osteoblast cells.

However, the use of vinyl phosphonic acid (VPA) and vinyl phosphonic acid diethyl ester (VPES) to crosslink the PPF polymer has not been reported so far. The use of these monomers as a bone filler material with high potential PPF polymers is expected to increase the biocompatibility and bone formation of PPF based systems.

In the majority of the studies on PPF conducted to date, low molecular weight poly-acrylate, methacrylate or fumarate resin has been used in the cross-linking of PPF except N-vinyl pyrrolidone, but comonomers that can be alternative to N-vinyl pyrrolidone have not been reported ever since. Besides, biocompatibility and osteoconductivity effects of the crosslinking agents were not found in the literature at the same time.

2.6. AIM

The main aim of this project is to use vinyl phosphonic acid diethyl ester (VPES) and vinyl phosphonic acid (VPA) instead of vinyl pyrrolidone (VP) for the curing process of PPF polymer in order to increase biocompatibility and investigate the effect of those comonomers on the mechanical and thermomechanical properties, thermal stabilities, surface hydrophilicity, biodegradation, cell attachment and osteoconductivity of the PPF polymer.

3. MATERIALS AND METHODS

3.1. SYNTHESIS OF POLY(PROPYLENE FUMARATE) (PPF)

3.1.1. Chemicals

All chemicals used for PPF synthesis and purification are listed in Table 3.1.

Table 3.1. Chemicals used for PPF synthesis and purification

Chemical	Chemical Formula	Company	Catalog Number
Fumaric acid	C ₄ H ₄ O ₄	Alfa Aesar	A10976
Propylene glycol	C ₃ H ₈ O ₂	Santra Cruz	SC-215754A
p-toluene sulfonic acid monohydrate	C ₇ H ₈ O ₃ S	Fluka	89762
Hydroquinone	C ₆ H ₆ O ₂	Sigma Aldrich	H9003
Dichloromethane	CH ₂ Cl ₂	Sigma Aldrich	24233-2.5L-R
Methanol	CH ₃ OH	Sigma Aldrich	24299
Calcium chloride	CaCl ₂	Sigma Aldrich	C1016
Diethyl ether	C ₄ H ₁₀ O	Sigma Aldrich	179272

3.1.2. PPF Synthesis

Polypropylene fumarate (PPF) was synthesized from propylene glycol and fumaric acid using hydroquinone as a radical inhibitor and p-toluene sulfonic acid as the catalyst. The synthesis reaction is presented in Figure 3.1.

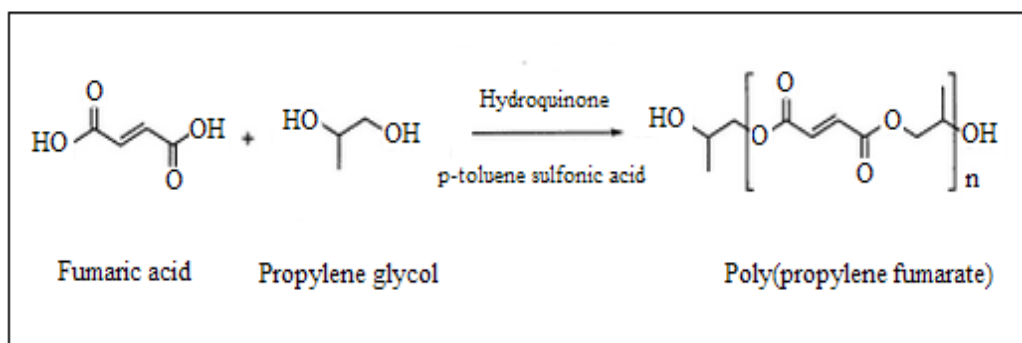


Figure 3.1. Reaction scheme of PPF synthesis

For the polycondensation reaction, the stoichiometric ratio used was 1.5:1.65 for fumaric acid and propylene glycol. The radical inhibitor, hydroquinone was used as 0.1 percent and the catalyst, p-toluene sulfonic acid was used as 0.4 percent of the total weight of propylene glycol and fumaric acid. Reaction mixture was stirred in a three necked round bottomed flask that was put on a heating mantle and that was equipped with Dean Stark apparatus connected to a distillation column; temperature controller and nitrogen gas inlets.. The reaction was carried out at 145°C for 3 hours and 180°C for 1 hour collecting water as the byproduct of the reaction. The set-up of the reaction is illustrated on Figure 3.2. The PPF product was then purified for the removal of unreacted fumaric acid and propylene glycol [50].



Figure 3.2. Set-up of the PPF synthesis

3.1.3. Purification of the PPF Resin

To purify the crude PPF product, PPF was dissolved in 120 mL of dichloromethane (CH_2Cl_2) and vacuum filtration was performed to eliminate unreacted fumaric acid. Filtered PPF was washed with 20:80 methanol-water solution (150 mL) to eliminate unreacted propylene glycol. Washed PPF was subsequently incubated with granular anhydrous calcium chloride (CaCl_2) to eliminate remaining water in the resin and second vacuum filtration was performed to remove CaCl_2 particles. Following rotary evaporation of CH_2Cl_2 , diethyl ether wash was performed and purified PPF was obtained.

3.1.4. Proton NMR (¹H-NMR) Spectroscopy and Gel Permeation Chromatography (GPC) Analysis of PPF Resin

Purified PPF resin was prepared by dissolving 0.1g of PPF in 1.0 ml deuterated chloroform (CDCl₃) for ¹H-NMR spectrometry. A Bruker AM250 instrument with a magnetic field strength of 250MHz was used as NMR spectrometer. A spectral window of 2000Hz, and a pulse width of 90° were used, and the digital resolution was 0.427 Hz/pt. Measurement was accomplished at room temperature (25°C).

GPC analysis of the PPF polymer was performed in tetrahydrofuran (THF) at a flow rate of 0.5 ml/min, using an Agilent 1100 Series GPC modular system equipped with a refractive index detector. The column used (PL-gel 5μm, Mixed D) was kept at 25°C. Polystyrene standards with Mp=500-300,000 g/mol were used for calibration.

3.1.5. FT-IR Spectroscopy Analysis of PPF

PPF was analysed by ATI Mattson Genesis Series FT-IR spectrometer. Viscous PPF resin was spread on a potassium bromide (KBr) pellet and pellets were formed under 10000 psi pressure, respectively. After a background scan of the pure KBr pellet was taken, sample was scanned 16 times with a resolution of 4 cm⁻¹, in the 400-4000 cm⁻¹ region.

3.2. PREPARATION OF THERMALLY CURED COPOLYMERS

All chemicals used for crosslinking of PPF with vinylphosphonic acid (VPA) or diethyl vinyl phosphonate (VPES) via thermal cure are listed in Table 3.2.

Table 3.2. Chemicals used for preparation of thermally cured copolymers

Chemical	Chemical Formula	Company	Catalog Number
Vinyl phosphonic acid	CH ₂ =CHP(O)(OH) ₂	Merck	8.43914.1000

(VPA) (90%)			
Diethyl vinyl phosphonate (VPES)	$C_6H_{13}O_3P$	Sigma Aldrich	116130-25G
Benzoyl peroxide	$C_{14}H_{10}O_4$	Merck	8.01641.0250

3.2.1. Crosslinking of PPF with VPA or VPES via Thermal Cure

PPF/VPA and PPF/VPES formulations containing 20, 30 and 40 weight percent comonomer (VPA or VPES), were cured in the presence of 2 and 3 weight percent benzoyl peroxide (BP) initiator. For this purpose the PPF pre-polymer was first heated to around 50 °C to decrease the viscosity, the comonomer and BP were introduced and the mixture was stirred for five minutes by pouring nitrogen gas through a pipette into the mixture. The prepared liquid mixtures were poured into glass vials or metal molds to get bars or discs with the desired shape for various tests. The molded mixtures were finally placed in an oven and cured for 2 hours at 65°C, 2 hours at 80°C and 5 hours at 100°C, respectively. Reaction scheme is presented in Figure 3.3.

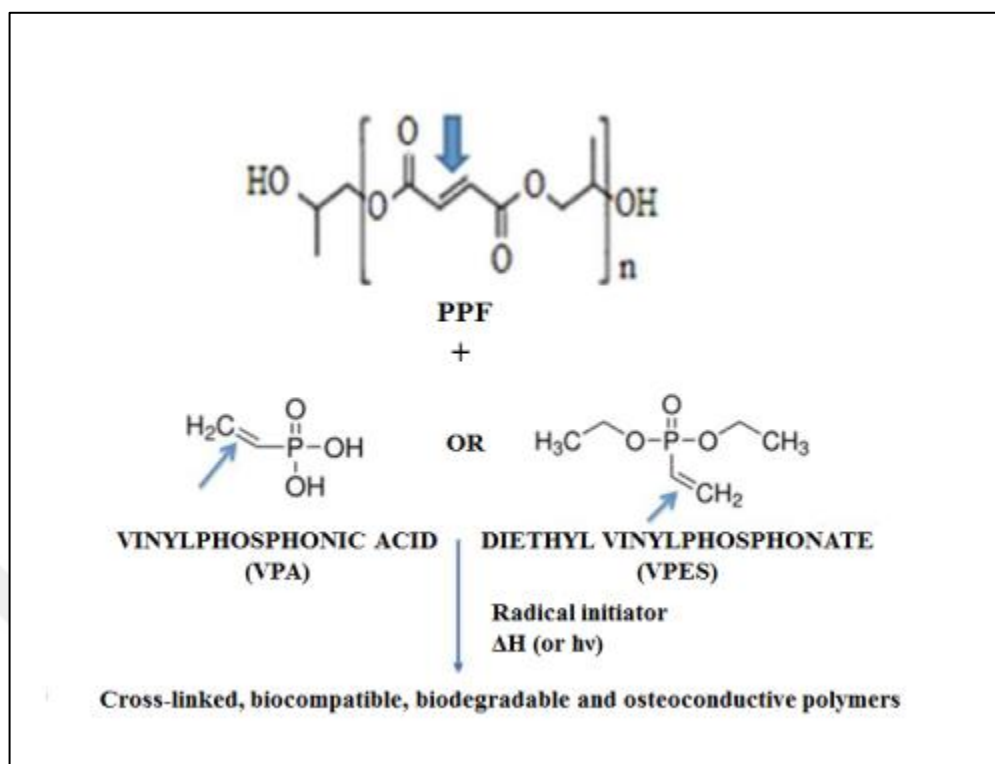


Figure 3.3. Radical polymerization scheme of PPF with comonomers

3.2.2. FT-IR Spectroscopy Analysis of Thermally Cured Copolymers

All end products were analysed by ATI Mattson Genesis Series FT-IR spectrometer. Samples were grinded and mixed with KBr powder and pellets were formed under 10000 psi pressure, respectively. After a background scan of the pure KBr pellet was taken, each sample was scanned 16 times with a resolution of 4 cm^{-1} , in the $400\text{-}4000\text{ cm}^{-1}$ region.

3.3. PREPARATION OF UV CURED COPOLYMERS

All chemicals used for crosslinking of PPF with vinylphosphonic acid (VPA) or diethyl vinyl phosphonate (VPES) via UV cure are listed in Table 3.3.

Table 3.3. Chemicals used for preparation of UV cured copolymers

Chemical	Chemical Formula	Company	Catalog Number
Vinyl phosphonic acid (VPA) (90%)	$\text{CH}_2=\text{CHP}(\text{O})(\text{OH})_2$	Merck	8.43914.1000
Diethyl vinyl phosphonate (VPES)	$\text{C}_6\text{H}_{13}\text{O}_3\text{P}$	Sigma Aldrich	116130-25G
Phenylbis (2,4,6-trimethylbenzoyl) phosphine oxide (BAPO)	$[(\text{CH}_3)_3\text{C}_6\text{H}_2\text{CO}]_2\text{P}(\text{O})\text{C}_6\text{H}_5$	Sigma Aldrich	511447-10G

3.3.1. Crosslinking of PPF with VPA or VPES via UV Cure

PPF/VPA and PPF/VPES formulations containing 30 weight percent comonomer (VPA or VPES), were cured in the presence of 1 and 2 weight percent phenylbis (2,4,6-trimethylbenzoyl) phosphine oxide (BAPO) UV catalyst. For this purpose the PPF prepolymer was first heated to around 50 °C to decrease the viscosity, the comonomer and BAPO were introduced and the mixture was stirred for five minutes by pouring nitrogen gas through a pipette into the mixture. The prepared liquid mixtures were poured into glass vials to get discs with the desired shape for various tests. The molded mixtures were finally placed under a UV light source ($\lambda=260$ nm) and cured for 2 hours at room temperature.

3.4. PPF BASED END PRODUCTS

All end products which were prepared by curing PPF resin with VPA and VPES comonomers are listed in Table 3.4. All analyses and experiments were performed for both thermal and UV cured copolymers.

Table 3.4. Cured PPF based copolymers

Copolymer	Method of Cure
PPF/VPA (80/20) – 2% BP	Thermal cure
PPF/VPA (70/30) – 2% BP	Thermal cure
PPF/VPA (60/40) – 2% BP	Thermal cure
PPF/VPA (80/20) – 3% BP	Thermal cure
PPF/VPA (70/30) – 3% BP	Thermal cure
PPF/VPA (60/40) – 3% BP	Thermal cure
PPF/VPES (80/20) – 2% BP	Thermal cure
PPF/VPES (70/30) – 2% BP	Thermal cure
PPF/VPES (60/40) – 2% BP	Thermal cure
PPF/VPES (80/20) – 3% BP	Thermal cure
PPF/VPES (70/30) – 3% BP	Thermal cure
PPF/VPES (60/40) – 3% BP	Thermal cure
PPF/VPA (70/30) – 2% BAPO	UV cure
PPF/VPA (70/30) – 3% BAPO	UV cure
PPF/VPES (70/30) – 1% BAPO	UV cure
PPF/VPES (70/30) – 2% BAPO	UV cure

3.5. CROSS-LINK DENSITY ANALYSIS OF PPF/VPA AND PPF/VPES POLYMERS

The cross-link density of the PPF copolymers was determined via swelling experiments. The cross-link density (γ) of swollen copolymers and molecular weight between cross-links were determined by using modified Flory–Rehner’s equation.

The swelling coefficient was determined by introducing the polymer piece (avr. 1 g) to reach equilibrium swelling in different solvents (dimethyl acetamide, dimethyl formamide, dH₂O, toluene, THF) with different solubility parameters. The solvent in which the polymer showed maximum swelling (THF) was used for determining the swelling coefficient.

Weighed polymer samples were allowed to swell in the solvent for 48 hours and the raise in weight was measured. The swelling coefficient is the ratio of volume of solvent in the swollen polymer to that of dry polymer and is defined by the equation:

$$\text{Swelling coefficient (Q)} = \frac{\text{Weight of the solvent in swollen polymer}}{\text{Weight of the swelled polymer}} \times \frac{\text{Density of the polymer}}{\text{Density of the solvent}} \quad (3.1)$$

The volume fraction of the polymer in the swollen polymer (V_r) was calculated from swelling coefficient. The solubility parameter of that solvent (δ_s), which relates maximum swelling, was accepted as the solubility parameter of the polymer (δ_p). The cross-link density (γ) of swollen polymers was determined by using modified Flory–Rehner's equation. The number average molecular weight between cross-links (M_c), which is correlative to crosslink density (γ) (mol/cm^3), was also calculated.

$$\text{Crosslink density, } \gamma = \frac{(V_r + \chi V_r^2 + \ln(1 - V_r))}{d_r V_o (V_r^{1/3} - V_r/2)} = \frac{1}{M_c} \quad (3.2)$$

Where

the volume fraction of the polymer in the swollen polymer, $V_r = \frac{1}{1+Q}$

V_o = Molar volume of the solvent (cm^3/mol), d_r = density of the polymer (g/cm^3)

χ , polymer-solvent interaction parameter is taken as 0.34 when ($\delta_s = \delta_p$).[51–53]

3.6. SCANNING ELECTRON MICROSCOPY (SEM) ANALYSIS

The scanning electron microscopy (SEM) analysis, was carried out on fracture surfaces of PPF/VPA and PPF/VPES samples using a Zeiss EVO 40 model instrument by applying 10 kV voltage under vacuum. Samples were fractured in liquid nitrogen. The fracture surfaces were coated with gold for 15 seconds (~5nm thickness) by using Baltec SCD 005 Sputter Coater before analysis [54].

3.7. DIFFERENTIAL SCANNING CALORIMETRY (DSC) AND THERMAL GRAVIMETRIC ANALYSIS (TGA)

Differential Scanning Calorimetry, or DSC, is a thermal analysis technique that observes how a material's heat capacity (C_p) is affected by temperature. A sample with a certain mass is heated or cooled and the changes in its heat capacity are followed via changes in the heat flow.

DSC is commonly used for analysing polymeric materials to arbitrate their thermal transitions. Melting points and glass transition temperatures for most polymers are accessible from standard compilations, cross-linking reaction temperature as well as the heat of cross-linking can be determined and the method also can indicate polymer degradation.

DSC analysis of the cured PPF/VPA and PPF/VPES samples was performed by using a SETARAM DSC 131 calorimeter and thermal analyzer. For each analysis, sample was scanned from 25°C to 250°C at 5°K/min heating rate under nitrogen atmosphere and heat flow (mW) versus sample temperature (°C) graph was plotted and analyzed. DSC analysis was performed to confirm the completion of the cure of the PPF copolymers and gain information about the thermal transitions of the prepared polymers.

Thermogravimetry (TG) is the section of thermal analysis which investigates the change in sample mass as a function of temperature in the scanning mode or as a function of time in the isothermal mode. Not all thermal incidents produce a change in the mass of the sample (for example melting, crystallization or glass transition), but there are some noteworthy special cases which cover desorption, absorption, sublimation, vaporization, oxidation, reduction and decomposition. TGA is used to identify the decomposition and thermal stability of materials under various circumstances and to investigate the kinetics of the physicochemical changes happening in the sample.

TGA analysis of the cured PPF/VPA and PPF/VPES samples was performed using a Pyris 1 TGA analyzer (PerkinElmer). For every analysis, a 5-7 mg sample was heated from 25°C to 800°C at 10°C/min heating rate under nitrogen gas atmosphere (20 mL/min).

According to the results, %weight and versus temperature (°C) graphs were plotted and analysed [52].

3.8. DETERMINATION OF EQUILIBRIUM WATER CONTENT AND DYNAMIC CONTACT ANGLE WITH WATER

Equilibrium water content (EWC) of the cured PPF/VPA and PPF/VPES polymer samples was determined gravimetrically and the values obtained were evaluated with regard to polymer composition. Each sample was first washed with dichloromethane and dried in open air for 24 hours, then kept in a vacuum oven at 40°C for 6 hours. At the end of the drying procedure, the weight of each sample was recorded as W_1 . Subsequently, samples were allowed to swell to equilibrium (appx. 36 hours) in 1X PBS buffer solution (pH=7.4). After samples were moved out of the PBS solution, they were dried with a paper towel and their weight was recorded as W_2 and equilibrium water content was calculated according to the following equation:

$$\text{EWC} = [(W_2 - W_1) / W_2] \times 100\% \quad (3.3)$$

Each composition was analyzed twice.

To perform dynamic contact angle measurements, a Hamilton syringe was used to obtain constant water droplet volume for each trial, and the measurement was performed using a KSV CAM 101 surface tension meter (optical contact angle measurement device). The first image was captured 30 seconds after the water droplet was released on the sample. Other images were taken with the interval of 10 seconds and a total of 15 images were taken. In analysis of the data, the contact angle value at 30th second was used to compare the hydrophilicity of the PPF copolymers. Two measurements were performed for each composition [52]

3.9. DYNAMIC MECHANICAL ANALYSIS (DMA)

Thermomechanical properties of the thermal cured PPF/VPA and PPF/VPES copolymers were determined via DMA using an AQ 800 Dynamic Mechanical Analyzer (TA Instruments LLC). Dynamic temperature ramp default tests were carried on polymers with dimensions of 12mm x 60mm, using a dual cantilever clamp at a frequency of 1Hz (single frequency mode) with a temperature ramp from -100 °C to 200 °C at a heating rate of 5°C/min. Two tests were performed for each sample. Storage modulus (E'), Loss modulus (E'') and tan delta values were plotted against temperature for each polymer sample and analyzed. The temperature at which the Loss modulus (and Tan delta) shows a maximum value was taken as the glass transition temperature (T_g) of the polymer.

3.10. MECHANICAL TESTING

For determining the compressive properties of the fully cured PPF/VPA and PPF/VPES copolymers, 6x15mm (length x diameter) cylindrical samples were prepared and faced to compressive load with a 1.0 mm/min crosshead speed by using 100 kN load cell using an INSTRON Universal Testing Machine. Five samples were tested for each composition. Compressive modulus was determined from the initial slope of the stress/strain plot and the compressive strength was recorded as the highest stress value reached on the stress/strain curve[52,55,56].

3.11. *IN VITRO* DEGRADATION

The analysis of biodegradation rate of the high temperature cured PPF/VPA and PPF/VPES polymer samples was carried out by both weight change and pH change measurements in PBS buffer solution (pH=7.4) at 37°C.

During the pH track experiment, all compositions of PPF/VPA and PPF/VPES samples were put into individual falcon tubes and 1X PBS buffer solution (pH=7.4) was introduced into each falcon tube. Each tube was put into a shaking water bath at 37°C and 75 rpm. In the first two days, the pH of the buffer was measured every 12 hours. After two days, pH

of the buffer was measured every 24 hours. After one week, the pH of the buffer was measured once a week throughout 84 days of incubation. After every pH measurement, the buffer solution inside the falcon tube was refreshed. The cumulative pH value of each sample was calculated and pH vs time graphs were plotted in order to simulate the behavior of samples inside the human body.

For the weight loss track experiment, all compositions of PPF/VPA and PPF/VPES samples were put into individual falcon tubes and 0.9 percent Na Azide containing 1X PBS buffer solution (pH=7.4) was introduced into each falcon tube. Each tube was put into a shaking water bath at 37°C and 75 rpm. After 1,2,3,4,5,6,7,14,21,28,35,42,56,70 and 84 days of incubation, solutions were removed, samples were lyophilized and weighed [57–60].

3.12. *IN VITRO* CELL INTERACTION STUDIES OF THERMALLY CURED PPF/VPA AND PPF/VPES POLYMERS

All chemicals, reagents and kits used for cell culture studies are listed in Table 3.5.

Table 3.5. Chemicals, reagents and kits used for cell culture studies

Chemical / Reagent / Kit	Company	Catalog Number
Dulbecco's phosphate buffered saline w/o calcium, w/o magnesium, 10X, sterile	SAFC Biosciences™	59331C-1000ML
TrypLE™ Express Dissociation Reagent 1X w/o phenol red sterile	Gibco® by life technologies™	12604-013 100mL
PenStrep Penicillin Streptomycin sterile	Gibco® by life technologies™	15140-122 100mL
Heat inactivated fetal bovine serum sterile, EU approved origin	Gibco® by life technologies™	10500-064
Dulbecco's modified eagle medium 1g/L D-glucose, with pyruvate, w/o L-glutamine w/o phenol red, sterile	Gibco® by life technologies™	11880-028
Primocin (100 µg/ml)	InvivoGen, USA	ant-pm-1
L-ascorbic acid 2-phosphate sesquimagnesium salt hydrate	SIGMA life science	A8960-5G
Silver nitrate solution 5%	Diagnostic BioSystems	33187
Sodium thiosulfate solution 5%	Diagnostic BioSystems	33187

Nuclear fast red solution	Diagnostic BioSystems	33187
β -glycerophosphate disodium salt hydrate BioUltra, suitable for cell culture	SIGMA life science	G9422-100g
Sodium azide, pure	AppliChem	A1430, 0500
CellTiter 96® AQueous One Solution Cell Proliferation Assay	Promega	G3581-5000 assays
Dexamethasone	SIGMA life science	D4902-1G
Ethanol CHROMASOLV®, absolute, for HPLC	Sigma-Aldrich	34870-2,5L
Dimethyl sulfoxide, cell culture reagent	ChemCruz™ Santa Cruz Biotechnology, INC.	#SC-358801
CellTiter 96® Aqueous One Solution Cell Proliferation Assay (MTS)	Promega, USA	G3581-5000 assays
Human Osteocalcin ELISA kit	Invitrogen™	#KAQ1381
TRACP & ALP Assay kit	TaKaRa	MK301

Human osteoblast cells (HOBs) (The European Collection of Cell Cultures, UK) (Cell line no. 406-05a) were seeded into cell culture plates by dissolving in no-phenol red Low Glucose DMEM which contains 10 percent Fetal Bovine Serum, 50 μ M ascorbic acid and 1 percent Pen-Strep, and were incubated at 37°C, 5 percent CO₂ and 90 percent humidity. Cell culture medium was replaced twice a week. When the cells reached confluency, they were passaged with no phenol red Gibco™ TrypLE Express (1X).

PPF based polymers with different formulations were sterilized before cell seeding by 1 hour long UV exposure to both sides (12 mm x 12 mm) and placed into well plates afterwards. Cells were seeded with concentration of 5x10³ cells/well and incubated through 28 days at the CO₂ incubator.

3.12.1. Cell Viability and Proliferation (MTS) Studies

CellTiter 96® Aqueous One Solution Cell Proliferation Assay (MTS; Promega, USA) was used to detect the cell concentration on the scaffolds. The procedure was carried out on days 1, 7, 14 and 21 after seeding the scaffolds with human osteoblast cells.

Scaffolds were rinsed with 1X, pH 7.40 PBS buffer and DMEM-low glucose without phenol red was mixed with MTS (5:1 v:v). Mixture (500 μ L) was added to each sample and

incubated for 3 hours. After incubation, 200 μ L solution from each well was transferred into a 96 wellplate. Absorbance was measured at 490 nm, using an Elisa Plate Reader (Bio-Tek, Elx800, USA). The alive cell amount in each scaffold was found by using the slope of the calibration curve plotted as absorbance vs cell number [59,61].

3.12.2. Scanning Electron Microscopy of Cell Seeded Polymers

After determined time intervals (7-14-21-28 days), cell culture media were aspirated, cell seeded scaffolds were rinsed with 0.1M, pH 7.40 cacodylate buffer, and fixed with 2.5 percent glutaraldehyde solution at room temperature for 1 hour. Samples were dried and coated with gold at 10 nm thickness before scanning electron microscopy.

3.12.3. Determination of Mineralization by Von Kossa Staining

Cell seeded scaffolds were prepared as indicated in section 3.12. This experiment was divided into two groups to compare the effect of osteogenic media on mineralization. Osteogenic differentiation (100 nm dexamethasone, 10 mM β -glycerophosphate, 50 μ g/mL ascorbic acid) media was added onto one group of samples, and normal low glucose DMEM is added (control group) onto other group of samples. All cell seeded samples were incubated in CO₂ incubators throughout 28 days.

After determined time intervals (7-14-21-28 days), cell culture media were aspirated, silver nitrate solution was introduced (Diagnostic biosystems calcium stain kit (modified von kossa)), and plates were incubated under UV light for 60 minutes. After incubation, wells were rinsed with dH₂O and sodium thiosulfate solution was added to stop the reaction. Plates were incubated for 3 minutes, subsequently. After incubation, wells were rinsed throughout tap water. Lastly, nuclear fast red solution was added and after 5 minutes incubation, they were rinsed quickly with absolute ethanol for three times. Following absolute ethanol wash, samples were dehydrated and become ready to observation.

3.12.4. Alkaline Phosphatase Assay (ALP)

Alkaline phosphatase is a ubiquitous, membrane-bound tetrameric enzyme linked to glycosyl-phosphatidylinositol moieties positioned on the outer cell surface. It has a notable duty in osteoid formation and mineralization [62].

Immunoassays act as most effective markers for bone formation. Briefly, alkaline phosphatase activity, mostly its quantification is automated, stand on the enzymatic hydrolysis of p-nitrophenyl phosphate, stays as the most frequently utilized marker of bone formation [63]. It is a functional option for detecting activity of osteoblasts [64].

After determined time intervals (7-14-21-28 days), cell culture media were aspirated, TaKaRa ALP activity test kit was applied to every sample regarding to kit instructions [59].

3.12.5. Osteocalcin Assay (OST)

Osteocalcin is a hydroxyapatite-binding protein uniquely synthesised by osteoblasts. One of the main properties of osteocalcin is vitamin-K dependent, gamma-carboxyglutamic acid (Gla) residues, that are accountable for the calcium binding characteristics. At its carboxy-terminus, osteocalcin can also synergize with other proteins, such as cell surface receptors. Such properties make osteocalcin an active molecule in the extracellular matrix organisation.

Osteocalcin is accepted as a specific marker of osteoblast activity. It is considered that, right after releasing from osteoblasts, the main portion of the freshly synthesised protein is get involved to the extracellular matrix of bone where it represents circa 15 percent of the non-collagenous protein. It is also slightly released into the flow where it can be determined by immunoassays [62].

After determined time intervals (7-14-21-28 days), cell culture media were aspirated, Invitrogen™ osteocalcin activity test kit was applied to every sample regarding to kit instructions [47,59–61].

4. RESULTS AND DISCUSSION

4.1. CHARACTERIZATION OF PPF BY FT-IR AND $^1\text{H-NMR}$ SPECTROSCOPY AND MOLECULAR WEIGHT ANALYSIS VIA GPC

The FT-IR spectrum of the synthesized PPF pre-polymer presented in Figure 4.1. shows the characteristic peaks associated with the PPF structure; the alcohol O-H stretching peak at 3444 cm^{-1} , alkyl C-H stretching peak at 3080 cm^{-1} , α unsaturated ester carbonyl (C=O) stretching peak at 1732 cm^{-1} , C=C stretching peak at 1645 cm^{-1} and carboxylic acid C-O stretching peak at 1360 cm^{-1} .

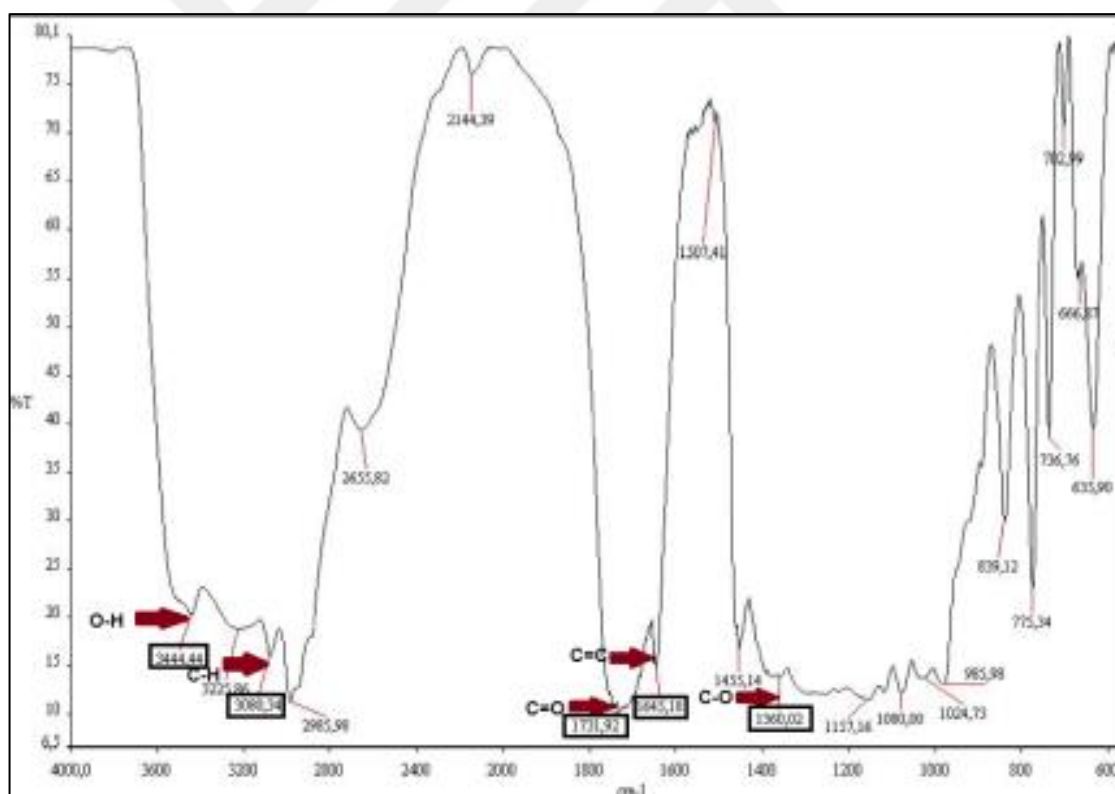


Figure 4.1. FT-IR spectrum of the synthesized PPF pre-polymer

The $^1\text{H-NMR}$ spectrum of the PPF pre-polymer and the different type of protons on PPF structure assigned to different peaks in this spectrum are shown in Figure 4.2. The structure of the PPF pre-polymer was confirmed via the characteristic peaks associated with the

CH=CH, CH₂, CH and CH₃ protons of the PPF backbone. Thus, the sharp peak at 1.2 ppm stands for the methyl (CH₃) protons, the multiple peaks in the 4.0-4.4 ppm region stand for the CH protons and the peak at around 5.15 ppm stands for the methylene (CH₂) protons of the propylene glycol unit whereas the sharp peak at around 6.7 ppm stands for the CH=CH protons of the fumarate unit (The minor multiplet peaks observed in the 2.5-4.0 ppm region may be assigned to the protons of the solvent residue such as diethyl ether used in the purification of the PPF pre-polymer.).

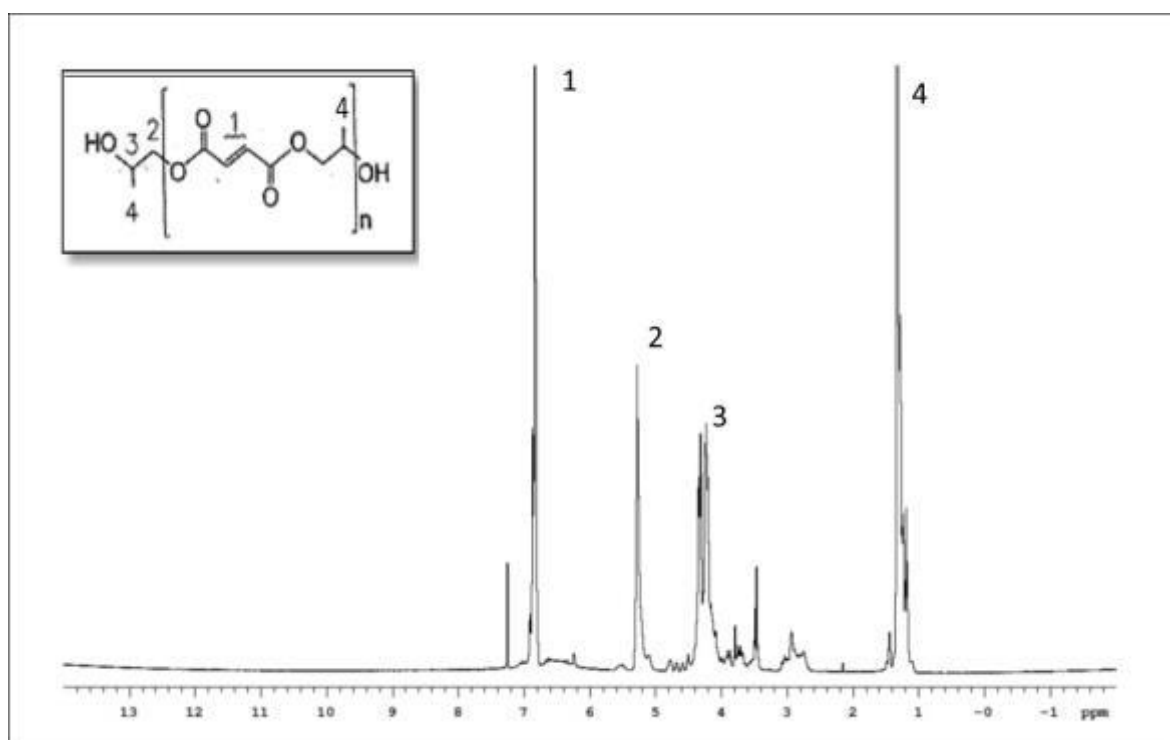


Figure 4.2. ¹H-NMR spectrum of the synthesized PPF pre-polymer

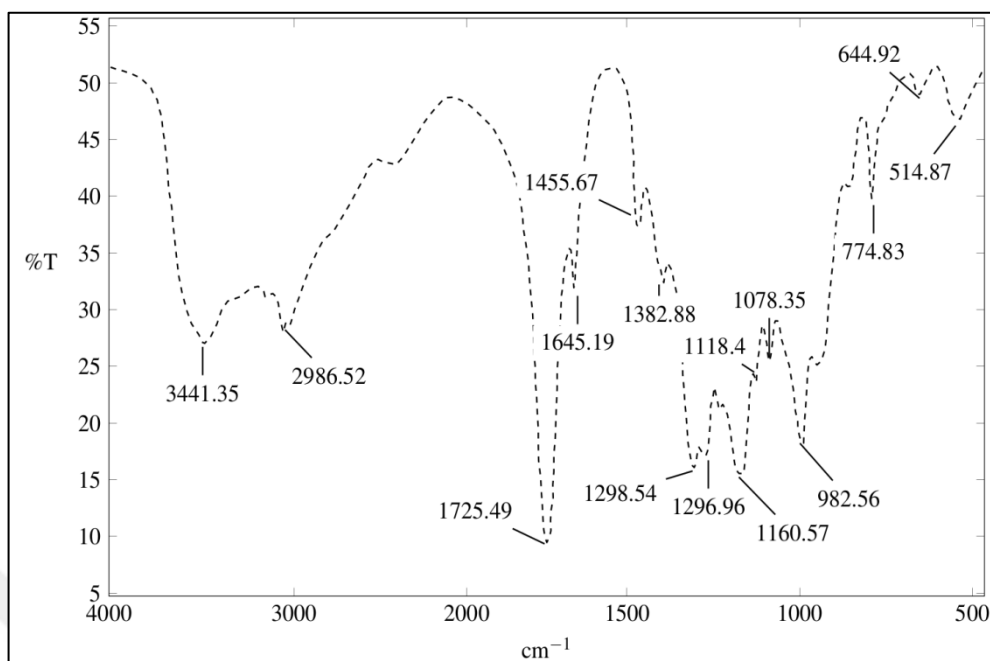
The number average molecular weight (M_n) and weight-average molecular weight (M_w) of the synthesized PPF pre-polymer were determined via GPC as 1653 g/mole, and 2880 g/mole respectively and the polydispersity index (PDI) was 1,74.

4.2. FT-IR ANALYSIS OF THE CURED PPF/VPA AND PPF/VPES POLYMERS

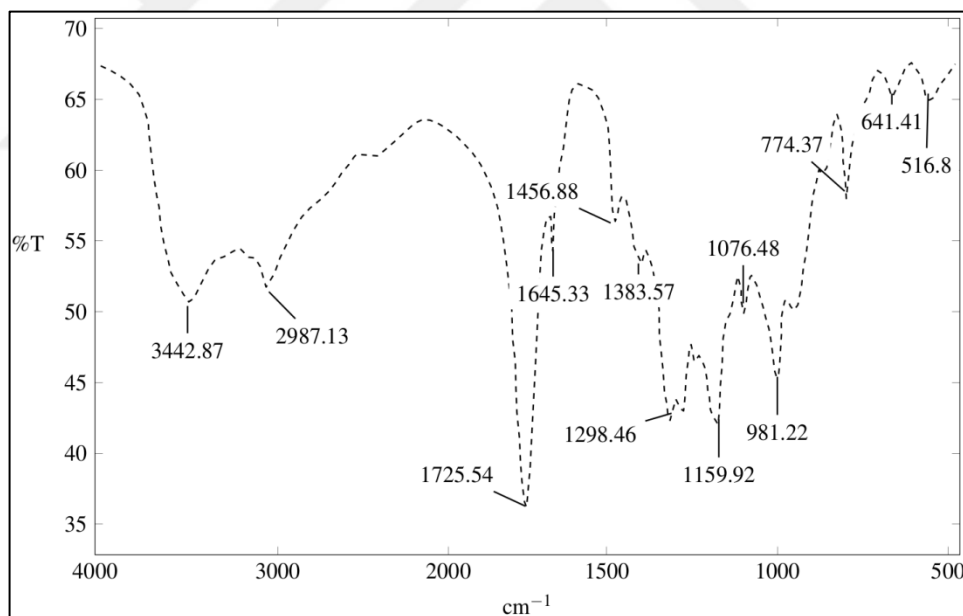
After the cure of the PPF polymer with VPA and VPES comonomers, they were characterized via FT-IR spectroscopy. In addition, the conversion of the polymerization cure reaction was analyzed qualitatively. The change in the absorption due to C=C stretching vibration (of the fumarate moiety) gave information about the conversion of the polymerization reaction.

4.2.1. PPF/VPA Products

The FT-IR spectra of the PPF/VPA (70/30) samples cured with 2 and 3 weight percent of initiator, are shown in Figure 4.3.(a) and (b) respectively. The characteristic peak of C=C stretching vibration of the fumarate moiety at 1645 cm^{-1} lost intensity for both of the PPF/VPA samples as compared to that of the PPF spectrum shown in Figure 4.1. But for the sample cured with 3wt% initiator this peak was more consumed indicating a higher conversion than the sample cured with 2wt% initiator. The presence of the 1645 cm^{-1} peak after the curing procedure shows that the conversion of the polymerization reaction was incomplete. The absence of the 1615 cm^{-1} peak characteristic of the VPA C=C stretching vibration may indicate the complete conversion of VPA or that no unreacted VPA was trapped in the PPF network. But since VPA content was only 30 weight percent of the total composition it is rather hard to observe the complete consumption of this weak peak. On the other hand, bands between 947 and 1069 cm^{-1} that correspond to the symmetric and asymmetric P-O(H) bands of phosphonic acid of VPA units and a peak at 1183 cm^{-1} that corresponds to P- O stretching of the phosphonic acid were observed as weak peaks in these spectra. The peaks corresponding to the POH bending and O-P-O asymmetric stretching vibrations of the phosphonic units were observed at around 2320 - 2325 cm^{-1} in these spectra. (Figure 4.3.(a) and (b))



(a)

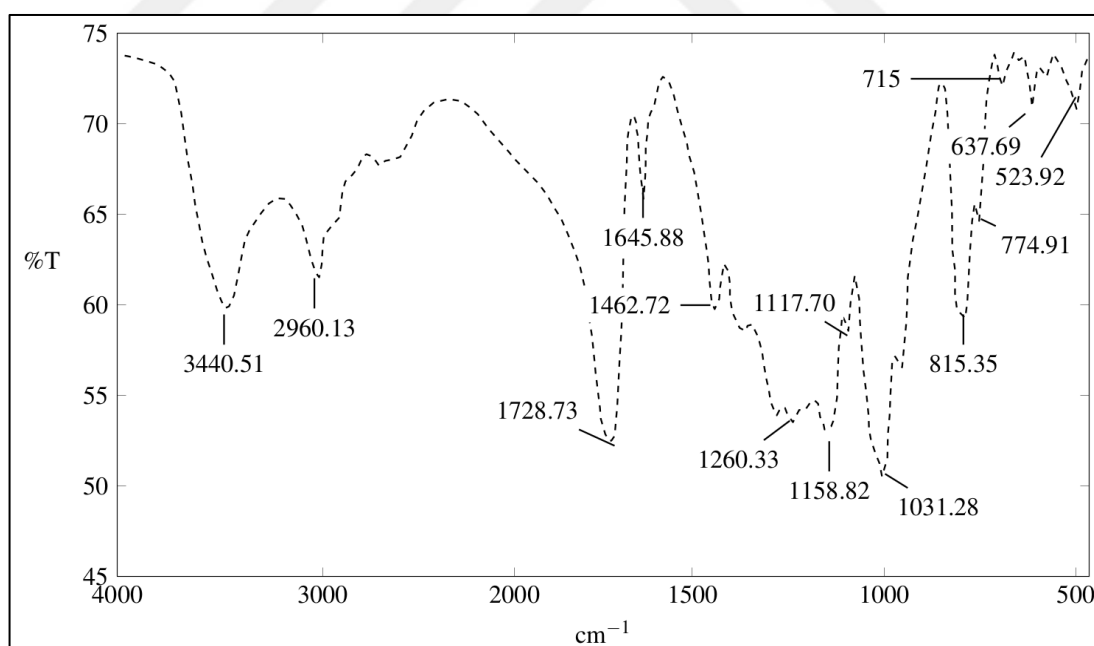


(b)

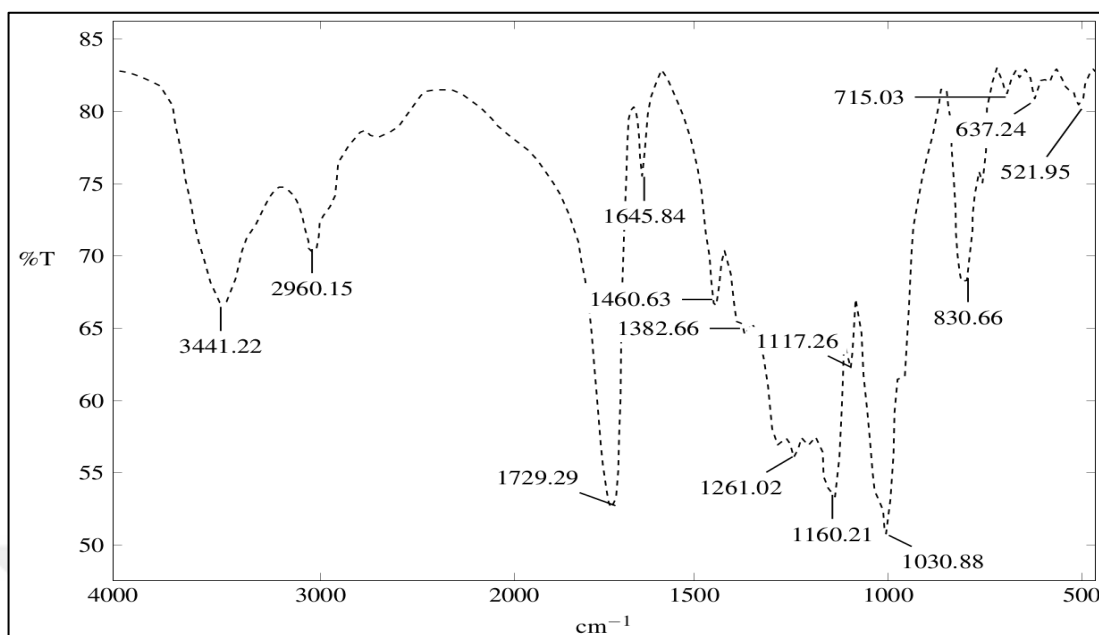
Figure 4.3. The FT-IR spectrum of the PPF/VPA (70/30) product cured with (a) 2 and (b) 3 weight percent initiator

4.2.2. PPF/VPES Products

The FT-IR spectra of the PPF/VPES (70/30) polymers cured with 2 and 3 weight percent of initiator are shown in Figure 4.4.(a) and (b) respectively. The presence of the 1034 and 1260 cm^{-1} characteristic peak of the VPES indicates that the VPES monomer was successfully incorporated into the PPF matrix structure. Here again, the characteristic peak of C=C stretching vibration of the fumarate moiety at 1645 cm^{-1} lost intensity for both of the PPF/VPES samples as compared to that of the PPF spectrum (Figure 4.1). The PPF/VPES sample cured with 3 weight percent of initiator exhibited a decreased intensity of this peak as compared to the sample cured with 2 weight percent of initiator, indicating a higher conversion of polymerization at the higher initiator concentration. Also, the 1615 cm^{-1} peak characteristic of the VPES C=C stretching vibration was absent which may indicate a conversion near to completion for the VPES units.



(a)



(b)

Figure 4.4. The FT-IR spectrum of the PPF/VPES (70/30) product cured with (a) 2 and (b) 3 weight percent initiator

4.3. CROSS-LINK DENSITY ANALYSIS OF THERMAL CURED PPF/VPA AND PPF/VPES POLYMERS

Crosslink density (mol/cm^3) and M_c (g) values are presented in bar graphs for PPF/VPA and PPF/VPES polymers for different compositions in Figure 4.5. (a) and (b), and all data are tabulated in Table.4.1. Crosslink density values of PPF copolymers varied between $1.80 \times 10^{-2} \text{ mol}/\text{cm}^3$ (PPF/VPA (60/40) – 3% BP) and $5.39 \times 10^{-3} \text{ mol}/\text{cm}^3$ (PPF/VPES (60/40) – 3% BP) and with same order, M_c values vary between 55.5 g (PPF/VPA (60/40) – 3% BP) and 185.5 g (PPF/VPES (60/40) – 3% BP).

For PPF/VPES copolymers with both BP amounts, PPF/VPES (70/30) showed the highest crosslink density values. PPF/VPES (70/30) were better cured than PPF/VPES (80/20) samples. While PPF polymer is a highly viscous resin at room temperature, VPES comonomer is liquid, thus with increasing VPES amounts, viscosity decreases in comparison to PPF and this situation results in increased effectiveness of cure procedure with ease of mixing. On the other hand, when VPES concentration increased from 30

percent to 40 percent, crosslink density started to decrease. This result demonstrated that reducing viscosity by increasing VPES concentration above 30 percent had no effect on crosslink density and increasing VPES amount which means decreasing PPF concentration also decreased crosslink density. Hence, 30 percent VPES was the ideal concentration in terms of crosslink density.

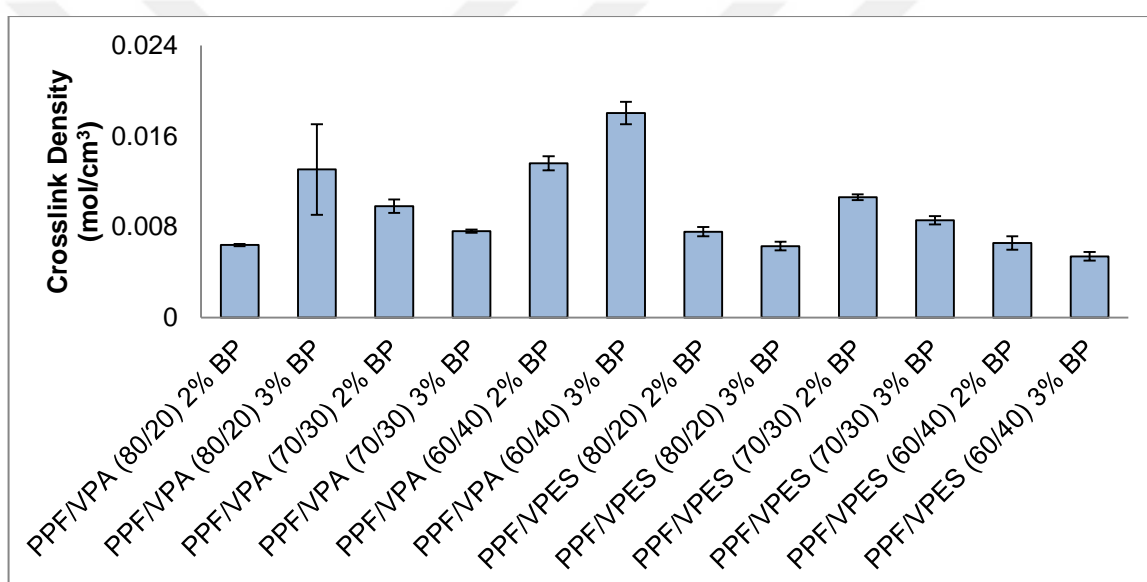
Considering initiator amounts of PPF/VPES copolymers, samples cured with 2 percent BP demonstrated higher crosslink density values compared to samples cured with 3 percent BP. Number average molecular weight between cross-links (M_c) (reciprocal of crosslink density) was inversely proportional to crosslink density values as expected.

For PPF/VPA copolymers, crosslink density generally increases with increasing VPA comonomer amount. In a study in which PPF was cured with NVP, it was reported that crosslink density increased with increasing NVP amount [48]. This condition is not related to decreasing viscosity in PPF mixtures as VPA possess higher viscosity than VPES, but can be explained with condensation of VPA via water loss from hydroxyls at high temperatures like 100°C and above and contribution to crosslinked structure. Condensation of VPA from phosphonic acid groups at high temperatures of 100°C and above was also reported in other studies [57]. Except 70/30 composition, 3 percent initiator amount resulted in higher crosslink density than 2 percent initiator amount, thereby much effective cure.

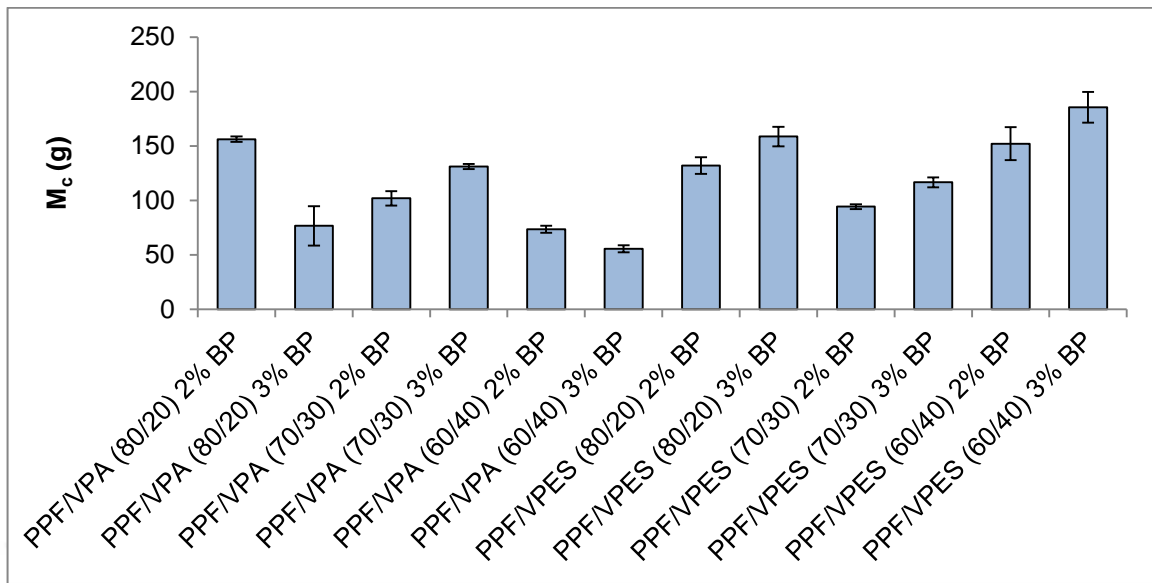
PPF/VPES (70/30) polymers with both initiator concentrations demonstrated higher crosslink densities compared to PPF/VPA (70/30) polymers, controversially for other compositions, PPF/VPA polymers resulted in higher crosslink densities. As the VPES comonomer is more reactive in the radical polymerization than the VPA comonomer, crosslink densities of VPES copolymers were expected to be higher, but the possible condensation reaction of VPA comonomer hydroxyls at the high temperature cure, increased the cross-link density of VPA copolymers.

Illustrated crosslink density values of PPF/VPA and PPF/VPES polymers are close to other PPF systems reported in literature. In a study of Jayabalan et. al., in which biodegradation and crosslink density analysis were performed with PPF/NVP copolymers, the cross-link density and number average molecular weight between cross-links (M_c) for the composition containing 36.4 percent by weight of NVP were determined as 22.69×10^{-3}

mol/cm³ and 44.08g respectively. The cross-link density and M_c values for the composition containing 45.3 percent NVP were found to be 24.64×10^{-3} mol/cm³ and 40.59g, respectively. Crosslink densities of PPF formulations which contain 30%-40% VPA and/or VPES were found to be slightly lower in this study than reported values. In another study in which PPF pre-polymer was cured with PPF diacrylate macromer (PPF-DA) (PPF/PPF-DA double bond ratio 0.5), cross-link density was reported to be 3.60×10^{-3} mol/cm³ and M_c value was 457g [53]. All compositions of PPF/VPA and PPF/VPES copolymers demonstrated higher crosslink density values than PPF/PPF-DA copolymers.



(a)



(b)

Figure 4.5. Bar graphs of (a) crosslink density and (b) number average molecular weight between cross-links (M_c) values of thermally cured PPF/VPA and PPF/VPES polymers

Table 4.1. Crosslink density and number average molecular weight between cross-links (M_c) values of thermally cured PPF/VPA and PPF/VPES polymers

Polymer	Cross-Link Density (mol/cm^3)	M_c (g)
PPF/VPA (80/20) 2% BP	$6.40 \times 10^{-3} \pm 1.0 \times 10^{-4}$	156.2 ± 2.5
PPF/VPA (80/20) 3% BP	$1.31 \times 10^{-2} \pm 4.0 \times 10^{-3}$	76.6 ± 18.1
PPF/VPA (70/30) 2% BP	$9.82 \times 10^{-3} \pm 5.9 \times 10^{-4}$	101.9 ± 6.5
PPF/VPA (70/30) 3% BP	$7.63 \times 10^{-3} \pm 1.4 \times 10^{-4}$	131.1 ± 2.4
PPF/VPA (60/40) 2% BP	$1.36 \times 10^{-2} \pm 6.2 \times 10^{-4}$	73.5 ± 3.2
PPF/VPA (60/40) 3% BP	$1.80 \times 10^{-2} \pm 9.9 \times 10^{-4}$	55.5 ± 3.2
PPF/VPES (80/20) 2% BP	$7.57 \times 10^{-3} \pm 4.2 \times 10^{-4}$	132.0 ± 7.7
PPF/VPES (80/20) 3% BP	$6.30 \times 10^{-3} \pm 3.8 \times 10^{-4}$	158.7 ± 8.9
PPF/VPES (70/30) 2% BP	$1.06 \times 10^{-2} \pm 2.6 \times 10^{-4}$	94.3 ± 2.2
PPF/VPES (70/30) 3% BP	$8.58 \times 10^{-3} \pm 3.6 \times 10^{-4}$	116.6 ± 4.7
PPF/VPES (60/40) 2% BP	$6.57 \times 10^{-3} \pm 6.0 \times 10^{-4}$	152.1 ± 15.2
PPF/VPES (60/40) 3% BP	$5.39 \times 10^{-3} \pm 3.8 \times 10^{-4}$	185.5 ± 14.1

4.4. SCANNING ELECTRON MICROSCOPY (SEM) ANALYSIS

SEM analysis was performed on fracture surfaces of thermal cured PPF/VPA and PPF/VPES samples. Fracture surfaces were analyzed for porosity.

4.4.1. Scanning Electron Microscopy Analysis of Thermal Cured Polymers

When fracture surface images of PPF/VPA materials were analyzed, micro and macro sized porous structure was observed. However, no porosity was observed on SEM images of fracture surfaces of PPF/VPES polymer samples. In Figure 4.6. and 4.7., fracture surface images of PPF/VPA (70/30) polymers are presented for samples cured with 2 and 3 percent BP, respectively. When the mentioned figures are examined, pore sizes of the PPF/VPA samples are measured to be between 2-10 micrometers. Also, the presence of porous structures inside another porous structure is observed. In addition, fracture surface images of thermally cured PPF/VPA (60/40) cured with 2 percent BP is presented in Figure 4.8. (a) and (b). Figure 4.8. (a) indicated that these materials exhibited macroporous structure and figure 4.8. (b) shows that these materials exhibit inter porous structure in the micro scale just like PPF/VPA (70/30) polymers. On the other hand, when SEM images of thermally cured PPF/VPA (80/20) samples for both initiator contents were examined (Fig 4.9.), smaller sized pores were observed when compared to the other PPF/VPA formulations. In addition, the fracture surface images of these materials show that the pores were not damaged. Also, the pores in these samples were located separately from each other.

In Figure 4.10., fracture surface images of thermally cured PPF/VPES (70/30) polymers cured with both initiator contents are presented. As it can be noticed from the figure, SEM images of this material support the non-porous structure of PPF/VPES materials. This situation is also valid for the other PPF/VPES formulations.

The main cause of the porosity of PPF/VPA samples may be explained by the evaporation of the small amount of water inside the VPA comonomer (10 weight percent) during thermal cure cycle. As VPES monomer does not contain this amount of water, such porosity due to water evaporation is not observed.

Variations in density and structure of pores due to VPA content in PPF/VPA samples can be observed from Figure 4.6. to 4.9. These differences in pore structure of PPF/VPA polymers affect the mechanical properties, biodegradation rate, cell attachment and growth rate.

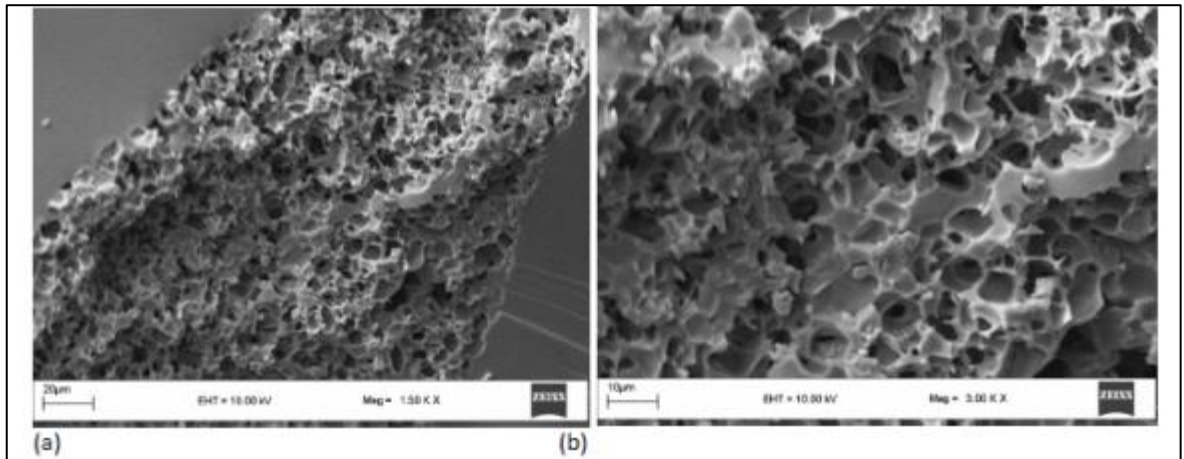


Figure 4.6. Scanning electron micrographs of PPF/VPA (70/30) sample cured with 2 weight percent BP at (a) 1500x and (b) 3000x magnification

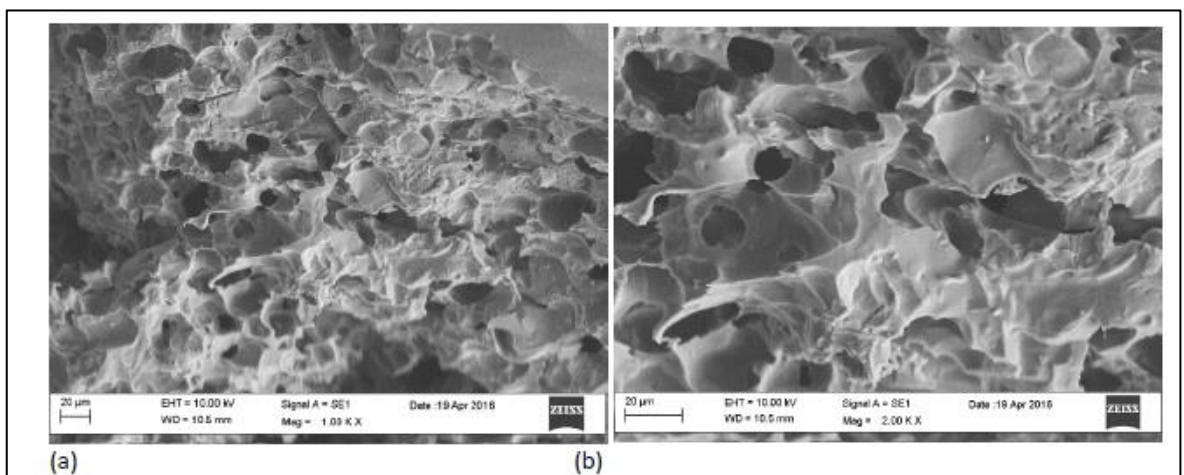


Figure 4.7. Scanning electron micrographs of PPF/VPA (70/30) sample cured with 3 percent BP at (a) 1000x and (b) 2000x magnification

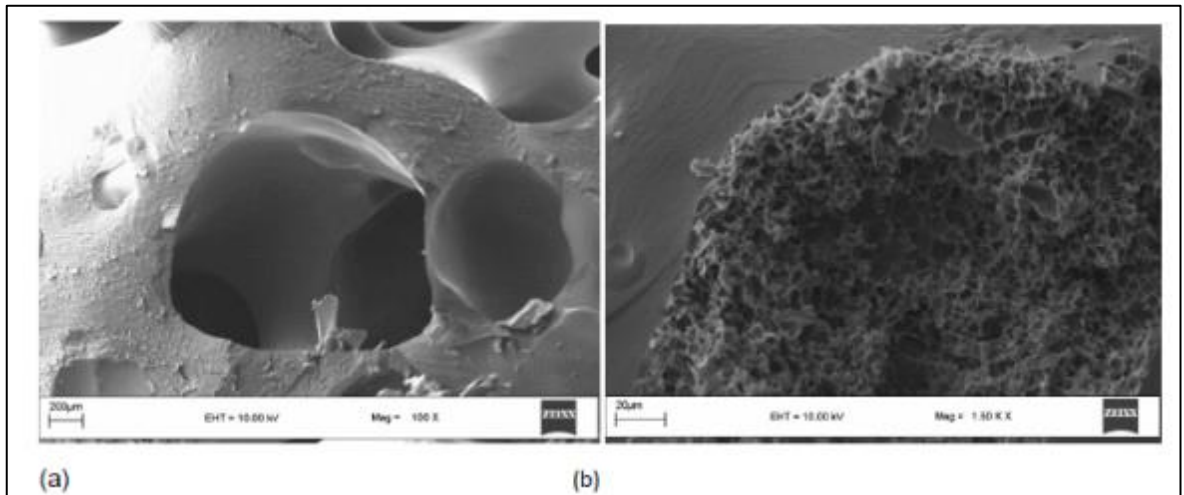


Figure 4.8. Scanning electron micrographs of PPF/VPA (60/40) sample cured with 2 percent BP at (a) 100x and (b) 1500x magnification

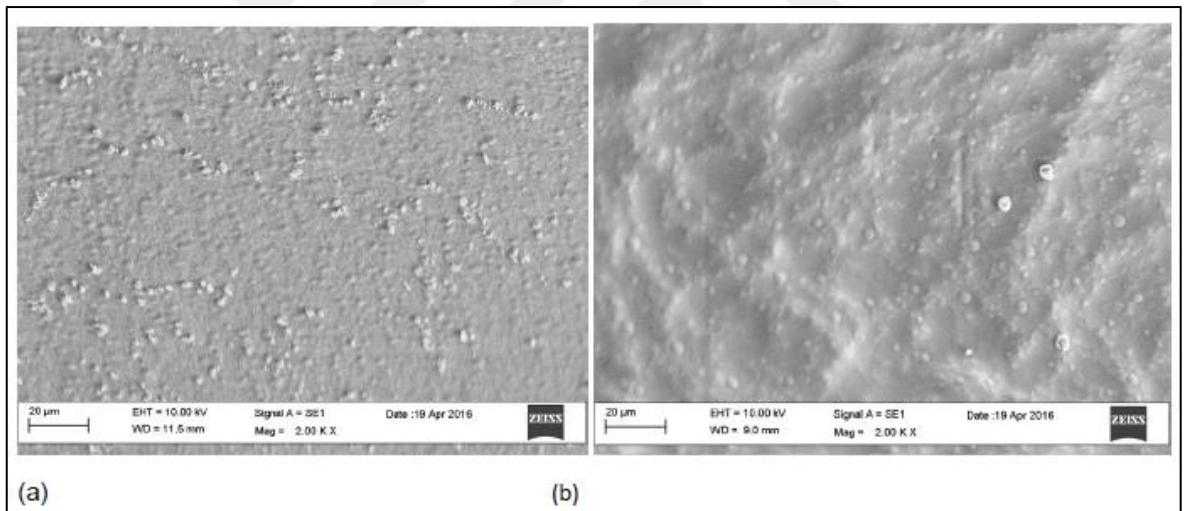


Figure 4.9. Scanning electron micrographs of PPF/VPA (80/20) sample cured with (a) 2 and (b) 3 weight percent BP at 2000x magnification

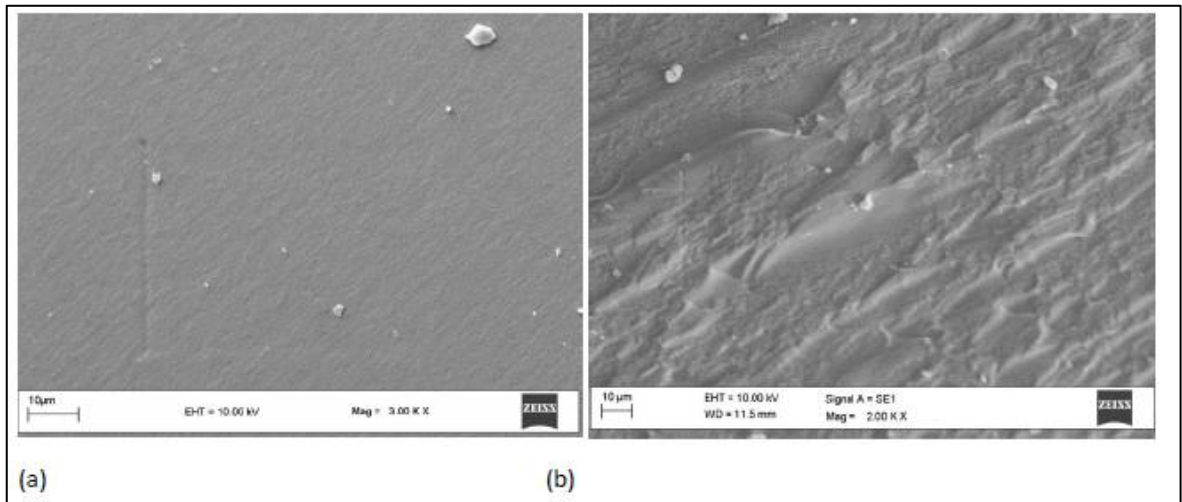
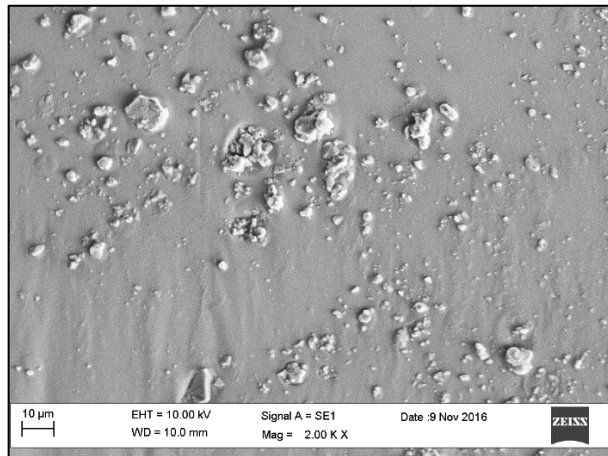


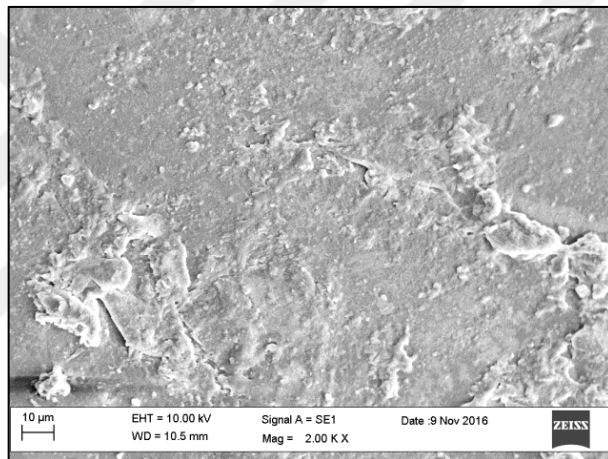
Figure 4.10. Scanning electron micrographs of PPF/VPES (70/30) sample cured with (a) 2 weight percent and (b) 3 weight percent BP at 3000x and 2000x magnification

4.4.2. Scanning Electron Microscopy Analysis of UV Cured Polymers

In Figure 4.11. (a) and (b), fracture surface images of PPF/VPA (70/30) polymers are presented for samples UV cured with 2 and 3 weight percent BAPO, respectively. Analyses of these images show that porous structure which was formed during thermal cure of PPF/VPA copolymers couldn't be obtained during UV cure. Since the water in VPA could not evaporate at room temperature and relatedly pores were not formed, it is an expected result. Fracture surface images of PPF/VPES (70/30) polymers are presented for samples cured with 2 and 3 percent BAPO in Figure 4.12. (a) and (b) respectively. When the mentioned figures are examined, similar to thermal cured PPF/VPES polymers, non-porous structures can be observed.

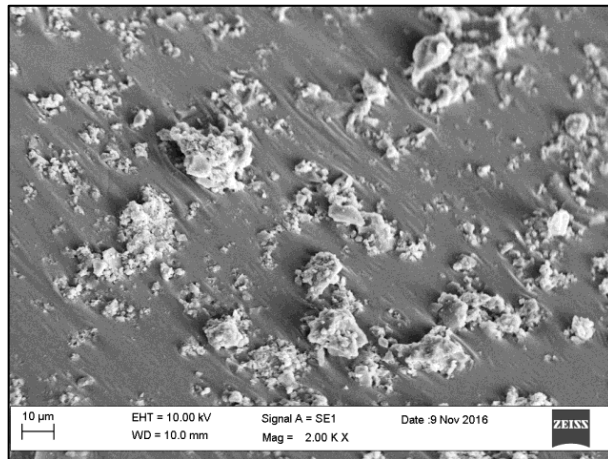


(a)

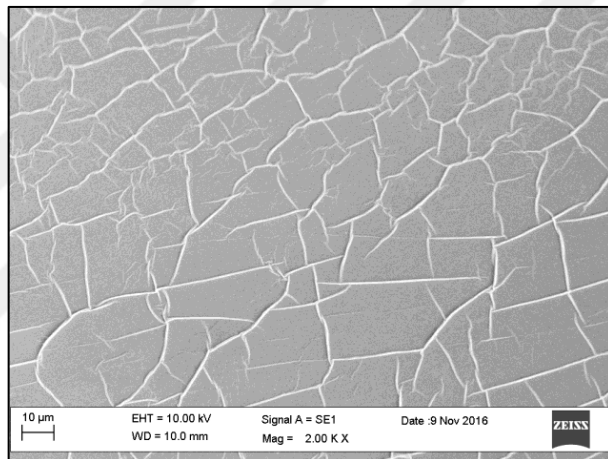


(b)

Figure 4.11. Scanning electron micrographs of UV cured PPF/VPA (70/30) samples containing (a) 2 percent BAPO and (b) 3 percent BAPO at 2000X magnification



(a)



(b)

Figure 4.12. Scanning electron micrographs of UV cured PPF/VPES (70/30) samples containing (a) 2 percent BAPO and (b) 3 percent BAPO at 2000X magnification

4.5. DIFFERENTIAL SCANNING CALORIMETRY (DSC) AND THERMAL GRAVIMETRIC ANALYSIS (TGA)

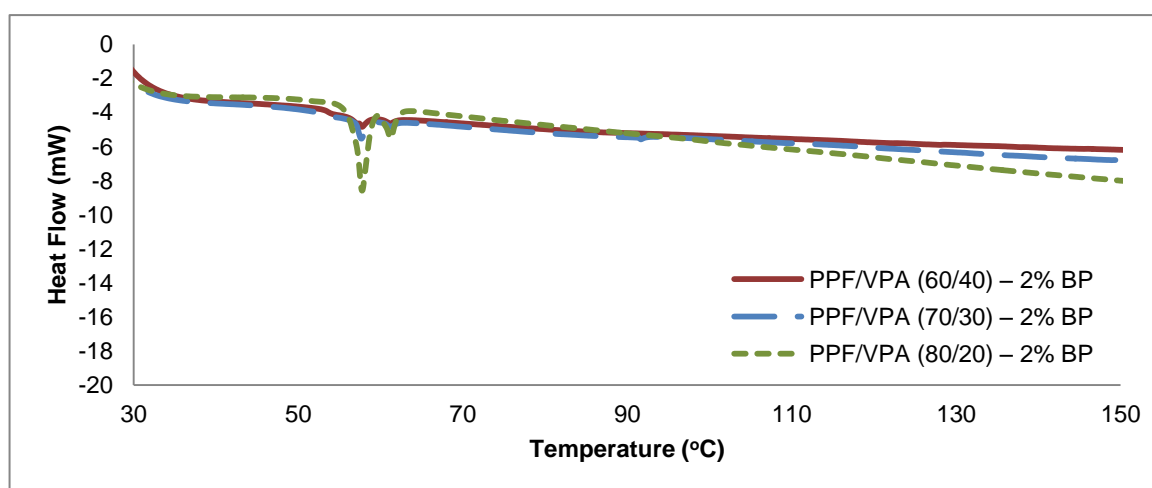
DSC analyses were carried out to get preliminary data about T_g values of samples and to see whether the cure reactions were completed or not.

4.5.1. DSC Analysis of Thermal Cured Polymers

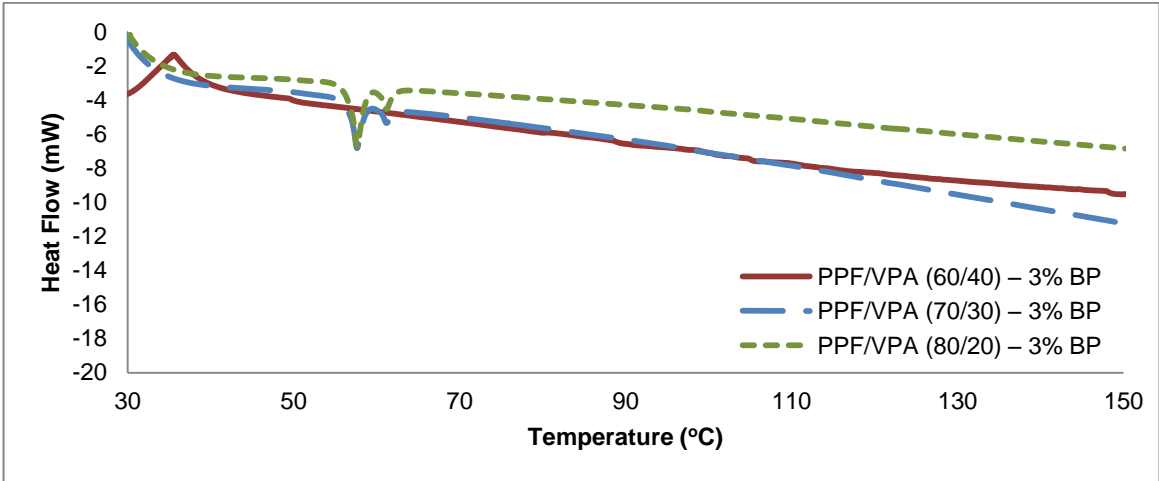
4.5.1.1. Effect of Change in Comonomer Content

Figure 4.13. shows the DSC plots of PPF/VPA samples cured with (a) 2 and (b) 3 weight percent initiator and Figure 4.14. shows the DSC plots of PPF/VPES samples cured with (a) 2 and (b) 3 weight percent initiator (BP).

The fact that none of the plots exhibit an exothermic peak in the 90 °C region indicates that the cure of the PPF/VPES and PPF/VPA polymers was complete. Each sample seem to exhibit two endothermic peaks at around 58°C and 61 °C. Although these endothermic peaks can be assigned to T_g 's of these polymers, the positions of these peaks are not effected by changing comonomer content and initiator content significantly. DSC analysis is not an appropriate method to analyze the effect of structural changes on the T_g of highly cross-linked polymers such as PPF/VPA and PPF/VPES copolymers and does not give meaningful results for the effect of cross-link density on T_g . Thus the T_g of the PPF copolymers were mainly analyzed via DMA.

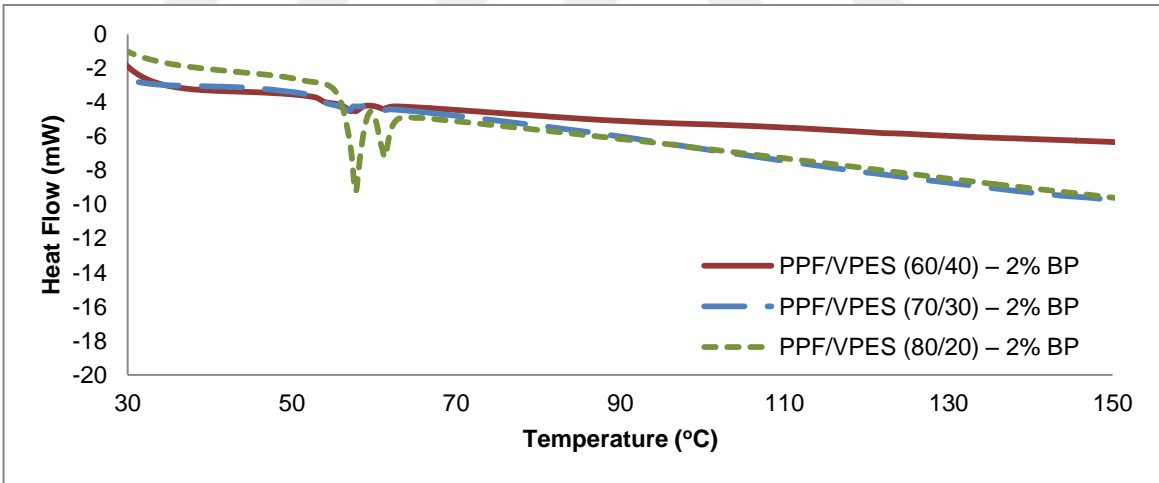


(a)



(b)

Figure 4.13. DSC plots of PPF/VPA samples cured with (a) 2 and (b) 3 weight percent initiator



(a)

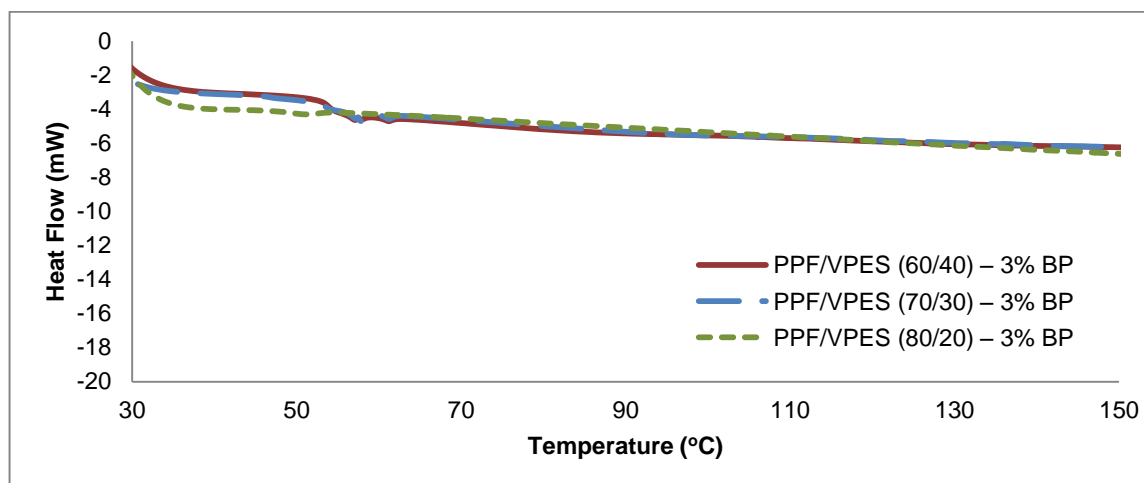


Figure 4.14. DSC plots of PPF/VPES samples cured with (a) 2 and (b) 3 weight percent initiator

4.5.1.2. Effect of Comonomer

Figure 4.15. shows the DSC plots of PPF/VPA and PPF/VPES (70/30) samples cured with 2 and 3 weight percent initiator. No exothermic peak was observed for the samples in the 90°C temperature region showing that the cure reaction was complete. The heat flow plots indicate a step change at 52 °C for the PPF/VPA (70/30) sample cured with 2 weight percent initiator, no such step change was observed for the PPF/VPA (70/30) sample cured with 3 weight percent initiator. The PPF/VPES (70/30) samples cured with 2 and 3 weight percent initiator exhibited a step change at around 52 °C and 53 °C respectively. If we consider these peaks as the T_g 's of the PPF polymers, it can be seen that the T_g was not affected by the comonomer identity at 2 weight percent initiator content and the increase of initiator content from 2 to 3 weight percent raised the T_g only by 1 °C for the PPF/VPES polymers. Thus, as mentioned earlier DSC analysis is not an appropriate method for analyzing the T_g 's of the highly cross-linked PPF/VPES and PPF/VPA polymers. The T_g 's of these polymers will be analyzed via DMA in the following sections.

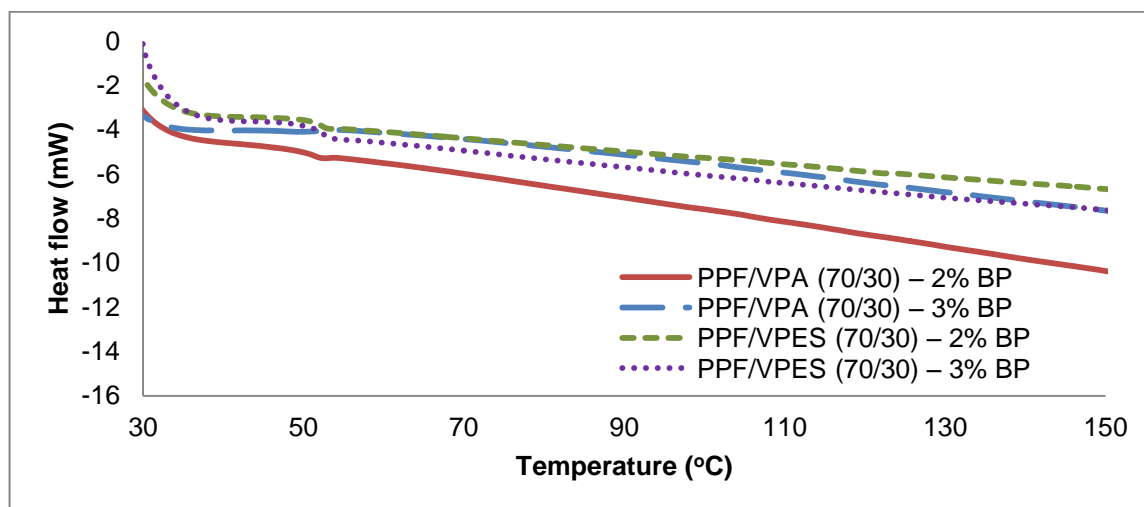
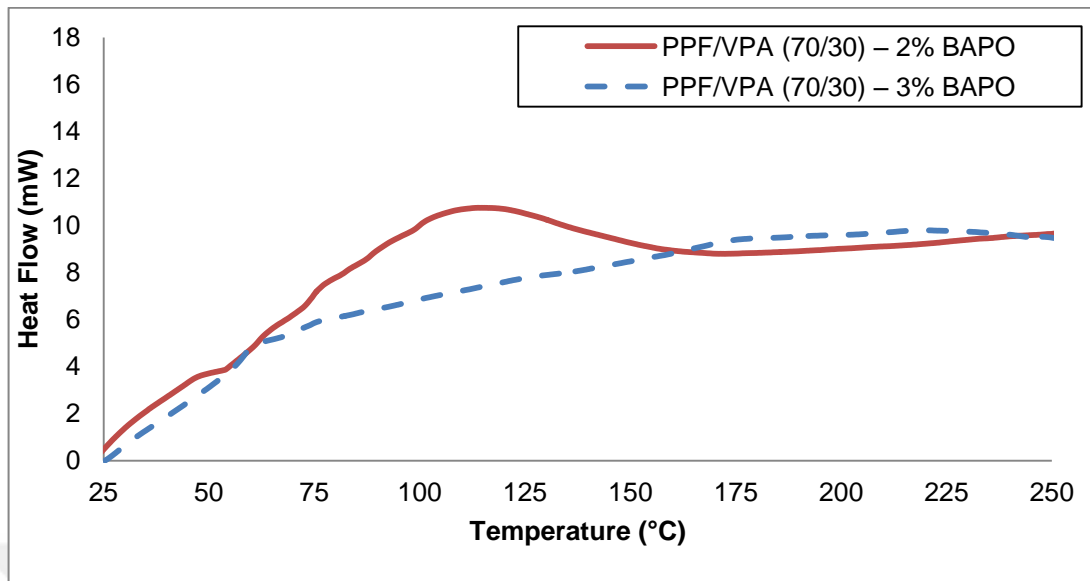


Figure 4.15. DSC plots of PPF/VPA and PPF/VPES (70/30) polymers cured with 2 and 3 weight percent initiator

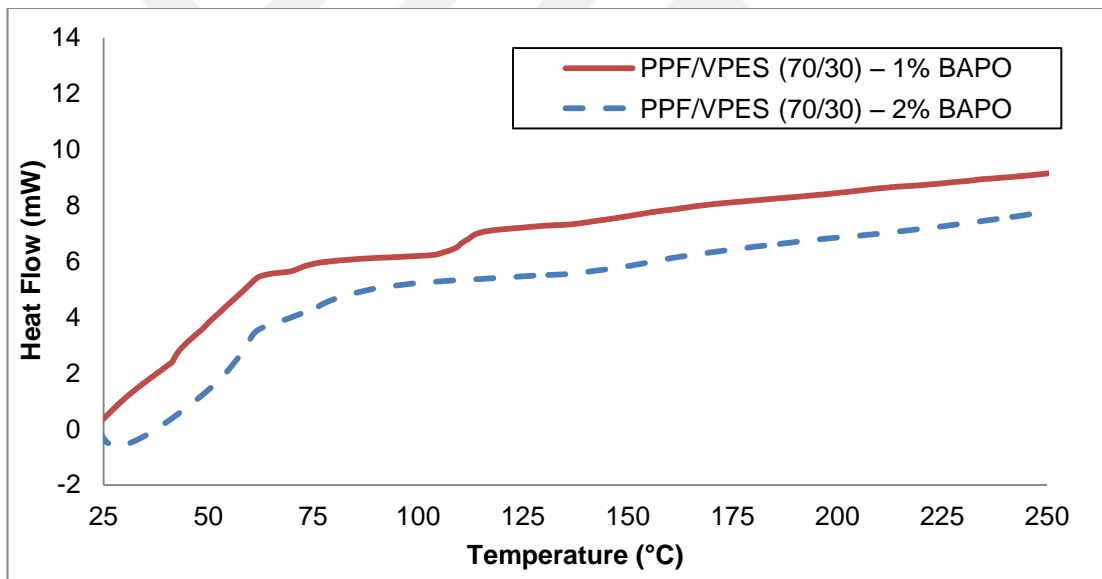
4.5.2. DSC Analysis of UV Cured Polymers

Figure 4.16. shows the DSC plots of UV cured PPF/VPA and PPF/VPES (70/30) samples. An exothermic peak was observed for the 2 percent BAPO containing PPF/VPA sample in the 110°C temperature region showing that the cure reaction was not complete, on the contrary the peak was not observed for the 3 percent BAPO containing PPF/VPA sample. This finding indicates that curing was complete for 3 percent BAPO containing PPF/VPA sample, however, 2 percent BAPO containing PPF/VPA sample needed a post-cure.

Observation of no major exothermic peaks on the DSC thermograms of UV cured PPF/VPES polymers indicates that both samples were completely cured for both initiator amounts.



(a)



(b)

Figure 4.16. DSC thermograms of UV cured (a) PPF/VPA and (b) PPF/VPES samples

4.5.3. Thermogravimetric Analysis of Thermal Cured PPF/VPA and PPF/VPES Polymers

The thermal degradation profiles of the PPF/VPA and PPF/VPES copolymers were analyzed via TGA.

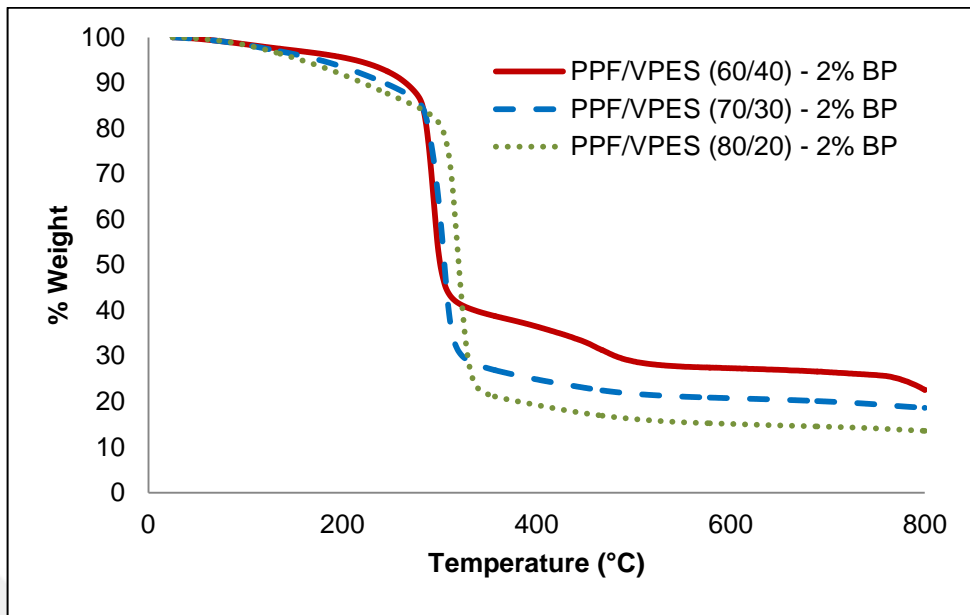
4.5.3.1. Effect of Change in Comonomer Content

Figure 4.17. shows the weight percentage vs temperature plots of PPF/VPES polymers cured with (a) 2 and (b) 3 percent initiator and Figure 4.18. shows the weight percentage vs temperature plots of PPF/VPA polymers cured with (a) 2 and (b) 3 percent initiator, respectively.

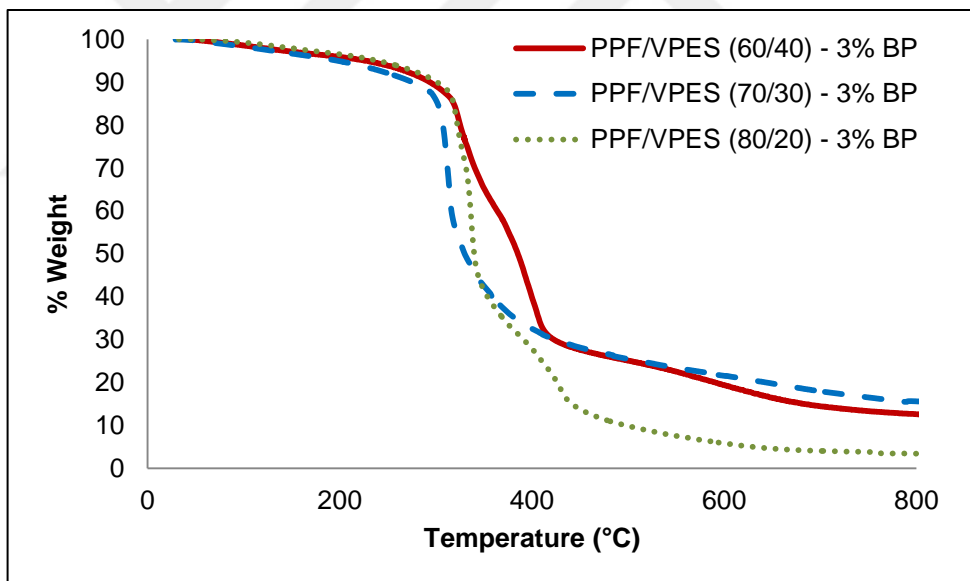
One-step thermal decomposition was observed from percentage weight-versus temperature graphs of PPF/VPES copolymers. Major decomposition started at 300°C for 2 percent BP containing PPF/VPES samples, and increase in weight loss was observed with increasing PPF amount. Major decomposition started at 350°C for 3 percent BP containing PPF/VPES samples, and similarly, increase in weight loss was observed with increasing PPF amount at above 500 °C.

Likewise, major decomposition started at 300°C for 2 percent BP containing PPF/VPA samples. Although PPF/VPA (60/40) polymer showed higher decomposition at the beginning, remaining char mass decreased as 80/20>70/30>60/40 at 700-800 °C. Char yield is expected to be proportional to crosslink density of the material.

Again, major decomposition started at 300°C for 2 percent BP containing PPF/VPA samples. PPF/VPA (60/40) polymer showed higher decomposition at the beginning, but no major difference was observed in terms of char yield at 700-800 °C. Besides, a two-step decomposition occurred for PPF/VPA (60/40) composition. The first step degradation can be attributed to the degradation of poly (vinyl phosphonic acid) which is believed to occur as a side product during the cure of PPF pre-polymer with VPA.

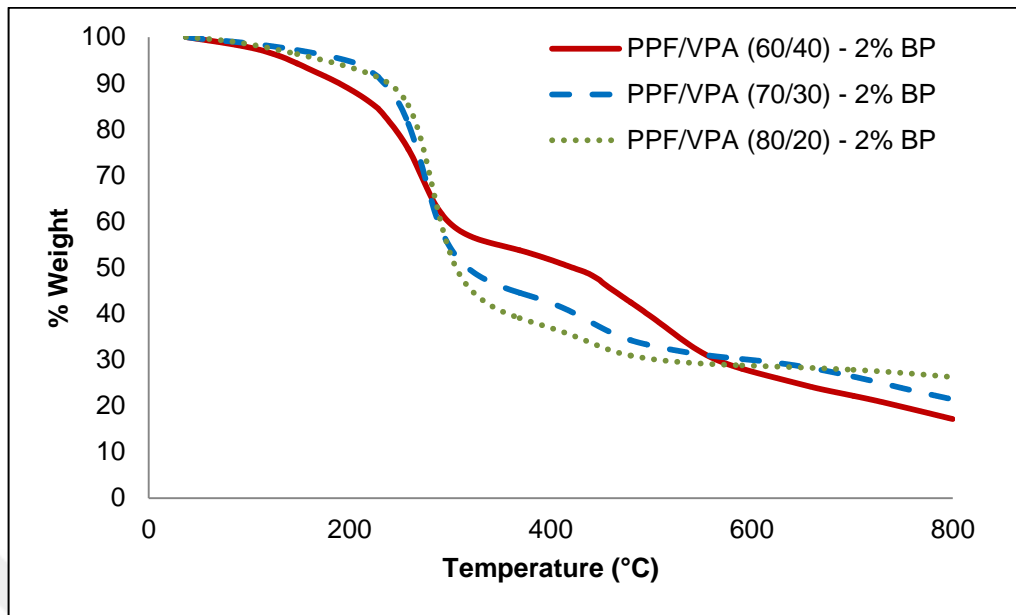


(a)

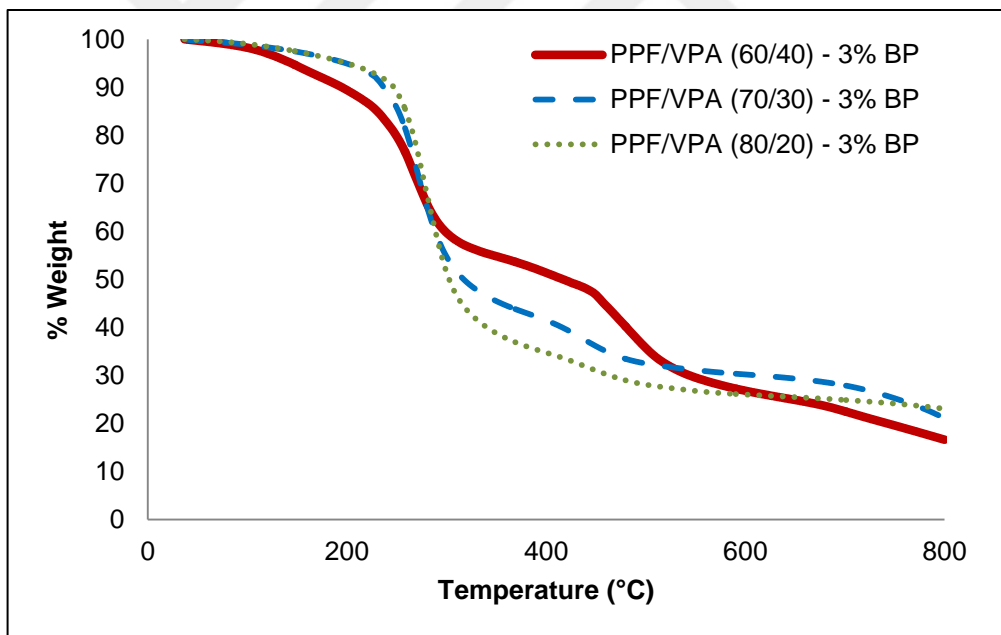


(b)

Figure 4.17. Weight percentage vs temperature plots of PPF/VPES polymers at changing VPES contents, cured with (a) 2 (b) 3 percent initiator



(a)



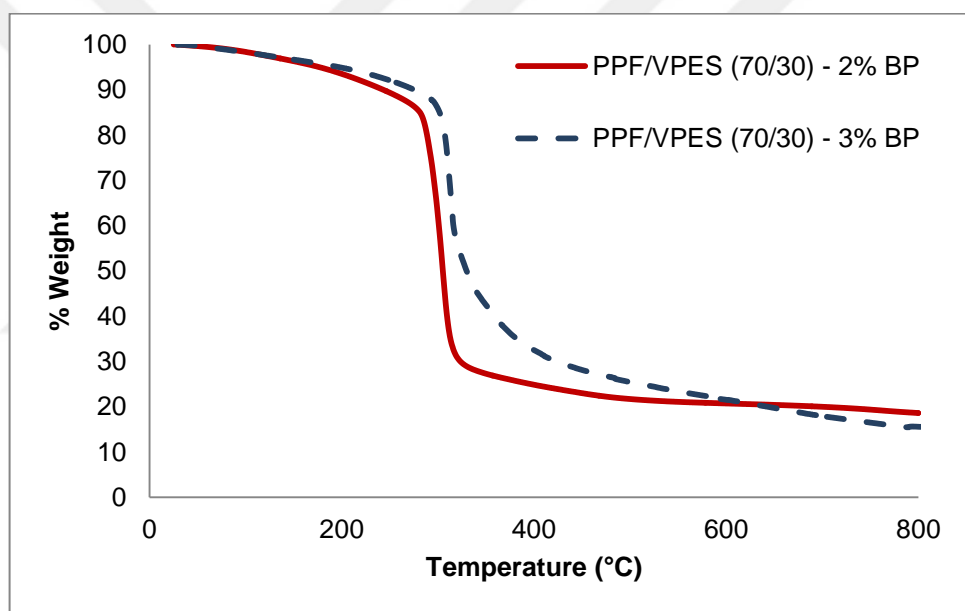
(b)

Figure 4.18. Weight percentage vs temperature plots of PPF/VPA polymers at changing VPA contents, cured with (a) 2 and (b) 3 percent initiator

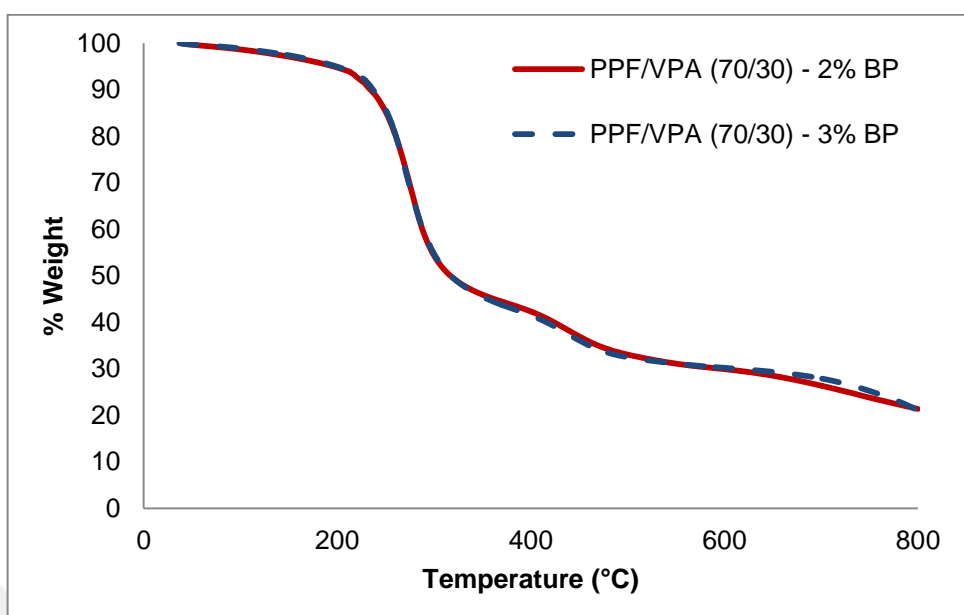
4.5.3.2. Effect of Initiator Amount

Figure 4.19. shows the weight percentage vs temperature plots of PPF/VPES (70/30) (a) and PPF/VPA (70/30) (b) polymers cured with 2 and 3 percent initiator amount.

Increasing initiator amount from 2 to 3 percent, results in beginning of the decomposition at higher temperatures for PPF/VPES (70/30) samples. Controversially, increase in initiator amount had no effect in terms of thermal stability and beginning temperature of decomposition.



(a)



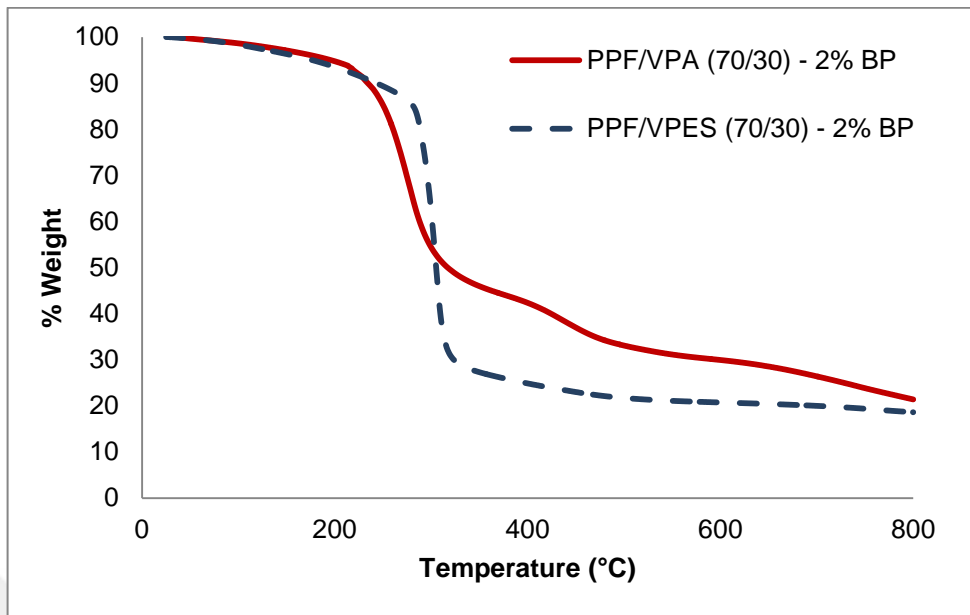
(b)

Figure 4.19. Weight percentage vs temperature plots of (a) PPF/VPES (70/30) and (b) PPF/VPA (70/30) polymers at changing initiator amounts

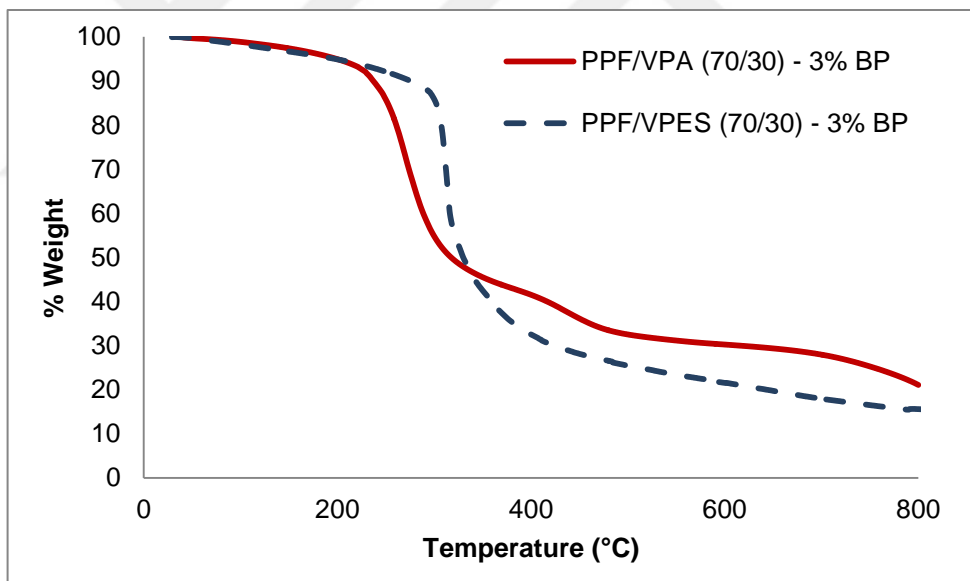
4.5.3.3. Effect of Comonomer

Figure 4.20 shows weight percentage versus temperature plots of PPF/VPA (70/30) and PPF/VPES (70/30) polymers cured with 2 (a) and 3 percent (b) initiator amount.

For both initiator amounts, PPF/VPES samples started major decomposition at higher temperatures than the PPF/VPA samples. The char residue at 600-800°C on the other hand was higher for the the PPF/VPA copolymers. The higher char residue for the PPF/VPA copolymers may be attributed to condensation of the VPA hydroxyl groups at the higher temperatures that contributes to cross-linking of the system.



(a)



(b)

Figure 4.20. Weight percentage vs temperature plots of PPF/VPA (70/30) and PPF/VPES (70/30) polymers cured with 2 (a) and 3 (b) percent initiator amount

4.5.4. Thermogravimetric Analysis of UV Cured Polymers

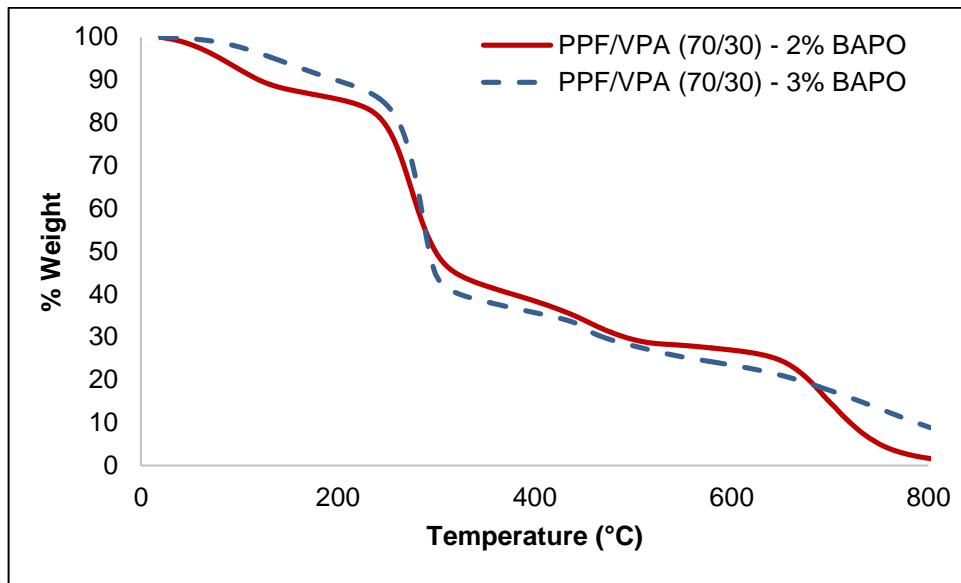
Weight percent versus temperature graphs of UV cured (a) PPF/VPA (70/30) and (b) PPF/VPES (70/30) samples with varying BAPO amounts are illustrated on Figure 4.21.

Major decomposition started at around 240 °C for UV cured PPF/VPA polymers (Fig.4.20.(a)). 2 percent BAPO containing PPF/VPA sample faced higher weight loss at between 25-240 °C by extension of incomplete cure, but yet there is no significant difference in terms of weight loss profiles at higher temperatures.

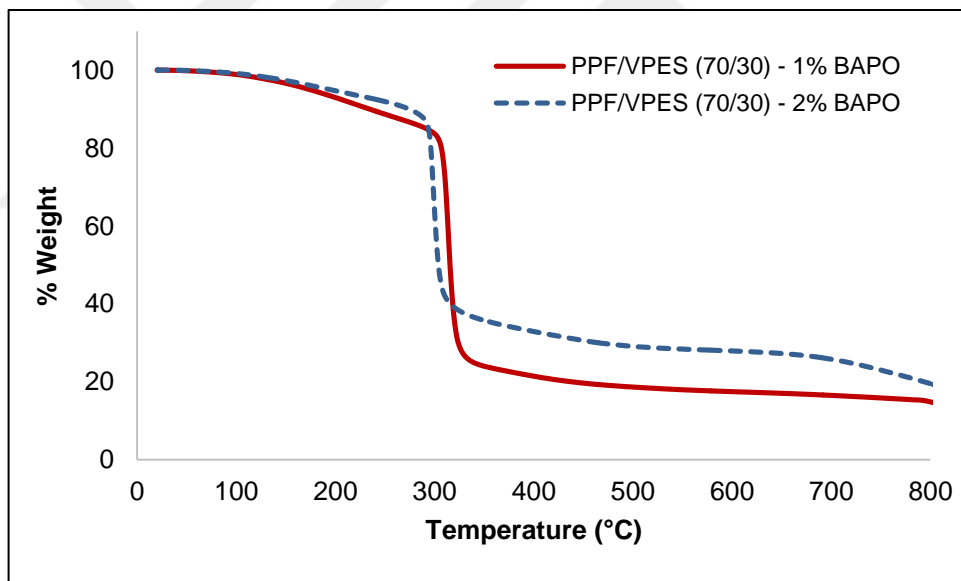
One-step thermal decomposition was observed from percentage weight-versus temperature graphs of UV cured PPF/VPES copolymers (Fig.4.21.(b)). Decomposition started at 290-295°C and char yield was higher for 2 percent BAPO containing PPF/VPES (70/30) samples, which was related to crosslink density of the polymer. This result indicates that 2 percent BAPO containing PPF/VPES (70/30) sample was more efficiently cured than 1 percent BAPO containing PPF/VPES (70/30) sample.

As a comparison, while PPF/VPA samples started major decomposition at 240 °C, PPF/VPES samples started major decomposition at 290 °C, additionally, char yields were higher between 700-800 °C. These results indicate that thermal stability of UV cured PPF/VPES polymers were higher than UV cured PPF/VPA polymers.

Furthermore, since there was no significant weight loss for all samples at between 25-90 °C, these samples will be thermally stable at body temperatures when they are used for tissue engineering applications.



(a)



(b)

Figure 4.21. Weight percent versus temperature graphs of UV cured (a) PPF/VPA (70/30) and (b) PPF/VPES (70/30) samples cured with varying amounts of UV initiator (BAPO)

4.6. EQUILIBRIUM WATER CONTENT AND DYNAMIC CONTACT ANGLE WITH WATER

As the PPF/VPA and PPF/VPES copolymers are designed to be used as scaffolds for bone tissue engineering, in order to analyze their water absorption capacity, the equilibrium water content of all the copolymers in PBS buffer solution (0.9wt% Sodium azide, pH=7.40) was determined. Dynamic contact angle with water at 30th second of measurements was used to compare the hydrophilicity of the PPF copolymers with different compositions.

4.6.1. EWC Analysis of Thermal Cured PPF/VPES and PPF/VPA Polymers

The equilibrium water content (weight percent) values of the PPF/VPES and PPF/VPA polymers are listed in Table 4.2. and the column plots for the equilibrium water content (wt%) data of the PPF/VPES and PPF/VPA polymers are presented in Figure 4.22. A quick examination of Figure 4.22. indicates that as the VPES content increases the equilibrium water content increases which can be related to the increase of the more hydrophilic VPES comonomer content as the crosslink density of the PPF/VPES polymers was found to increase from 20 to 30 weight percent VPES and then decrease slightly from 30 to 40 weight percent VPES content. This trend is valid for 20 and 30 weight percent comonomer content for PPF/VPA polymers as VPA is the hydrophilic comonomer, however, equilibrium water content decreased significantly at 40 weight percent VPA content. As previous work showed an increase in cross-link density, especially at 40wt% VPA content, the increased cross-link density should lead to a lower water absorption. Also, apart from the 60/40 composition, for all other compositions at both initiator contents, PPF/VPA polymers exhibited a higher equilibrium water content than the PPF/VPES polymers. This result is rather expected as VPA structure is more hydrophilic than the VPES structure and also the PPF/VPA polymers exhibited a rather porous structure whereas such porosity was not present in PPF/VPES copolymers.

In addition, it can be seen that both the PPF/VPES and PPF/VPA polymers exhibited a higher equilibrium water content at 2 weight percent initiator content as compared to those

at 3 weight percent initiator content. This result is in agreement with the fact that the crosslink density increases with increasing initiator content from 2 to 3 weight percent for PPF/VPES polymers.

Table 4.2. Equilibrium water content (wt%) values of the PPF/VPES and PPF/VPA polymers

Polymer	Equilibrium Water Content (wt %)
PPF/VPES (80/20) (2% BP)	8.49± 1.48
PPF/VPES (70/30) (2% BP)	9.02± 0.22
PPF/VPES (60/40) (2% BP)	10.36± 0.16
PPF/VPES (80/20) (3% BP)	4.43± 0.11
PPF/VPES (70/30) (3% BP)	7.19± 1.67
PPF/VPES (60/40) (3% BP)	11.26± 0.71
PPF/VPA (80/20) (2% BP)	15.93± 1.16
PPF/VPA (70/30) (2% BP)	33.24± 1.045
PPF/VPA (60/40) (2% BP)	8.89± 0.74
PPF/VPA (80/20) (3% BP)	14.92± 1.83
PPF/VPA (70/30) (3% BP)	14.60± 2.93
PPF/VPA (60/40) (3% BP)	4.44± 1.08

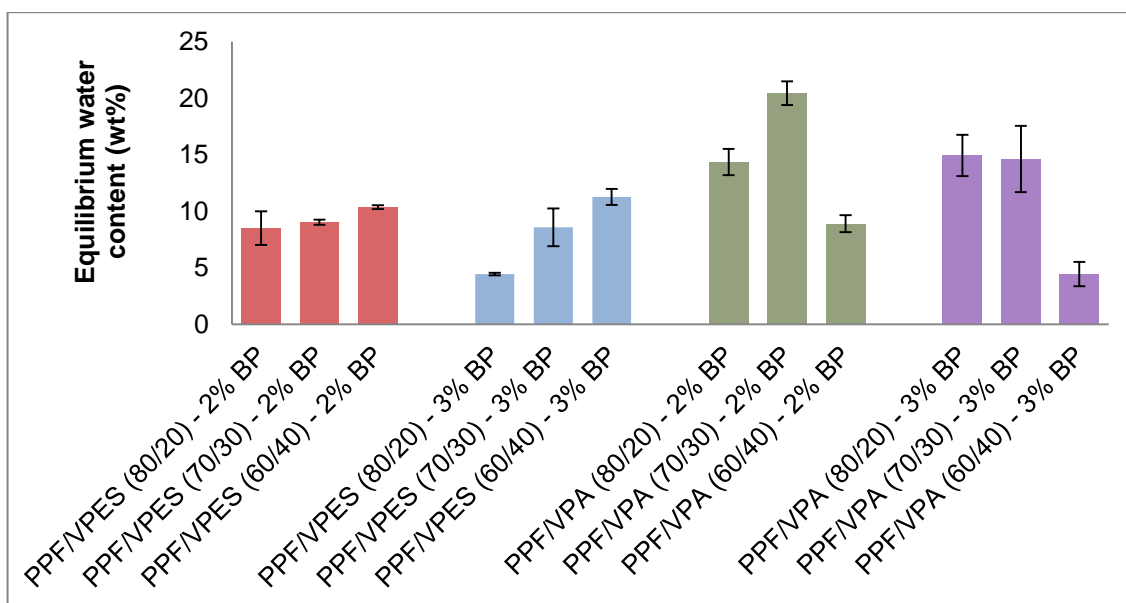


Figure 4.22. Column plots for the equilibrium water content (weight percent) data of the PPF/VPES and PPF/VPA polymers.

4.6.2. EWC Analysis of UV Cured PPF/VPA and PPF/VPES Polymers

Equilibrium water content results of UV cured PPF/VPA and PPF/VPES samples with different BAPO amounts are given as column plots in Figure 4.23, and the corresponding equilibrium water content (wt%) values are tabulated in Table 4.3.

As it can be seen on Figure 4.23., increasing BAPO amount from 1 to 2 weight percent in PPF/VPES samples have resulted in a decrease in equilibrium water content. Similarly increasing BAPO amount from 2 to 3 percent in PPF/VPA samples decreased the equilibrium water content. These results may be related to a higher cross-link density and therefore a more efficient cross-linking with the increasing initiator amounts for both PPF/VPA and PPF/VPES polymers. Equilibrium water content of the polymers is expected to decrease with increasing cross-link density.

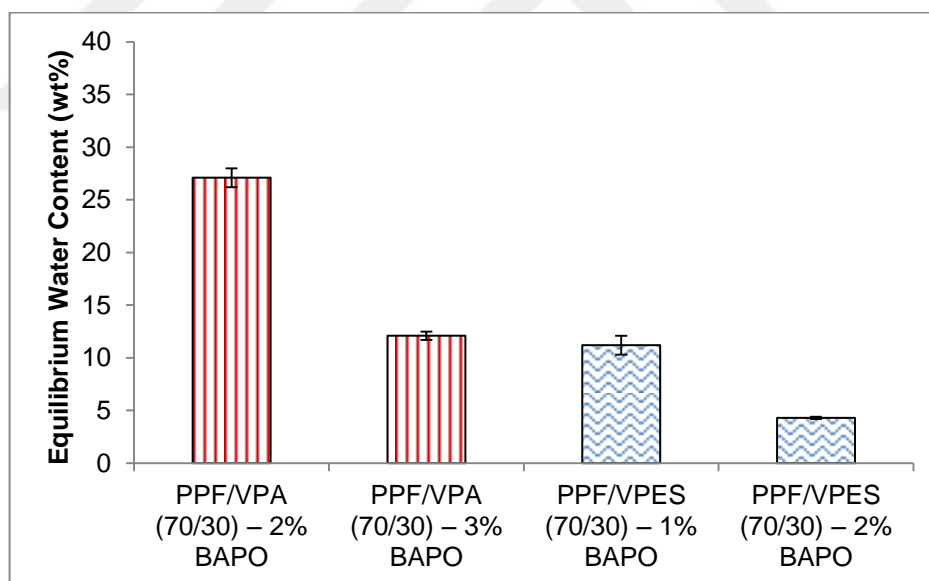


Figure 4.23. Equilibrium water content values of UV cured PPF/VPA and PPF/VPES samples

Table 4.3. Equilibrium water content results of UV cured PPF/VPA and PPF/VPES samples

Polymer	Equilibrium Water Content (wt%)
PPF/VPA (70/30) – 2% BAPO	27.1±0.9
PPF/VPA (70/30) – 3% BAPO	12.1±0.4
PPF/VPES (70/30) – 1% BAPO	11.2±0.9
PPF/VPES (70/30) – 2% BAPO	4.3±0.1

4.6.3. Dynamic Contact Angle With Water

The average dynamic contact angle with water values at the 30th second of measurements for all thermal cured PPF/VPA and PPF/VPES polymers are listed in Table 4.4. and also presented in column graphs in Figure 4.24.

As can be noticed from Figure 4.24., the contact angle with water for both PPF/VPA and PPF/VPES samples decreased generally with increasing VPA and VPES content respectively. This result can be related to the higher hydrophilicity of the VPA or VPES comonomer as compared to the PPF backbone. In addition, PPF/VPA samples generally exhibited lower contact angle values with water as compared to those of PPF/VPES samples at the same composition. This result may again be related to the greater polarity and hydrophilicity of the VPA comonomer as compared to the VPES comonomer, as contact angle with water must decrease with increasing hydrophilicity or polarity of the sample. As increasing hydrophilicity of the surface of a biomaterial will favor cell interaction, it can be proposed that samples with higher VPA or VPES content and samples containing VPA as compared to VPES may be more favorable in terms of biocompatibility and tissue regeneration[58].

Table 4.4. Average dynamic contact angle with water values at the 30th second of measurements for all thermal cured samples

Polymer	Mean Contact Angle (°) (30 th second)
PPF/VPES (80/20) (2% BP)	52.70 ± 3.80
PPF/VPES (70/30) (2% BP)	48.15 ± 2.65
PPF/VPES (60/40) (2% BP)	43.15 ± 1.25
PPF/VPES (80/20) (3% BP)	60.60 ± 0.80
PPF/VPES (70/30) (3% BP)	55.30 ± 2.10
PPF/VPES (60/40) (3% BP)	50.00 ± 1.00
PPF/VPA (80/20) (2% BP)	50.40 ± 0.20
PPF/VPA (70/30) (2% BP)	50.65 ± 2.35
PPF/VPA (60/40) (2% BP)	39.25 ± 0.55
PPF/VPA (80/20) (3% BP)	43.98 ± 2.58
PPF/VPA (70/30) (3% BP)	45.97 ± 2.03
PPF/VPA (60/40) (3% BP)	31.25 ± 1.15

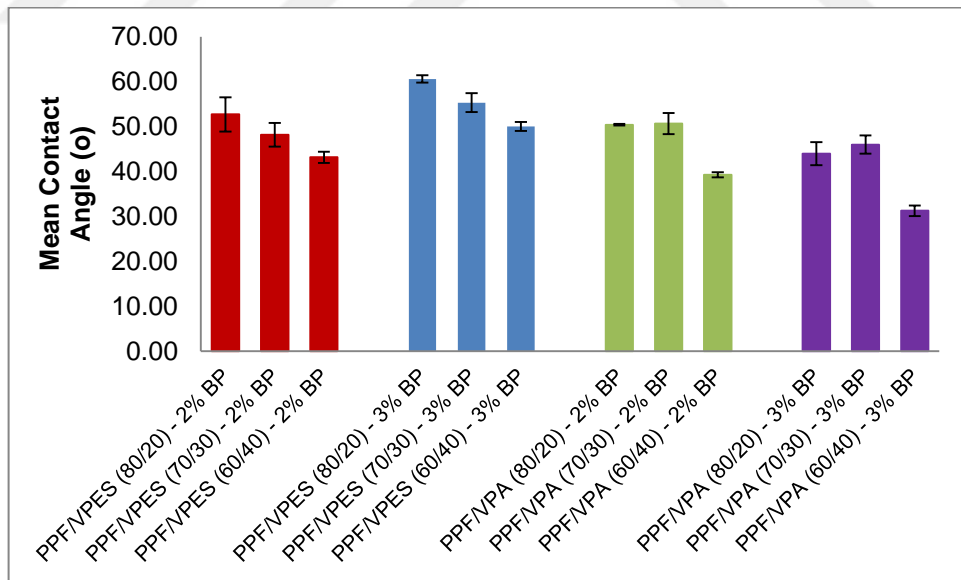


Figure 4.24. Dynamic contact angle with water values at the 30th second of measurements for all thermal cured samples

4.7. DYNAMIC MECHANICAL ANALYSIS (DMA)

Dynamic mechanical analysis (DMA) gives information about the mechanical features of a sample positioned in minor, usually sinusoidal, oscillation as a function of time and temperature by facing it to a small, usually sinusoidal, oscillating force. The subjected mechanical force, which is, stress, brings out a corresponding strain (deformation) whose amplitude and phase shift can be found out. While the modulus (stiffness) of the material is influenced by the temperature and the assigned stress, the modulus points out how properly a material will function in a certain usage in a real world. As mentioned earlier, dynamic temperature ramp default tests were carried on polymer samples in single cantilever mode. Cantilever bending is a good general purpose mode for evaluating thermoplastics, some thermosets and highly damped materials (e.g., elastomers). Glass transition temperature (T_g) of the polymer was taken as the temperature at which the Loss modulus (as well as Tan delta) shows a maximum value.

4.7.1. Dynamic Mechanical Analysis of Thermal Cured PPF/VPA and PPF/VPES Polymers

Storage modulus (E'), Loss modulus (E'') and tan delta values were plotted with respect to temperature for PPF/VPA and PPF/VPES polymers for different compositions in Figure 4.26 - 4.33. In addition, storage and loss modulus values at 37°C , and T_g values as determined from the maxima of the loss modulus and tan delta curves for all thermal cured PPF/VPA and PPF/VPES compositions are listed in Table 4.5.

As can be seen from Table 4.5., for different compositions of PPF/VPES polymers, storage modulus values at 37°C varied between 845-2430 MPa and for different compositions of PPF/VPA polymers they varied between 1134-6330 MPa. For PPF/VPES samples cured with 3 percent BP, increasing VPES amount caused a decrease in storage modulus and for PPF/VPES samples cured with 2 percent BP, just the opposite condition was observed. Moreover, for PPF/VPA polymers cured with both amounts of BP, the PPF/VPA (60/40) composition showed highest storage modulus, and for the other two compositions (70/30 and 80/20), increase in VPA amount resulted in a decrease in storage modulus. Alteration of glass transition points (T_g) of PPF polymers were tracked by determining maxima of

loss modulus and tan delta plots. As expected, T_g values obtained from tan delta maxima were higher than T_g values obtained from loss modulus [67].

In general, T_g values increased with increase in VPA amount but decreased with increasing VPES amount. For PPF/VPA polymers, the predicted crosslink density increasing effect of VPA condensation which occurs during thermal cure (2 hours 60°C, 2 hours 85 °C, 5 hours 100 °C) was thought to increase the T_g values with increase in VPA amount. Moreover, acid structure of VPA causes an increase in T_g values. For PPF/VPES polymers, there is no such condensation reaction; decrease in T_g related to decrease in crosslink density with increasing VPES amount was an expected result.

Additionally, since PPF/VPA polymers showed a porous structure, the increase in porosity with increasing VPA content is resulted in a decrease in storage modulus. At this point, the highest storage modulus values observed for the PPF/VPA (60/40) for both initiator amount was an unexpected result. This result may be explained by the increase of the extent of VPA phosphate groups' condensation at increased VPA content, that must contribute to the crosslinking of the system.. In case of PPF/VPES polymers, for example in 3 percent BP containing samples, decreasing storage moduli with increasing VPES amount can be explained by decreasing crosslink density with decreasing amount of PPF.

Table 4.5. Storage and loss modulus values at 37°C and T_g values which are determined from loss modulus and tan delta maxima of all thermal cured polymer compositions

Polymer	Storage Modulus (E')(37°C) (MPa)	Loss Modulus (E'')(37°C) (MPa)	T_g (tan delta max.) (°C)	T_g' (loss mod. max.) (°C)
PPF/VPA (80/20) - 3% BP	2590 ± 239	416 ± 36	67.4 ± 3.9	26.7 ± 4.0
PPF/VPA (70/30) - 3% BP	1236 ± 134	287 ± 15	73.4 ± 9.5	20.6 ± 6.0
PPF/VPA (60/40) - 3% BP	6331 ± 706	500 ± 56	88.5 ± 0.04	56.5 ± 4.7
PPF/VPA (80/20) - 2% BP	1391 ± 273	302 ± 40	61.1 ± 2.96	19.6 ± 2.0

PPF/VPA (70/30) - 2% BP	1134 ± 44	243 ± 29	59.0 ± 2.0	25.9 ± 1.2
PPF/VPA (60/40) - 2% BP	4107 ± 483	546 ± 67	69.5 ± 0.1	35.2 ± 0.5
PPF/VPES (80/20) - 3% BP	2432 ± 109	338 ± 32	70.9 ± 4.8	32.6 ± 3.9
PPF/VPES (70/30) - 3% BP	1713 ± 251	388 ± 10	67.3 ± 1.3	20.9 ± 7.8
PPF/VPES (60/40) - 3% BP	845 ± 147	246 ± 21	58.3 ± 8.2	7.9 ± 0.04
PPF/VPES (80/20) - 2% BP	1670 ± 16	388 ± 38	55.1 ± 8.2	24.6 ± 2.6
PPF/VPES (70/30) - 2% BP	2135 ± 73	531 ± 27	53.0 ± 1.6	13.6 ± 1.9
PPF/VPES (60/40) - 2% BP	2313 ± 251	773 ± 38	34.3 ± 3.2	-0.8 ± 0.6

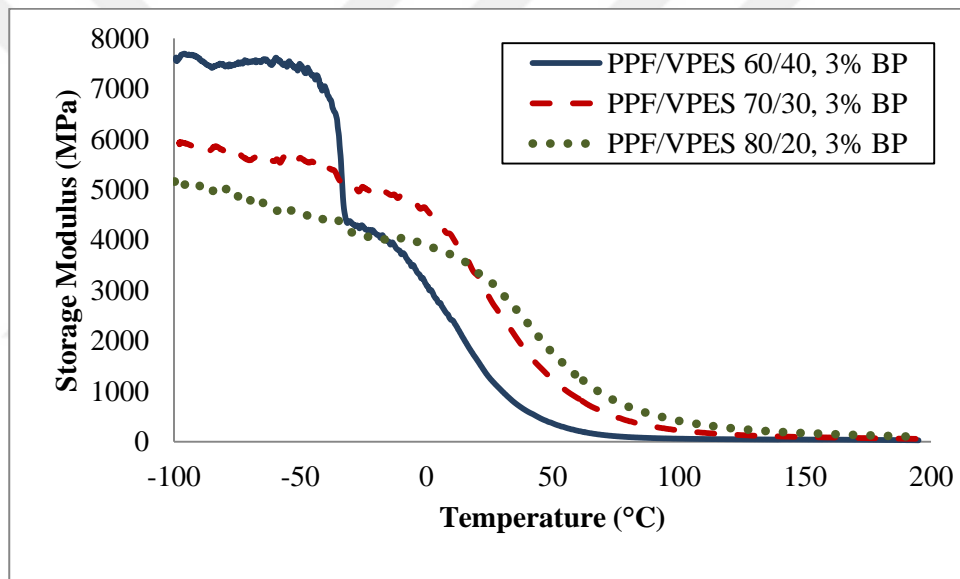
Storage modulus, loss modulus and tan delta versus temperature graphs of PPF/VPES polymers cured with 3 percent BP are illustrated in Figure 4.26. ((a),(b),(c)). For PPF/VPES polymers, storage modulus values below T_g were decreasing like 60/40>70/30>80/20 respectively, however it is just the opposite above T_g (Figure 4.26. (a)).

As it is presented in Figure 4.26.(b), two peaks were observed on loss modulus versus temperature graphs. The observed broad peaks (first peaks) between -50°C and -60°C for all compositions were thought to correspond with β -transitions in alkyl chains of PPF [67]. The second peak which was observed above 0°C is referring to T_g values of polymers. As it can be seen in the graph, for PPF/VPES polymers cured with 3 percent BP, T_g values which were obtained from loss moduli graphs, increased with decrease in VPES amount. This situation may be explained with increasing crosslink density, which is a result of increasing crosslinker unit of PPF, by a decrease in VPES amount. Tan delta versus temperature graphs which are presented in Figure 4.26.(c) show broad bands which refer to glass transition but second peaks which refer to β -transitions of alkyl chains which are at negative temperatures were observed to be very weak.

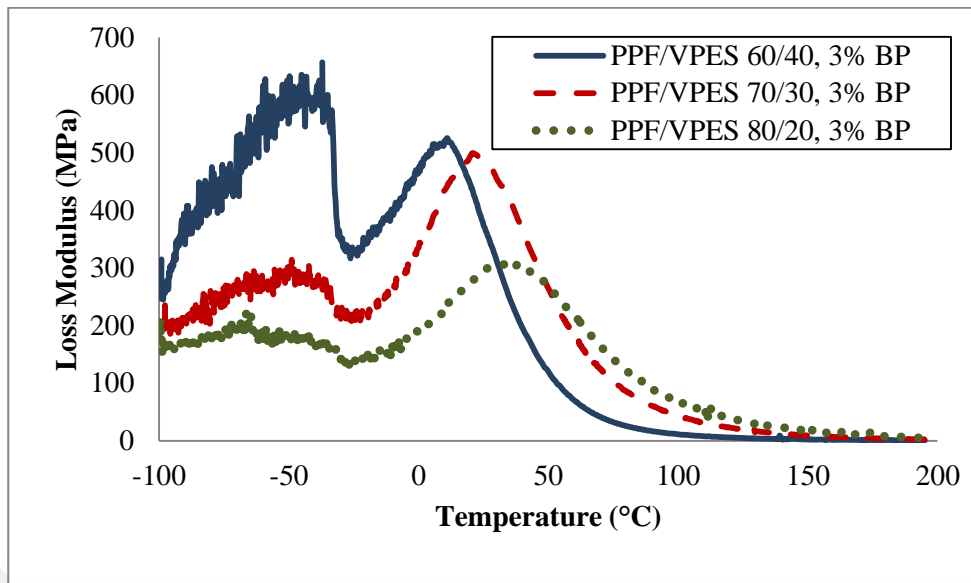
Additionally, T_g values which are determined from tan delta maxima increased with decrease in VPES amount. Moreover, increase in VPES amount resulted in an increase in

Tan delta values, and this situation showed that energy absorbing capabilities of PPF/VPES polymers were increasing with increase in VPES amount in their compositions.

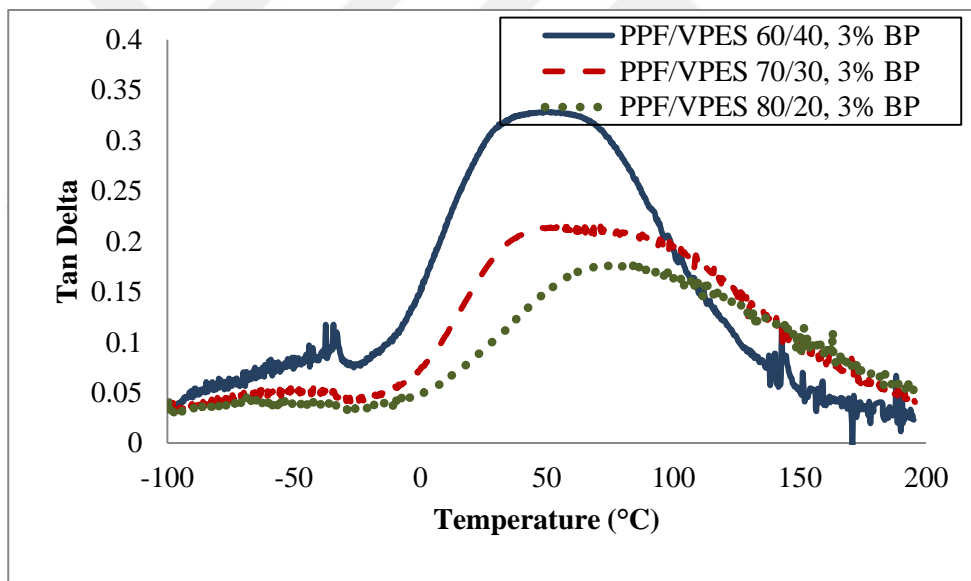
Storage modulus, loss modulus and tan delta versus temperature graphs of PPF/VPES polymers cured with 2 percent BP are presented in Figure 4.27. (a), (b), (c) below, respectively. Storage modulus values were increasing with increase in comonomer amount. Except that, 2 percent BP containing PPF/VPES polymers showed similar trends as observed for 3 percent BP containing PPF/VPES polymers in terms of loss modulus and tan delta profiles.



(a)

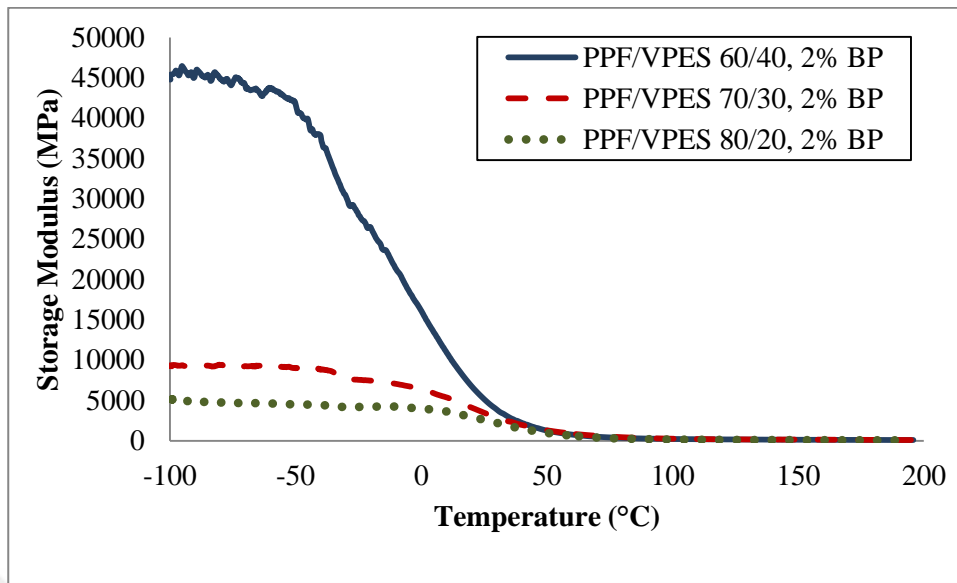


(b)

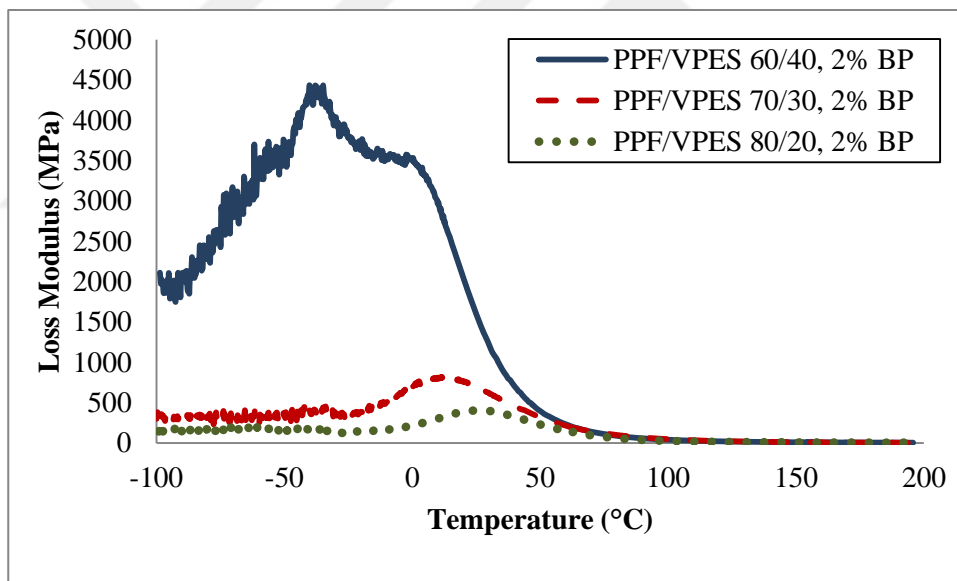


(c)

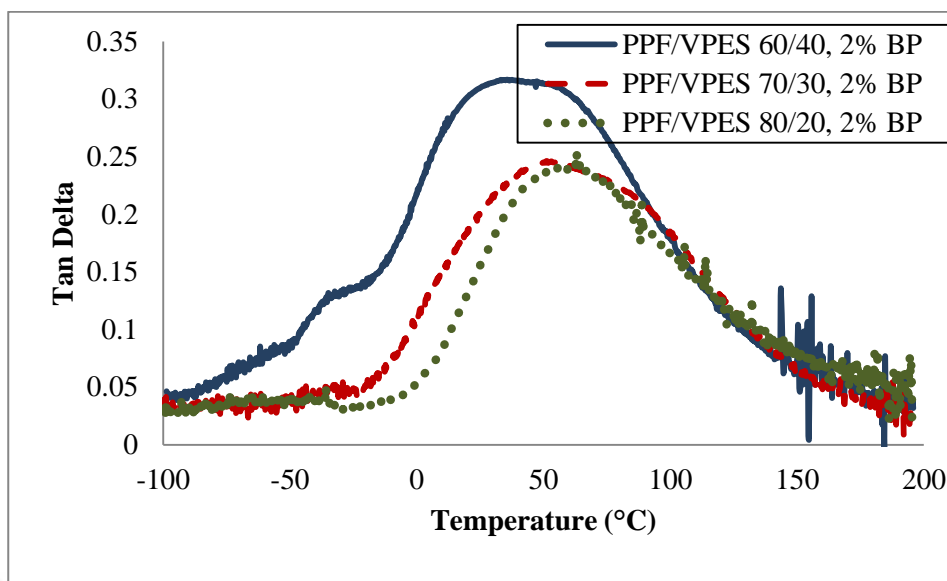
Figure 4.25. (a) Storage modulus, (b) loss modulus and (c) tan delta versus temperature graphs of 3 percent BP containing PPF/VPES samples



(a)



(b)



(c)

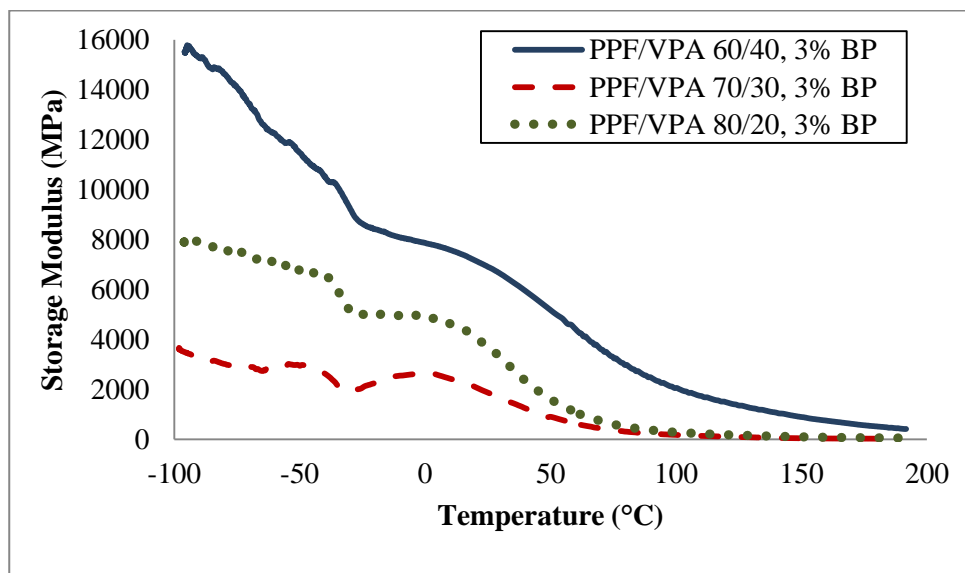
Figure 4.26. (a) Storage modulus, (b) loss modulus and (c) tan delta versus temperature graphs of 2 percent BP containing PPF/VPES samples

Storage modulus, loss modulus and tan delta versus temperature graphs of PPF/VPA polymers cured with 3 percent BP are illustrated in Figure 4.28.((a),(b),(c)). Storage modulus values for PPF/VPA polymers are decreasing like $60/40 > 80/20 > 70/30$, respectively (Figure 4.28.(a)). In loss modulus versus temperature graph which is shown in Figure 4.28.(b), two peaks were observed between $-100\text{ }^{\circ}\text{C}$ and $100\text{ }^{\circ}\text{C}$, the first peaks were thought to refer to β -transitions in alkyl groups of PPF in a similar way. The peaks which were observed above $0\text{ }^{\circ}\text{C}$ and refer glass transition points (T_g) of polymers, were appearing at similar temperatures ($20\text{--}25\text{ }^{\circ}\text{C}$) for the 80/20 and 70/30 compositions but for 60/40 composition this transition was observed as a broad band. Moreover, in tan delta graphs which is presented in Figure 4.28.(c), in addition to broad glass transition peaks between $0\text{--}100\text{ }^{\circ}\text{C}$, one more broad band was observed at above $150\text{ }^{\circ}\text{C}$. These peaks are thought to be related to VPA degradation. Also T_g values obtained from tan delta maxima were increasing with increase in VPA amount.

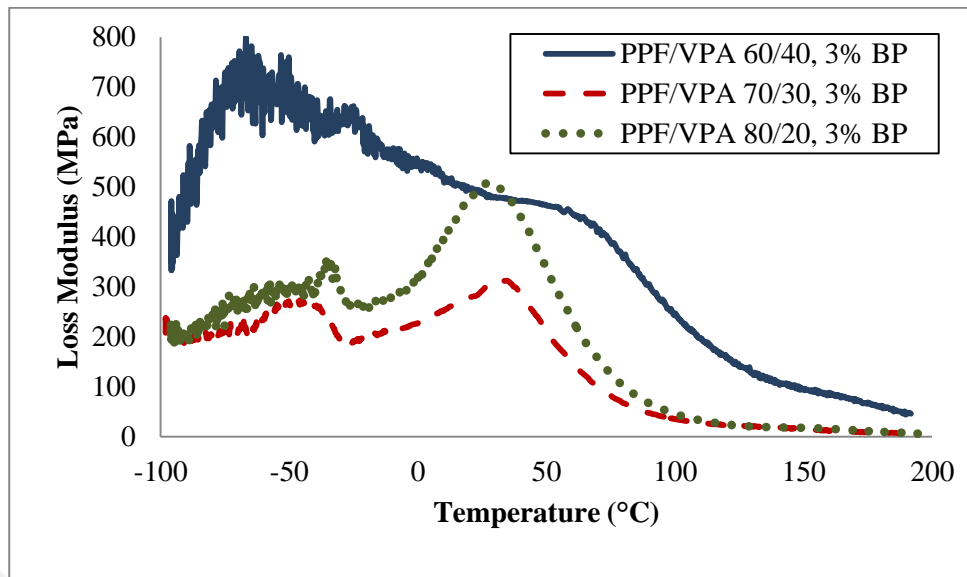
Storage modulus, loss modulus and tan delta versus temperature graphs of PPF/VPA polymers cured with 2 percent BP are presented in Figure 4.29.((a), (b), (c)) below. Although the highest storage modulus value of PPF/VPA polymers, (Figure 4.29.(a)) belonged to 60/40 composition again, PPF/VPA 80/20 and 70/30 compositions showed

similar storage modulus values above T_g temperatures. In loss modulus graph which is presented in Figure 4.29.(b), the two peaks can be obviously observed for all compositions. At negative temperatures, the temperature of the first peak which belongs to β -transitions of alkyl chains of PPF was increasing with increase in VPA amount. The temperature of the peak which was observed between 0-70 °C and accepted as T_g of PPF/VPA polymers was increasing with the increase in VPA amount. As it was also discussed before, increase in T_g with increasing VPA amount can be explained by increasing crosslink density as a result of VPA condensation during thermal cure and T_g increasing effect of acidic structure. The broad peaks which are observed in tan delta graph (Figure 4.29.(c)) between 50-70°C present T_g and it is obvious that T_g which is determined from tan delta peak was increasing with increase in VPA amount.

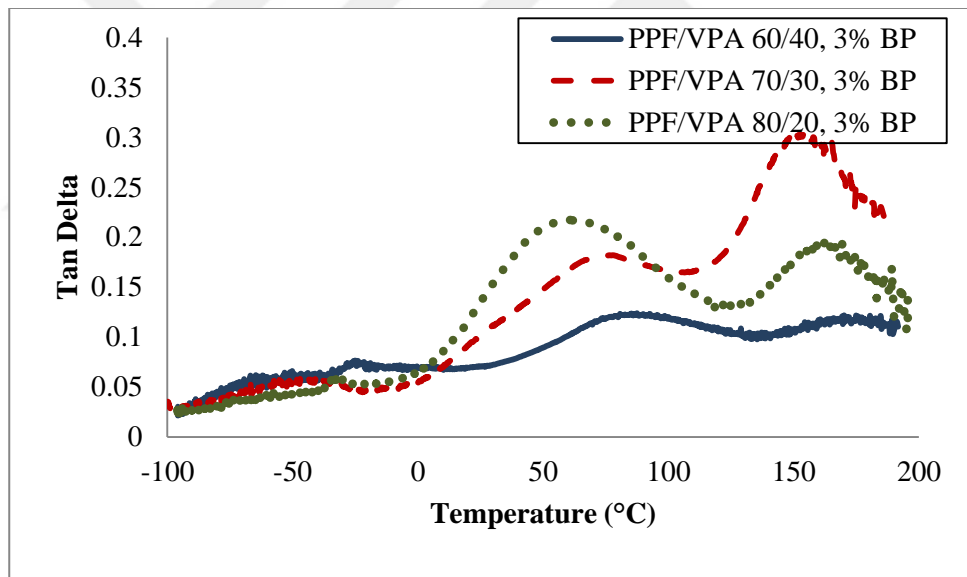
The weak and broad peaks, which were observed after 150°C were thought to present VPA degradation, which also exist in 3 percent BP containing PPF/VPA polymers. Moreover, tan delta values were increasing with decrease in VPA amount and this situation shows that, energy absorbing capabilities were decreasing with increase in VPA amount for PPF/VPA polymers.



(a)

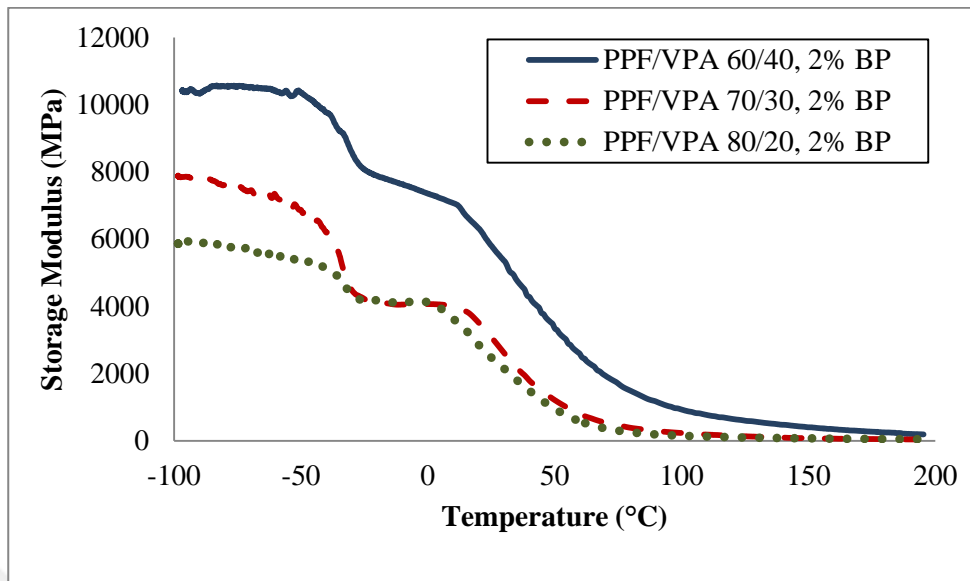


(b)

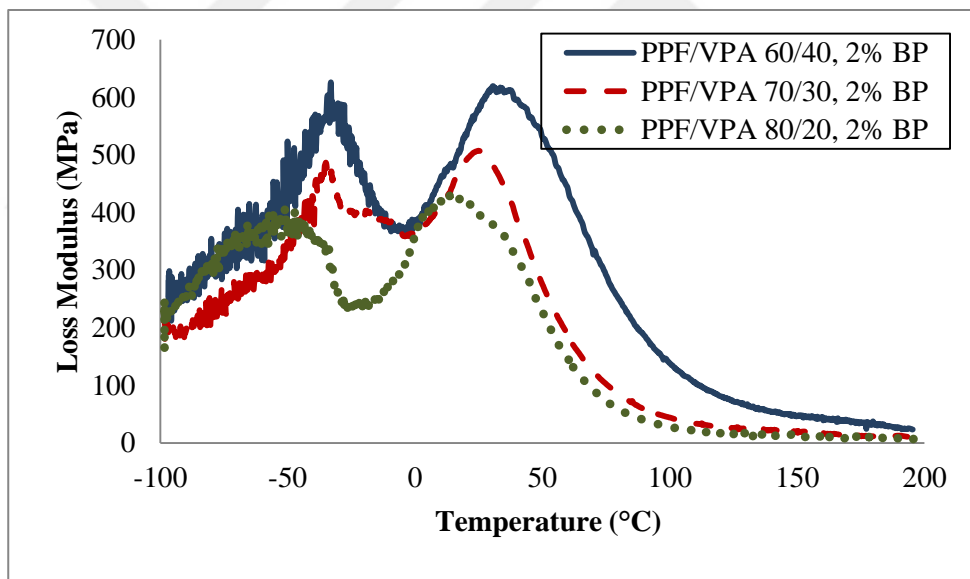


(c)

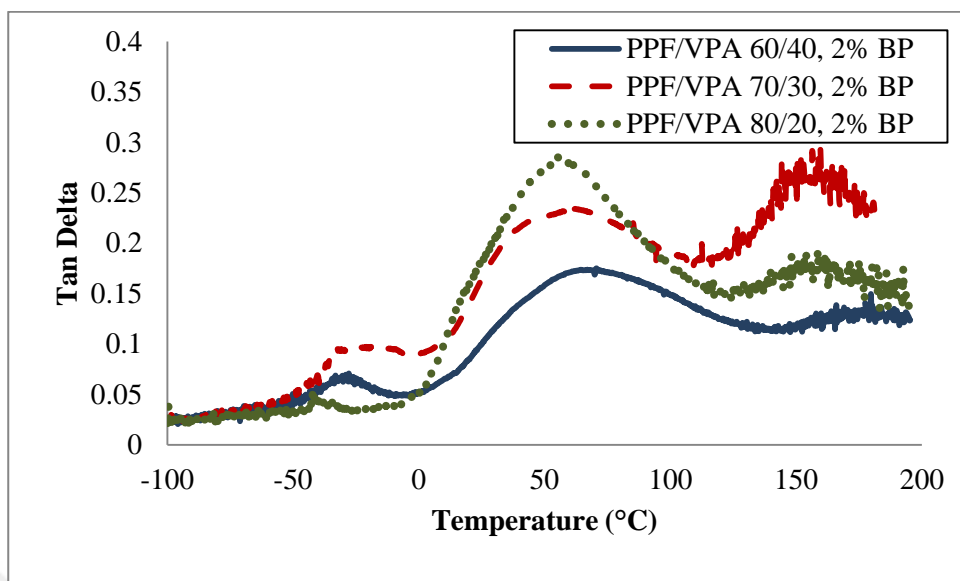
Figure 4.27. (a) Storage modulus, (b) loss modulus and (c) tan delta versus temperature graphs of 3 percent BP containing PPF/VPA samples



(a)



(b)



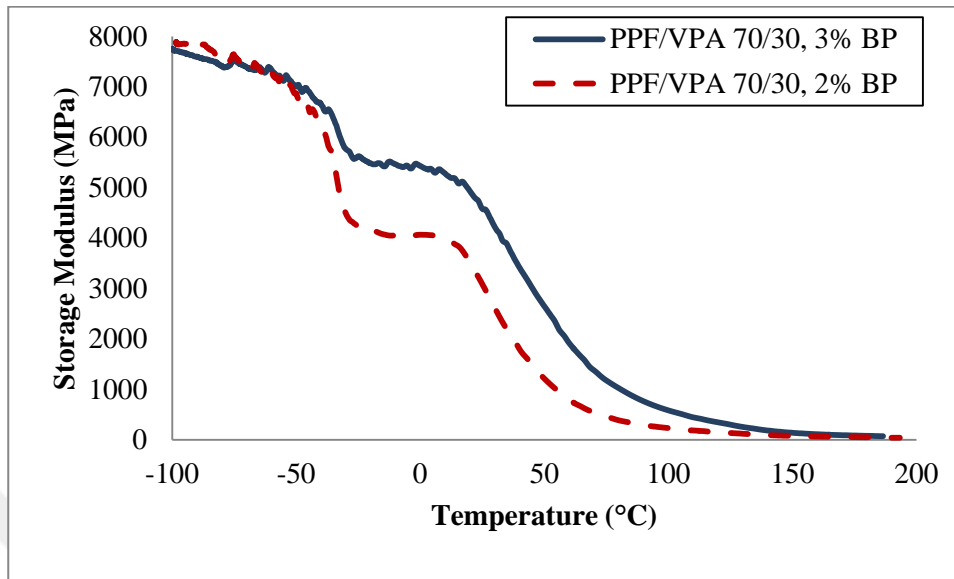
(c)

Figure 4.28. (a) Storage modulus, (b) loss modulus and (c) tan delta versus temperature graphs of 2 percent BP containing PPF/VPA samples

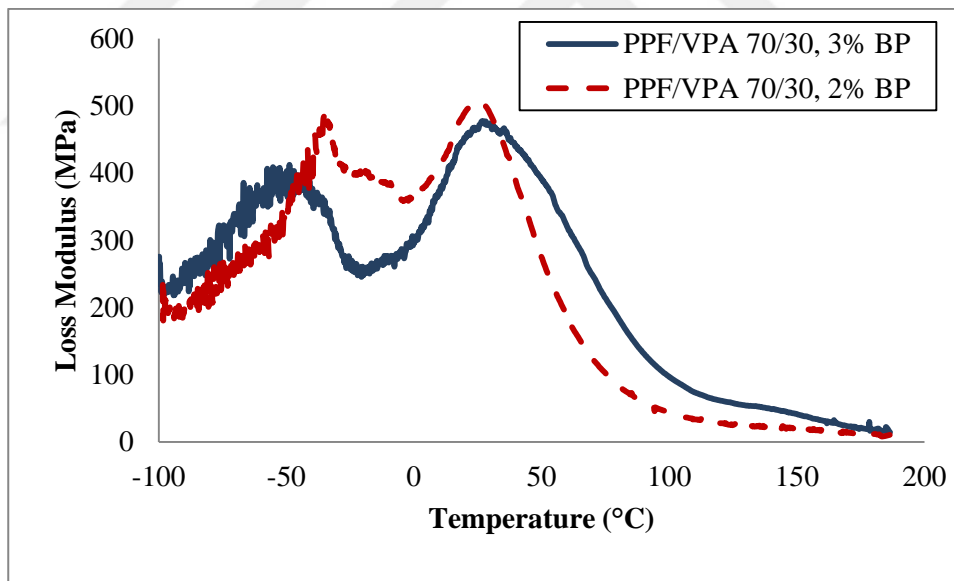
Comparison graphs of storage modulus and loss modulus versus temperature which belong to PPF/VPA polymers cured with 3 percent BP and 2 percent BP are illustrated in Figure 4.30.((a), (b)). And comparison graphs of storage modulus and loss modulus versus temperature which belong to PPF/VPES polymers cured with 3 percent BP and 2 percent BP are also illustrated in Figure 4.31.((a), (b)).

For this composition of PPF/VPA polymers, samples cured with 3 percent BP showed higher storage modulus values rather than samples cured with 2 percent BP above T_g values. Additionally, T_g values which were obtained from loss modulus maxima were also higher than 2 percent BP containing samples. Data in Table 4.5. show that, increase of BP from 2 to 3 percent caused increase in T_g and storage modulus values also for other compositions.

For PPF/VPES (70/30) polymers which were cured with 2 and 3 percent BP, storage modulus for 2 percent BP containing sample was higher (at temperatures below T_g) but tan delta and T_g values obtained from loss modulus peaks were higher for 3 percent BP containing samples. This trend was also valid for other compositions of PPF/VPES polymers (Table 4.5.).

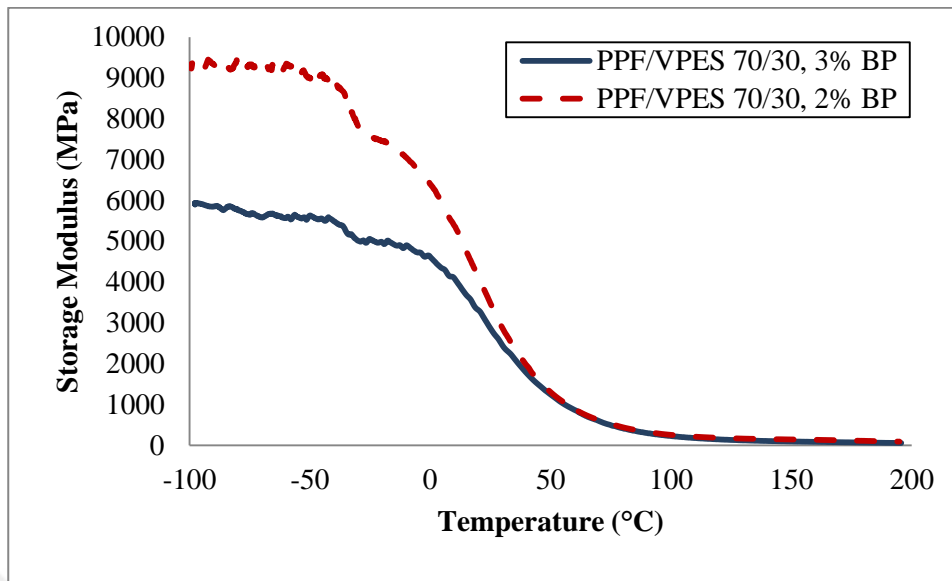


(a)

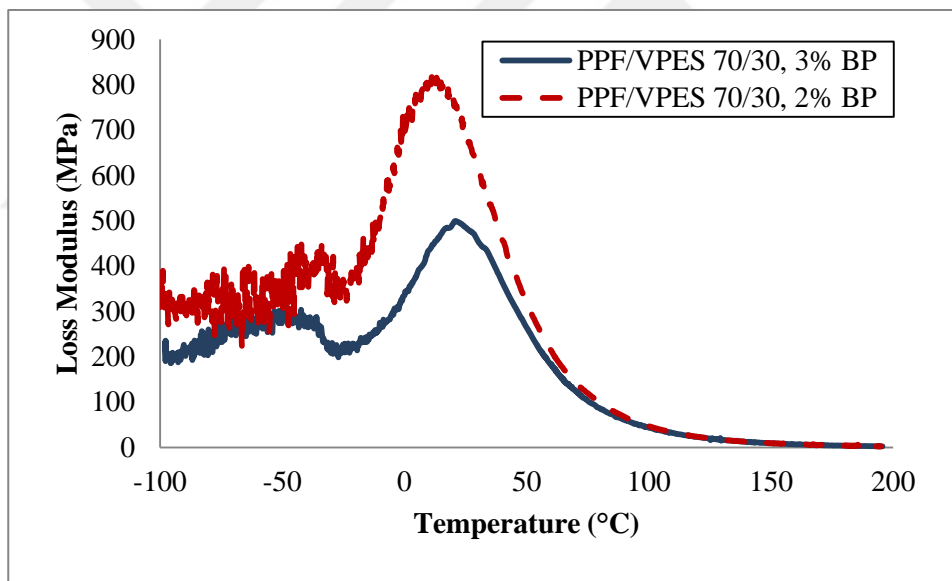


(b)

Figure 4.29. Comparison graphs of 3 and 2 percent BP containing PPF/VPA (70/30) samples in terms of (a) storage and (b) loss modulus



(a)

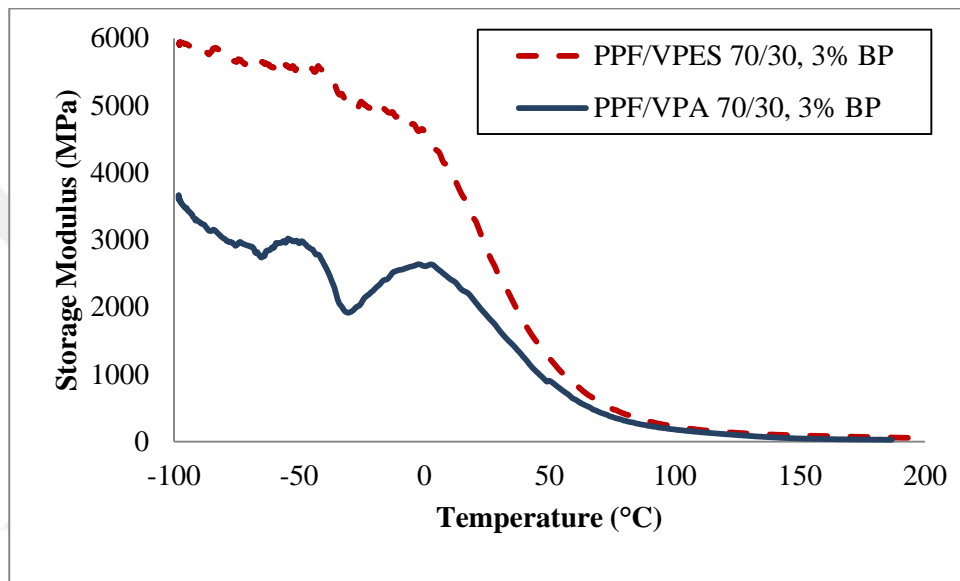


(b)

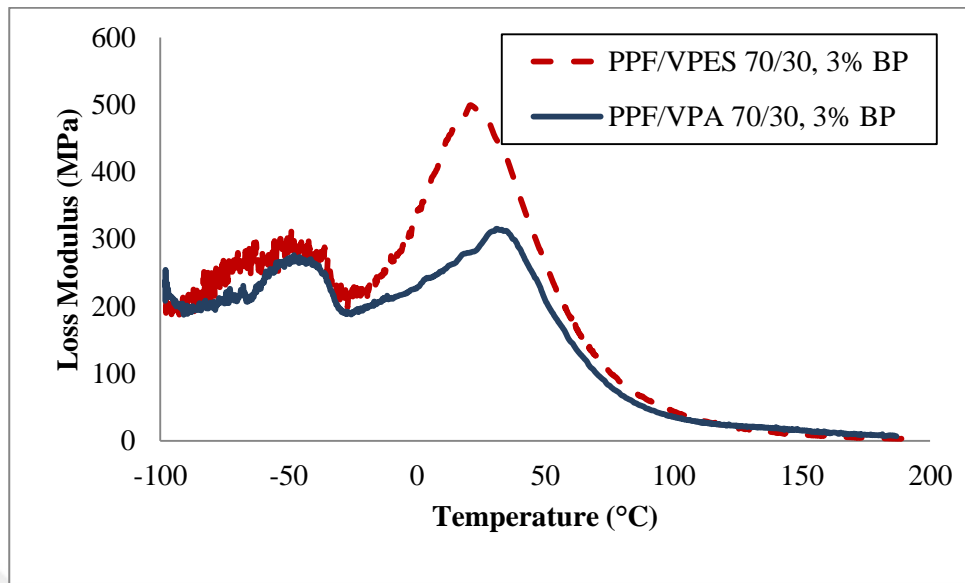
Figure 4.30. Comparison graphs of 3 and 2 percent BP containing PPF/VPES (70/30) samples in terms of (a) storage and (b) loss modulus

Comparison graphs of (a) storage and (b) loss modulus versus temperature which belong to PPF/VPA (70/30) and PPF/VPES (70/30) polymers cured with 3 percent BP are given in Figure 4.32. ((a), (b)). Moreover in Figure 4.33. ((a), (b)), comparison graphs of (a) storage and (b) loss modulus versus temperature which belong to PPF/VPA (70/30) and

PPF/VPES (70/30) polymers cured with 2 percent BP are also given. As it is obvious from both figures, at similar comonomer and radical initiator amounts PPF/VPES polymers showed higher storage modulus values than PPF/VPA polymers however, PPF/VPA polymers showed higher T_g values than the PPF/VPES polymers. This trend was also valid for other compositions except the 60/40 composition (Table 4.5.) [68].

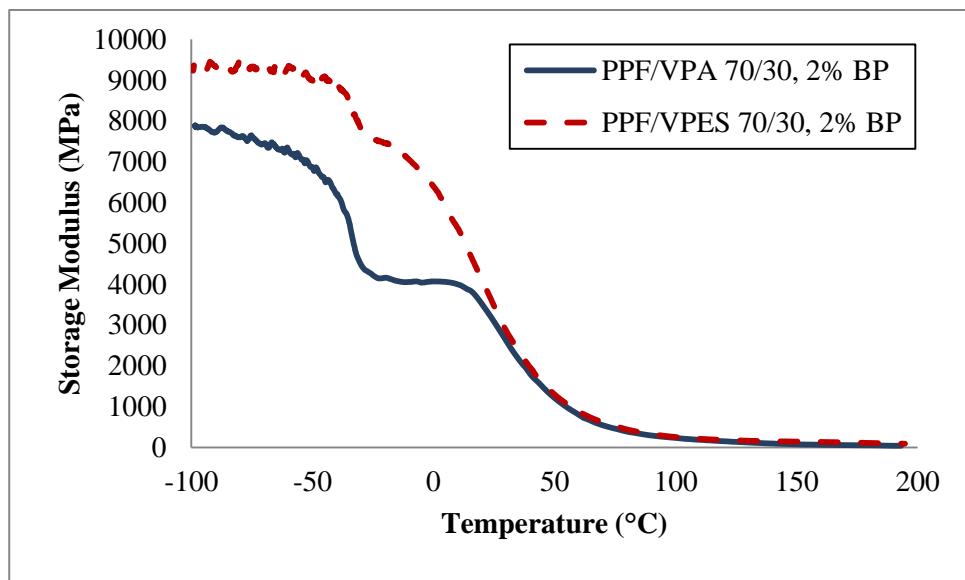


(a)

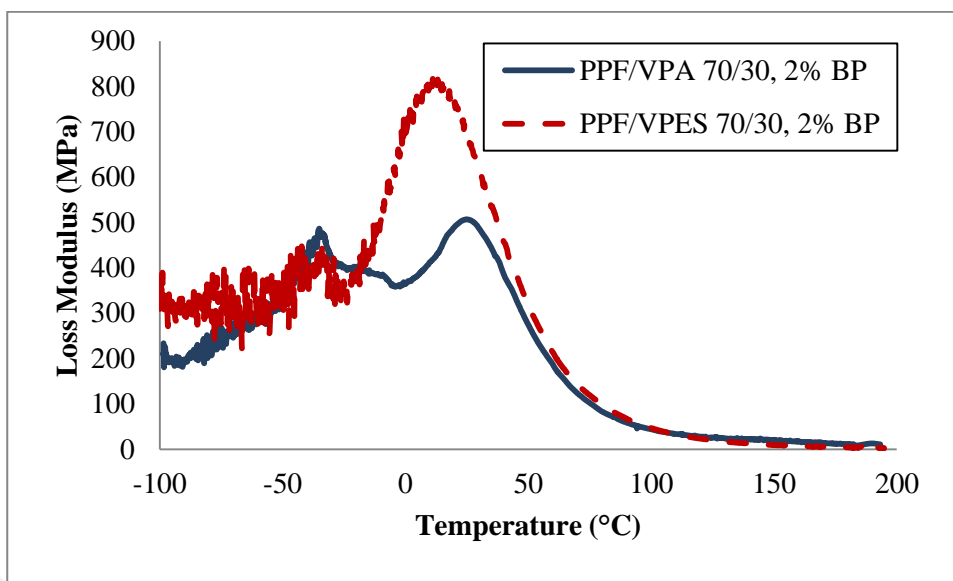


(b)

Figure 4.31. Comparison graphs of PPF/VPA and PPF/VPES (70/30) samples with 3 percent BP in terms of (a) storage and (b) loss modulus



(a)



(b)

Figure 4.32. Comparison graphs of PPF/VPA and PPF/VPES (70/30) samples with 2 percent BP in terms of (a) storage and (b) loss modulus

4.8. MECHANICAL TESTING

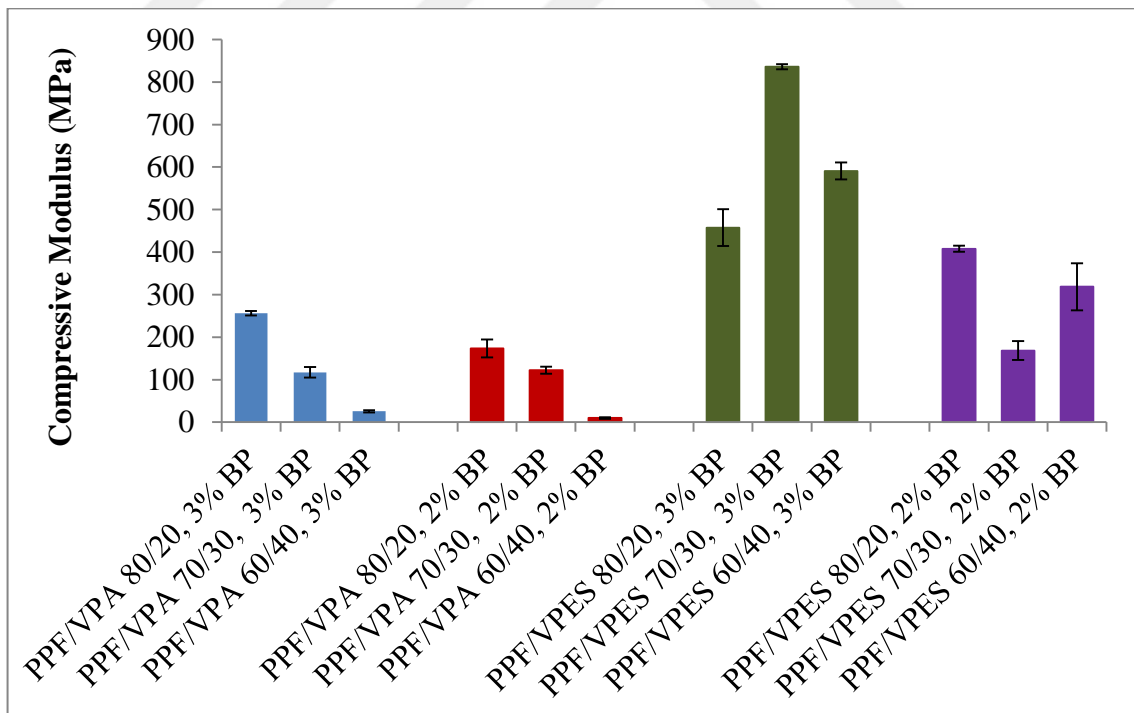
For the compression tests, 6x15mm (length x diameter) cylinder samples were prepared and faced to compressive load with a 1.0 mm/min crosshead speed by using 100 kN load cell using an INSTRON Universal Testing Machine as described in Section 3.10. The obtained compressive modulus and strength values were analyzed with respect to composition of the copolymers.

4.8.1. Compressive Properties of Thermal Cured Polymers

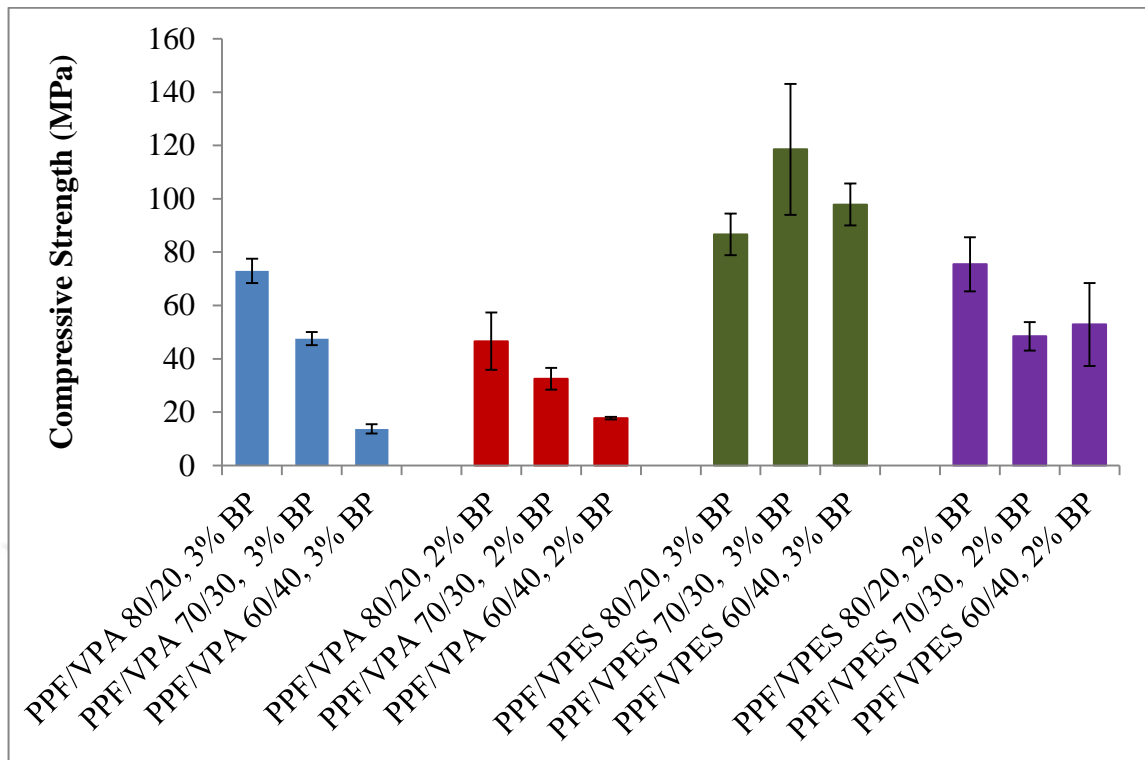
In this section, compressive properties (compressive modulus and compressive strength) of thermally cured PPF/VPA and PPF/VPES polymers were analyzed with varying PPF-comonomer and initiator contents as shown in Table 4.6. In addition, comparison of compressive modulus and compressive strength of these materials are presented in bar graphs in Figure 4.34. (a) and (b) respectively.

Table 4.6. Compressive modulus and strength of all thermal cured materials

Polymer	Compressive Modulus (MPa)	Compressive Strength (MPa)
PPF/VPA (80/20) - 3% BP	256.28±5.16	72.97±4.58
PPF/VPA (70/30) - 3% BP	117.26±12.44	47.57±2.48
PPF/VPA (60/40) - 3% BP	25.80±2.65	13.71±1.70
PPF/VPA (80/20) - 2% BP	173.17±21.04	46.60±10.72
PPF/VPA (70/30) - 2% BP	121.91±8.27	32.50±4.05
PPF/VPA (60/40) - 2% BP	9.77±1.77	17.76±0.52
PPF/VPES (80/20) - 3% BP	457.66±43.08	86.61±7.81
PPF/VPES (70/30) - 3% BP	835.97±6.16	118.57±24.54
PPF/VPES (60/40) - 3% BP	590.82±20.06	97.87±7.90
PPF/VPES (80/20) - 2% BP	407.91±7.41	75.45±10.14
PPF/VPES (70/30) - 2% BP	168.52±21.94	48.44±5.32
PPF/VPES (60/40) - 2% BP	318.38±55.54	52.88±15.53



(a)



(b)

Figure 4.33. (a) Compressive modulus and (b) compressive strength bar graphs

For PPF/VPES polymers, compressive modulus values were found to be between 169-836 MPa and compressive strength values were obtained between 18 and 119 MPa for the different compositions. On the other hand, compressive modulus of PPF/VPA materials were found to be between 10 and 256 MPa and compressive strength values were determined to be between 14 and 73 MPa for the different compositions. Increase in comonomer content negatively affected the compressive properties of PPF/VPA materials at both initiator contents (2 and 3 weight percent). For PPF/VPES materials cured with 3 percent BP, lowest compressive modulus and strength were obtained from the 80/20 composition and highest compressive modulus and strength were obtained from the 70/30 composition. However, for the PPF/VPES (70/30) and (60/40) formulations, increase in VPES content decreased compressive modulus and strength of the materials. For thermally cured PPF/VPES samples in the presence of 2 percent BP, increase in VPES content generally decreased the compressive modulus and strength of these materials. Also, compressive modulus and strength of PPF/VPES polymers were found to be higher than those of PPF/VPA polymers at all compositions. This result can be justified by the non-

porous structure of PPF/VPES polymers. PPF/VPA polymers on the other hand exhibited porous structure as confirmed via SEM analysis of the fracture surfaces of these materials. Porosity is expected to decrease the compressive modulus and strength of a material.

It is known that compressive modulus and strength of a human bone vary with bone density. Compressive moduli of a human trabecular bone range between 10 and 1000 MPa and compressive strength values vary between 0.5 and 70 MPa. Thus, our results indicate that the PPF copolymers can be easily utilized with or without inorganic additives (e.g. β -TCP) as scaffolds in bone tissue engineering applications [69].

4.9. IN VITRO DEGRADATION

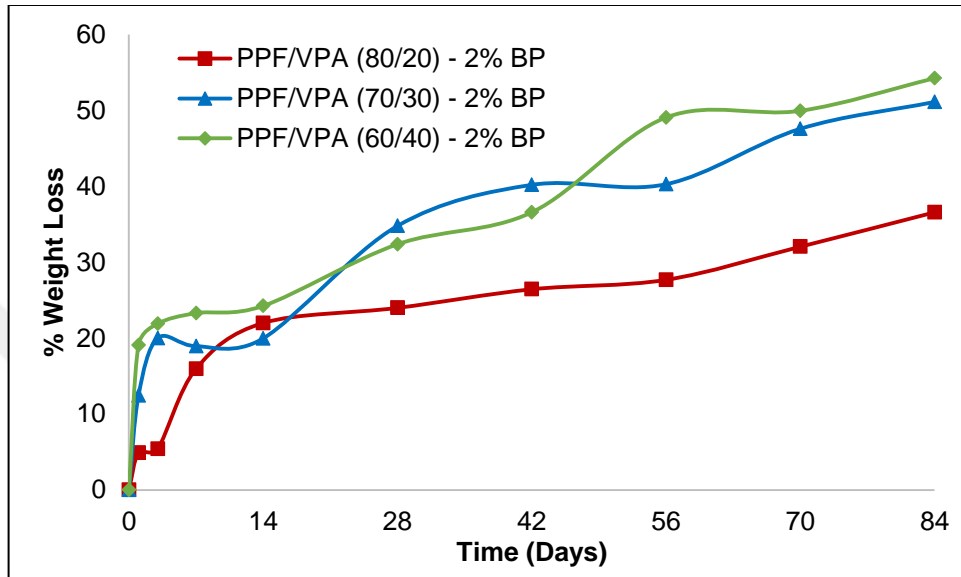
4.9.1. In Vitro Degradation of Thermal Cured Polymers

Biodegradation of the thermal cured PPF/VPA and PPF/VPES polymer samples was followed via both weight change and pH change measurements in 0.9 percent Na Azide containing 1X PBS buffer solution (pH=7.4) at 37°C.

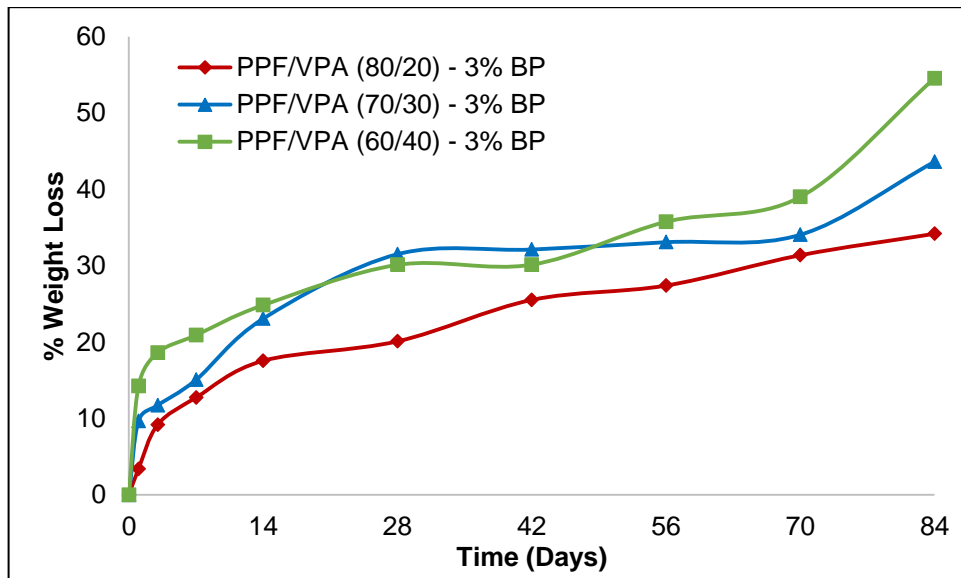
4.9.1.1. Analysis of Biodegradation via Weight Loss Measurements

Figure 4.35. (a) and (b) show percentage weight loss versus time plots of thermally cured PPF/VPA polymers cured with 2 and 3 percent initiator contents in pH=7.4 (1X) PBS solution for 84 days, respectively. When the weight loss profiles of the PPF/VPA polymers are analyzed, it can be observed that biodegradation rate of these materials differed according to the comonomer and initiator content. At the end of 84 days, percentage weight losses of the PPF/VPA polymers were determined to be between 30 and 55 percent. From these graphs, it can be postulated that the biodegradation rate of these polymers were faster in the first 7 to 14 days. After this period, a decrease in biodegradation rate was observed. The higher initial weight loss of PPF/VPA polymers can be explained by the leakage of VPA comonomers or VPA homopolymer which were not incorporated into the network structure. The following slower weight loss of PPF/VPA polymers can be attributed to the hydrolysis of PPF polyester structure. For both initiator contents, the

weight loss at the end of 84 days increased with increasing VPA content. And it can be generally claimed that the biodegradation rate of PPF/VPA materials increased with increasing VPA content.



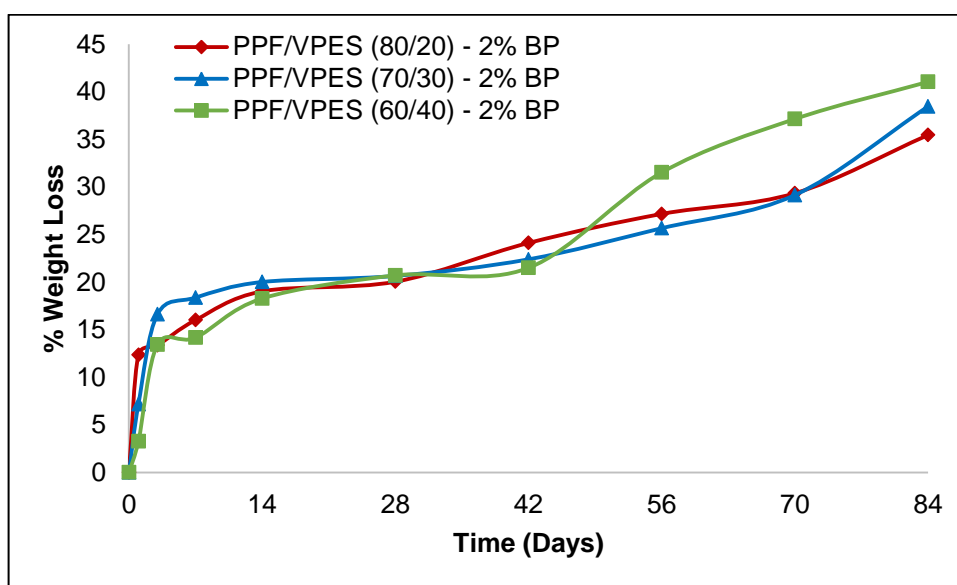
(a)



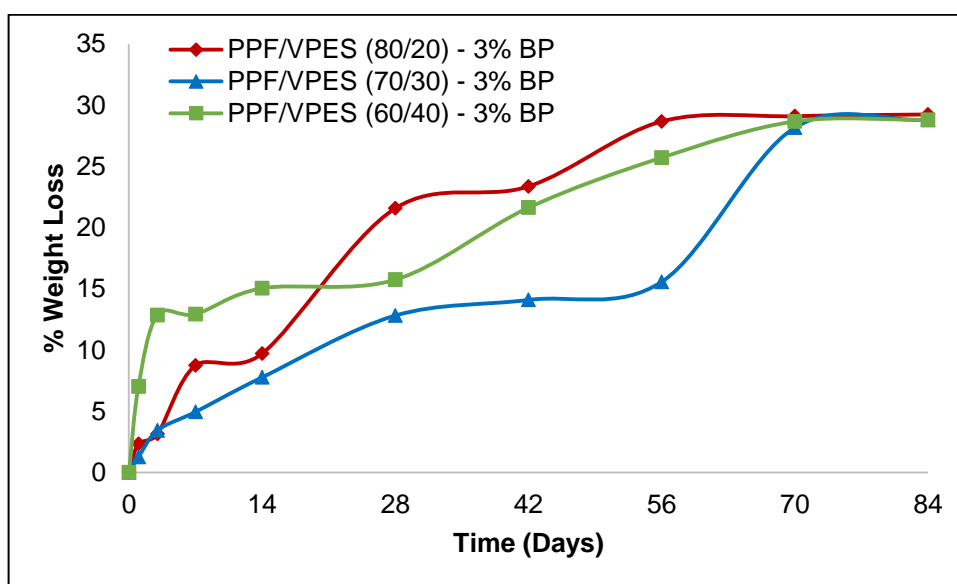
(b)

Figure 4.34. Weight loss versus time graphs of (a) 2 percent BP and (b) 3 percent BP containing PPF/VPA samples

Figure 4,35. (a) and (b) show percentage weight loss versus time plots of thermally cured PPF/VPES polymers cured with 2 and 3 percent initiator contents in pH=7.4 (1X) PBS solution for 84 days, respectively. Biodegradation rate of PPF/VPES polymers in the first 7-14 days was higher and after this period there was a slower weight loss and degradation similar to the PPF/VPA polymers. Higher degradation rate of these materials in the first 7 to 14 days can also be explained by the release of VPES comonomer or VPES homopolymer which was not incorporated in the network structure. Similarly, after 14 days, the slower weight loss occurred due to hydrolysis of the PPF polyester structure. The biodegradation rates of PPF/VPES polymers were also affected by the VPES comonomer and initiator content. At the end of 84 days, percentage weight losses of these samples were determined to be between 28 and 41 percent. When PPF/VPES samples cured with 2 percent BP are analyzed, it can be seen that percentage weight loss at the end of 84 days increased with increasing VPES content. For PPF/VPES samples cured with 3 percent BP, the PPF/VPES (80/20) composition showed the highest biodegradation rate when compared with other compositions. For the degradation related to PPF hydrolysis the PPF/VPES (60/40) composition with the higher VPES content degraded more than the PPF/VPES (70/30) composition. The higher biodegradation rate of the PPF/VPES (80/20) composition may be related to the lower cross-link density of this material due to initial higher viscosity.



(a)



(b)

Figure 4.35. Weight loss versus time graphs of (a) 2 percent BP and (b) 3 percent BP containing PPF/VPES samples

Figure 4.36 and 4.37 show percentage weight loss versus time plots of thermally cured (70/30) PPF/VPA and PPF/VPES polymers cured with 2 and 3 percent initiator, which were plotted to compare polymers in terms of used initiator amount. Increasing amount of BP from 2 to 3 percent resulted in a decrease in weight loss which means a lower extent of biodegradation for both of the PPF copolymers.

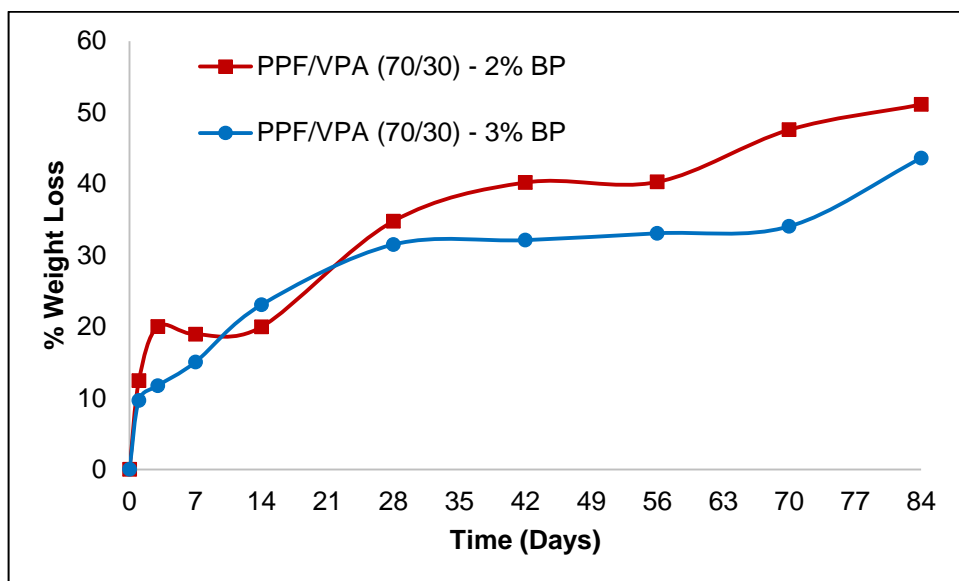


Figure 4.36. Comparison of weight loss profiles of 2 and 3 percent BP containing PPF/VPA (70/30) samples

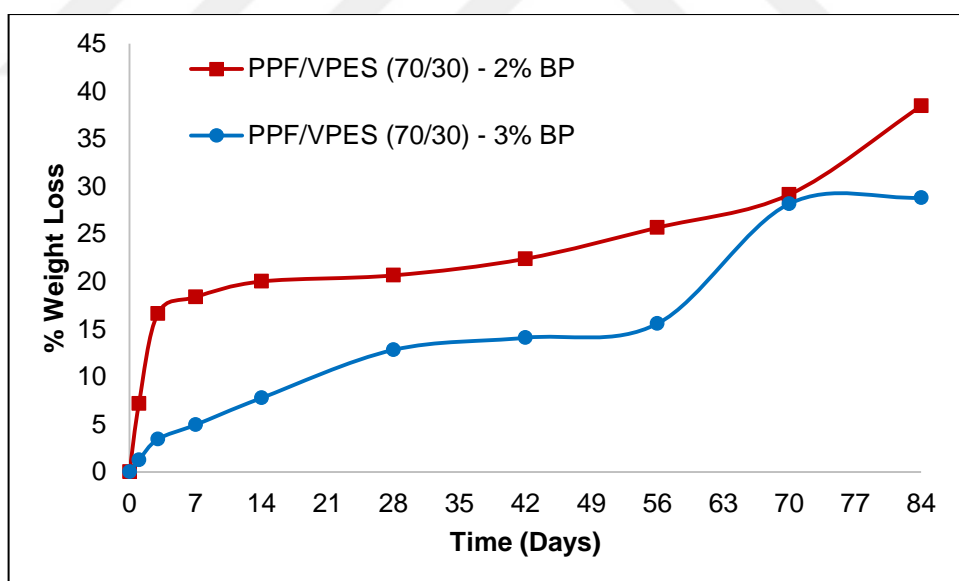
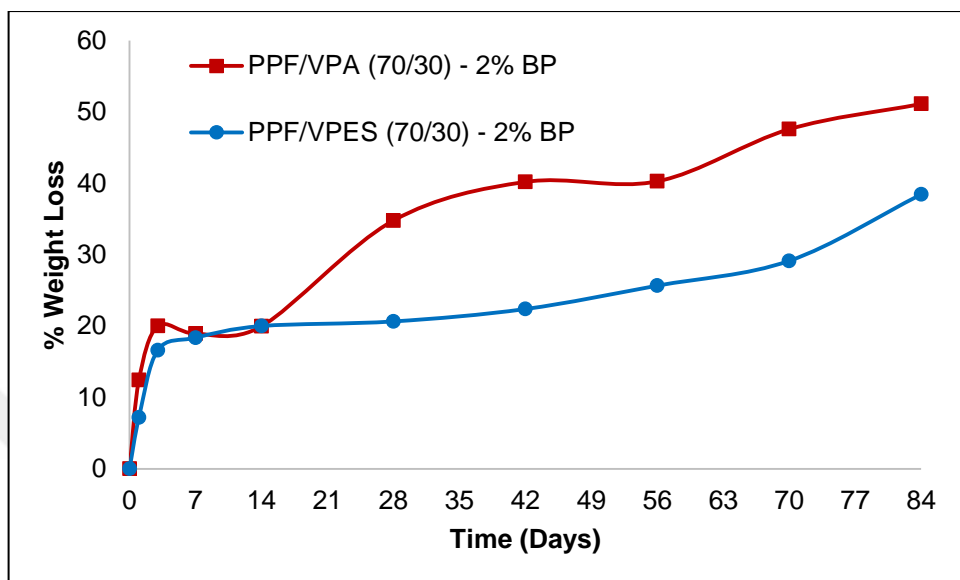


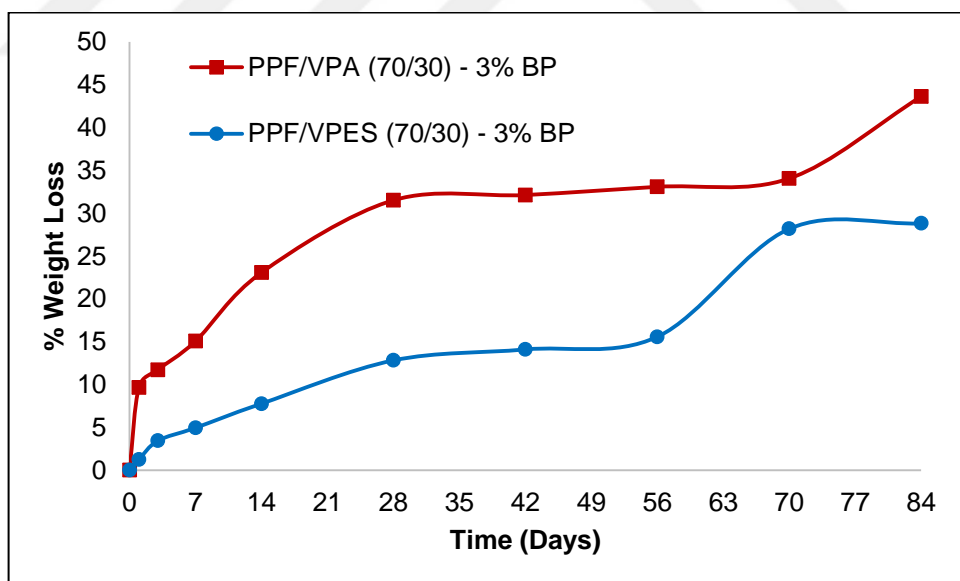
Figure 4.37. Comparison of weight loss profiles of 2 and 3 percent BP containing PPF/VPES (70/30) samples

Figure 4.38 shows percentage weight loss versus time plots of thermally cured (70/30) PPF/VPA and PPF/VPES copolymers cured with (a) 2 and (b) 3 percent initiator, which were plotted to compare copolymers in terms of comonomer type. PPF/VPA copolymers had higher weight loss which means higher biodegradation rate than PPF/VPES

copolymers for both initiator amounts. This result can be attributed to the porous structure of PPF/VPA copolymers.



(a)



(b)

Figure 4.38. Comparison of weight loss profiles of (a) 2 and (b) 3 percent BP containing PPF/VPA and PPF/VPES (70/30) samples

4.9.1.2. Analysis of Biodegradation via pH Track

Since degradation products of PPF/VPA and PPF/VPES polymers contain acidic contents, degradation profiles of these samples in 1X PBS buffer solution (pH =7.4) were tracked by pH change. Rate of decrease in pH is proportional to rate of degradation.

Figures 4.39 and 4.40. show the pH change results of PPF/VPA samples cured with 3 and 2 weight percent initiator content, respectively. For all compositions, VPA or VPA homopolymer that couldn't incorporate into the crosslinked structure was initially released to the buffer and the VPA and fumaric acid which come from degradation of the network were released to the buffer subsequently and therefore the pH decreased significantly in the first seven days. After this significant decrease in pH, a slower decrease was observed for the samples cured with 3 weight percent initiator and a plateau was reached for samples cured with 2 weight percent initiator. For samples cured with 2 weight percent initiator the degradation rate increased with increasing VPA content, since a lower pH indicates a higher extent of degradation. This trend was true for samples cured with 3 weight percent initiator till 20 days. This trend contradicts the cross link density analysis which indicated an increase in cross-link density with increasing VPA content. This result can be explained by the fact that VPA is acidic and more VPA or VPA homopolymer may have been released to the buffer with increasing VPA content.

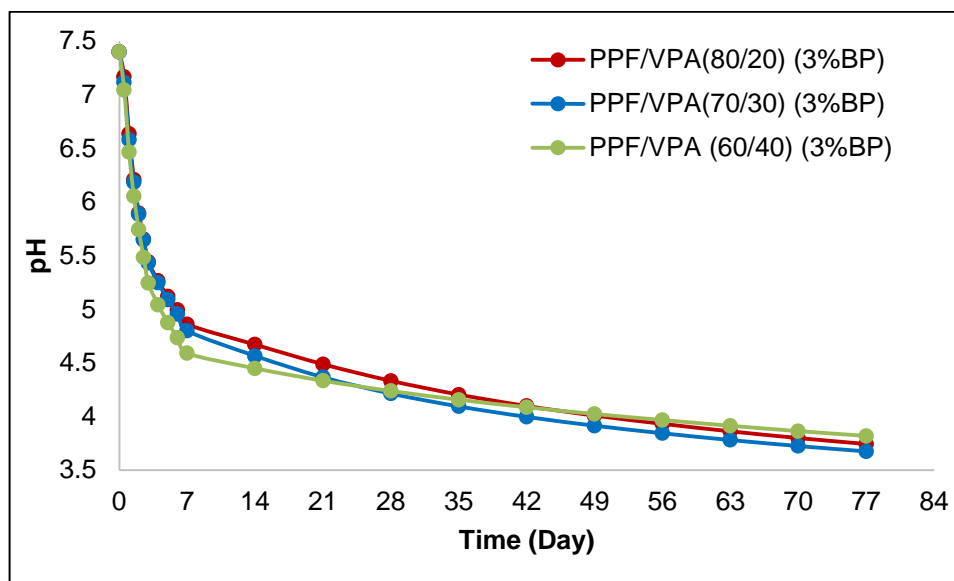


Figure 4.39. pH versus time graphs of 3 percent initiator containing PPF/VPA samples

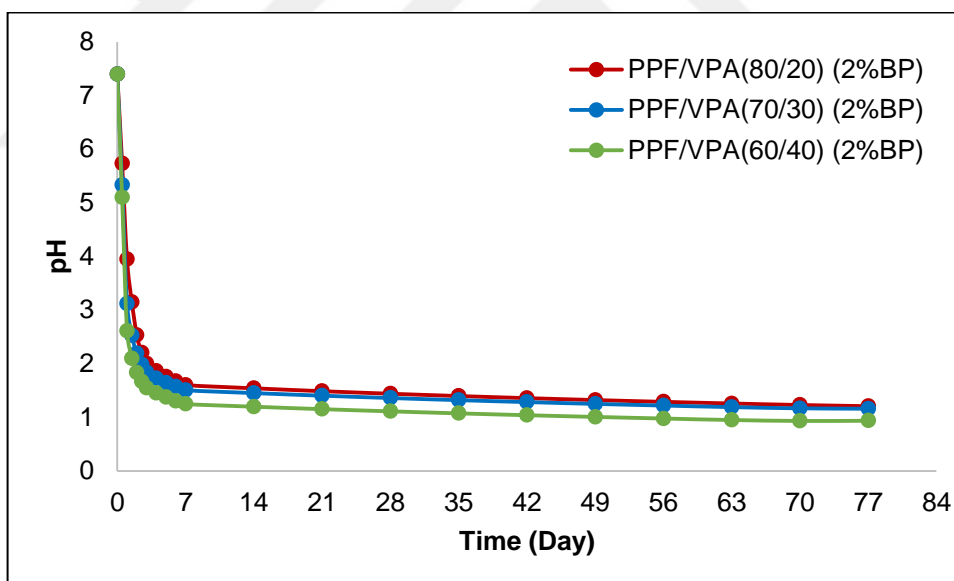


Figure 4.40. pH versus time graphs of 2 percent initiator containing PPF/VPA samples

Figures 4.41 and 4.42 show pH change results of PPF/VPES samples cured with 3 and 2 weight percent initiator content, respectively. Again similar profiles were observed, first there was a sudden decrease in pH due to release of VPES or VPES homopolymer that were not incorporated into network structure, and then a plateau was reached where pH decrease was less significant. Here again for samples cured with 3 weight percent

initiator, degradation rate increased with increasing VPES content. For samples cured with 2 weight percent initiator, the slowest degradation rate was observed in the 80/20 PPF/VPES sample, and compositions of 60/40 and 70/30 followed it. Samples cured with 3 weight percent initiator exhibited pH values in the range of 1.5 and samples cured with 2 weight percent initiator reached pH values in the range of about 4.0 at the end of 84 days. This result can be justified by the higher crosslink density of samples cured with 2 weight percent initiator which caused a lower degradation rate and a lower pH change within the same time interval.

Although initially, a large drop in pH was observed in PBS buffer solution (pH=7.4), as decrease in pH, in other words H^{1+} ion concentration, was calculated cumulatively, actual decrease in pH was not dramatic.

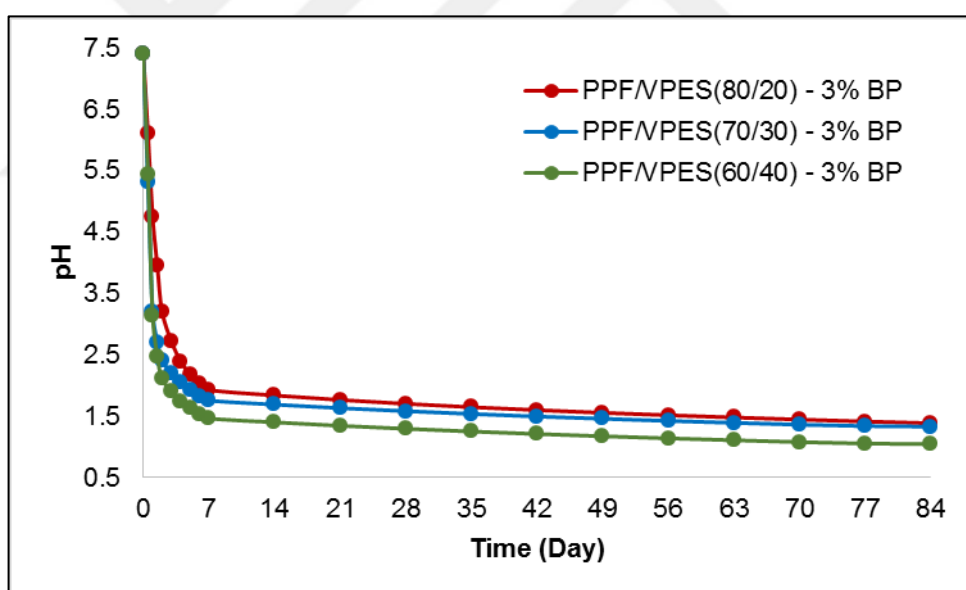


Figure 4.41. pH data of 3 percent initiator containing PPF/VPES samples

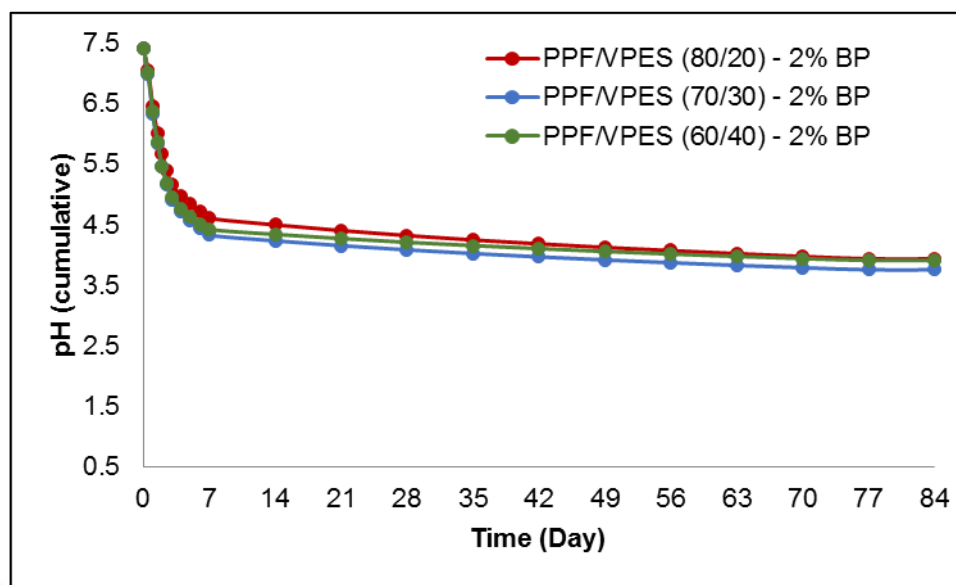


Figure 4.42. pH data of 2 percent initiator containing PPF/VPES samples

In Figure 4.43. below, results of comparison of pH data of 2 and 3 percent initiator containing PPF/VPA samples are illustrated. The pH decrease was higher in 2 percent initiator containing sample which means degradation rate was higher than the 3 percent initiator containing sample.

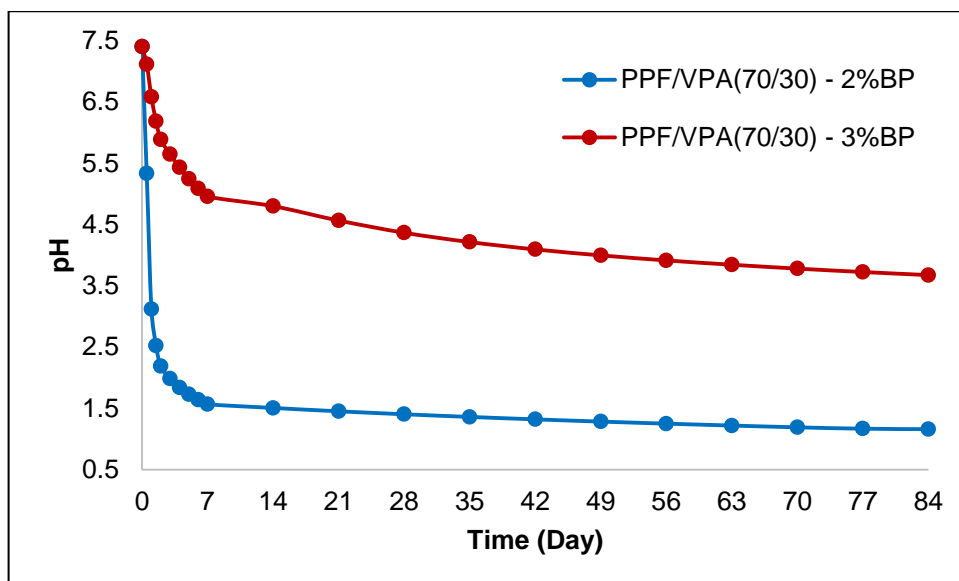


Figure 4.43. Comparison of pH data of 2 and 3 percent initiator containing PPF/VPA samples

In Figure 4.44 below, results of comparison of pH data of 2 and 3 percent initiator containing PPF/VPES samples are illustrated. Here, pH decrease was higher for the sample cured with 3 weight percent initiator which means degradation rate was higher as compared to sample cured with 2 weight percent initiator. These results are in agreement with the crosslink density results which indicated a higher crosslink density at 2 weight percent initiator content for PPF/VPES samples and a higher crosslink density at 3 weight percent initiator content for PPF/VPA samples.

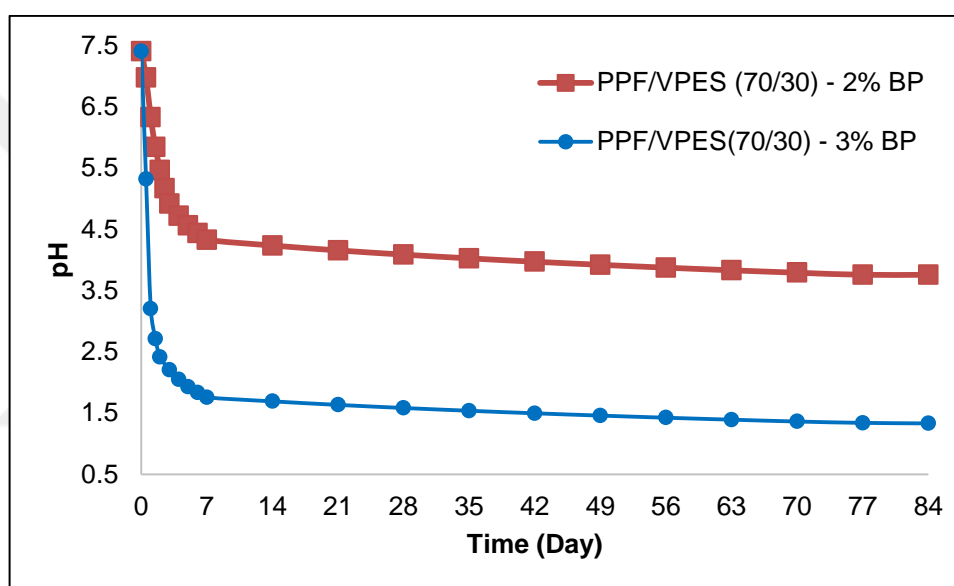


Figure 4.44. Comparison of pH data of 2 and 3 percent initiator containing PPF/VPES samples

In Figure 4.45 below, results of comparison of pH data of 2 percent initiator containing PPF/VPA and PPF/VPES samples are illustrated. Here, the decrease in pH was higher for PPF/VPA sample which means its degradation rate was higher than the PPF/VPES sample or this result can also be attributed to the higher acidity of VPA comonomer.

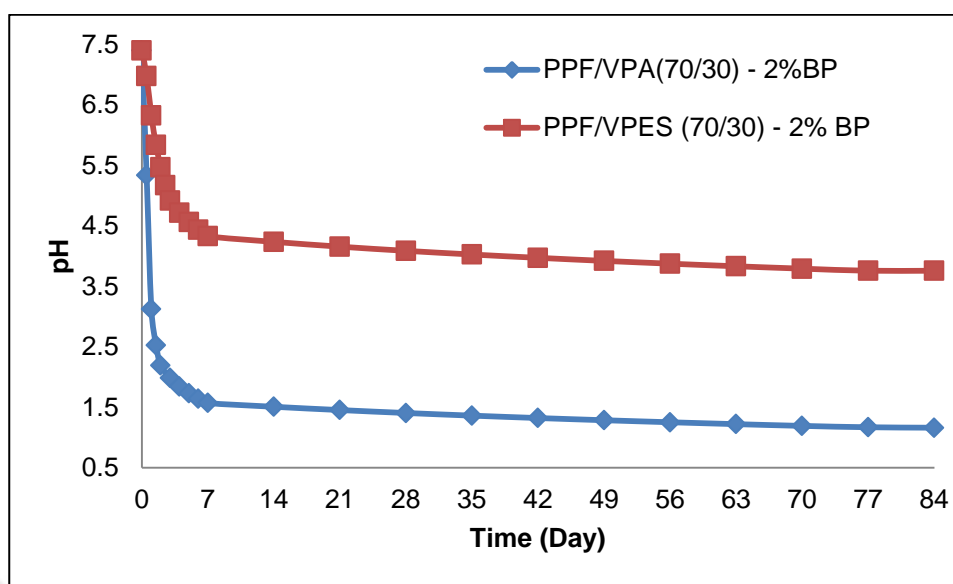


Figure 4.45. Comparison of pH data of 2 percent initiator containing PPF/VPA and PPF/VPES samples

In Figure 4.46 below, results of comparison of pH data of 3 percent initiator containing PPF/VPA and PPF/VPES samples are illustrated. It can be seen that the decrease in pH was higher for the PPF/VPES sample and the degradation rate was also higher for the PPF/VPES sample than the PPF/VPA sample. This result can be attributed to the less efficient crosslinking of the PPF/VPES copolymer at 3 percent initiator content.

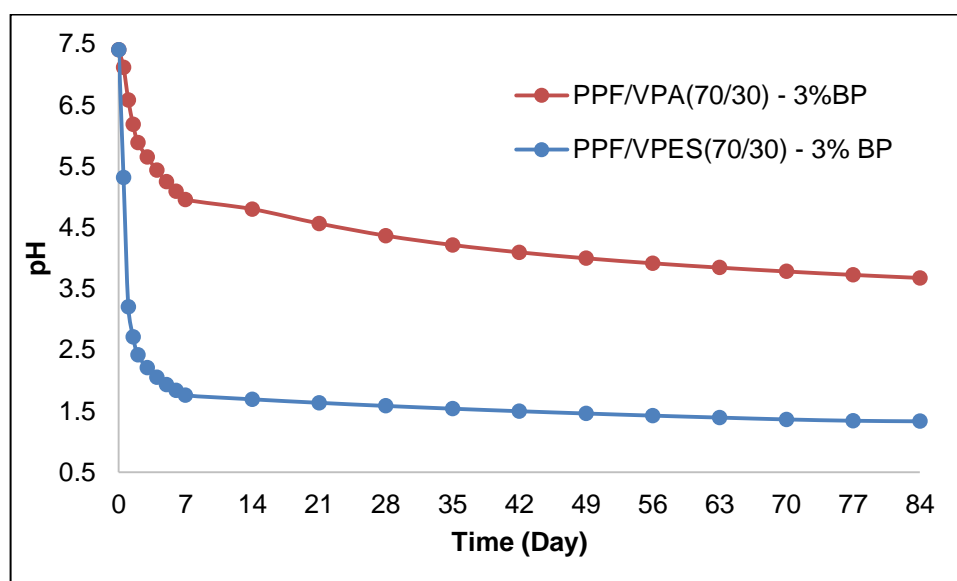


Figure 4.46. Comparison of pH data of 3 percent initiator containing PPF/VPA and PPF/VPES samples

4.9.2. *In Vitro* Degradation of UV Cured Polymers

Biodegradation of the UV cured PPF/VPA and PPF/VPES polymer samples was followed via both weight change and pH change measurements in 0.9 percent Na Azide containing 1X PBS buffer solution (pH=7.4) at 37°C.

4.9.2.1. *Analysis of Biodegradation via Weight Loss Studies*

In Figure 4.47 below, weight loss profiles of all UV cured polymers over time is presented. Like the thermal cured samples, while biodegradation rate of these UV cured polymers was faster in the first seven days, after this period, a decrease in biodegradation rate was observed. This initial weight loss was caused by release of unreacted or homopolymerized VPA and VPES comonomers. Higher initial weight loss of UV cured PPF/VPA polymers than that of the PPF/VPES polymers can be explained by higher reactivity of VPES comonomer at radical copolymerization with fumarate double bonds.

The reason of the lower weight loss, in other words the lower biodegradation rate of PPF/VPES polymers than the PPF/VPA polymers, is the more efficient UV cure of PPF/VPES polymers than the PPF/VPA polymers.

Weight loss values of UV cured PPF/VPES polymers at the end of 84 days were similar to percentage weight loss values of thermal cured PPF/VPES polymers at the end of 84 days for similar compositions. Percentage weight loss values of thermal cured PPF/VPA polymers at the end of 84 days on the other hand, were approximately 20 percent lower than the percentage weight loss values of UV cured PPF/VPA polymers at the end of 84 days for similar compositions. This situation can be understood as UV cure is not as effective as thermal cure for PPF/VPA compositions.

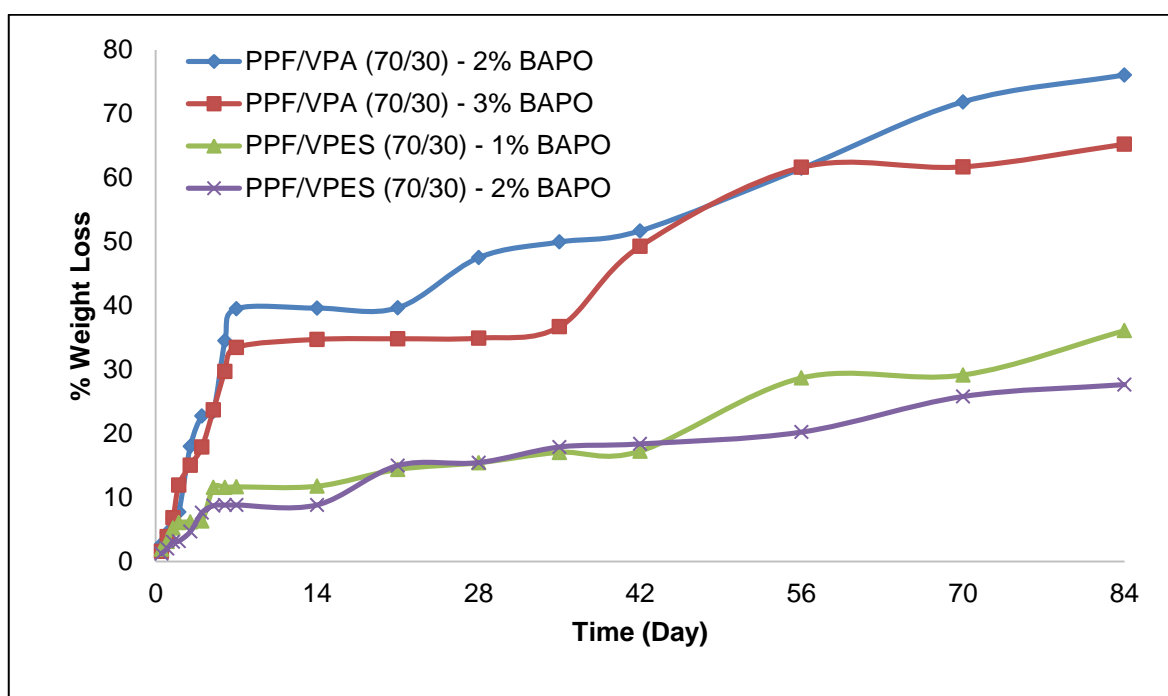


Figure 4.47. Weight loss profiles of all UV cured polymer compositions

4.9.2.2. Analysis of Biodegradation via pH Track

Figures 4.48 and 4.49 show the pH change results over time of UV cured PPF/VPA and PPF/VPES samples, respectively.

Similar to the thermal cured PPF/VPA samples, for all compositions, VPA or VPA homopolymer formed that could not incorporate into the crosslinked structure was initially released to the buffer and decreased the pH significantly within first few days and the VPA and fumaric acid which come from degradation of the network were released to the buffer subsequently. After the initial significant decrease in pH, a plateau was reached for all samples.

For UV cured PPF/VPES samples, similar profiles were observed with thermal cured PPF/VPES samples, first there was again a fast, considerable decrease in pH due to release of VPES or VPES homopolymer that could not incorporate into network structure. Then a plateau was reached where pH decrease was less significant due to network degradation.

When the effect of comonomer was examined at the same initiator (BAPO) content (2wt percent), the decrease in pH was found to be significantly higher for UV cured PPF/VPA samples than the UV cured PPF/VPES samples within the same time period which means the degradation rate of PPF/VPA polymers was higher than that of the PPF/VPES polymers. This result is in agreement with the weight loss results. In addition the higher acidity of VPA comonomer should also contribute to this result.

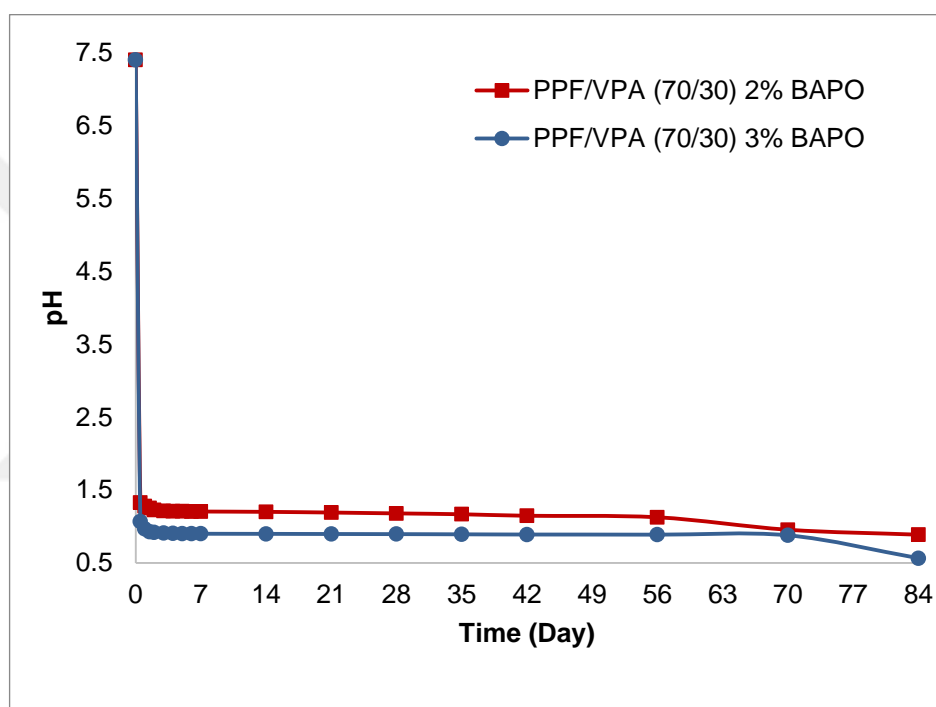


Figure 4.48. pH track of UV cured PPF/VPA polymers

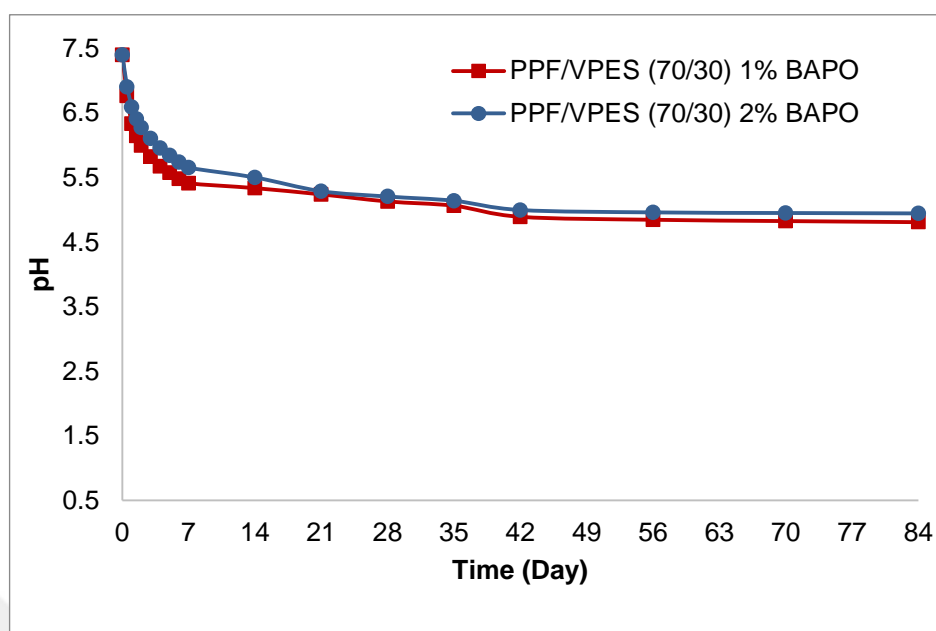


Figure 4.49. pH track of UV cured PPF/VPES polymers

4.10. *IN VITRO* CELL INTERACTION STUDIES OF THERMAL CURED SAMPLES

Human osteoblast cells (HOBs) (The European Collection of Cell Cultures, UK) (Cell line no. 406-05a) were seeded into cell culture plates by dissolving in no-phenol red Low Glucose DMEM which contains 10 percent Fetal Bovine Serum, 50 μ M ascorbic acid and 1 percent Pen-Strep, and incubated at 37°C, 5 percent CO₂ and 90 percent humidity. Cell culture medium was replaced twice a week. When the cells reached confluency, they were passaged with Gibco™ TrypLE Express (1X) without phenol red.

PPF based polymers with different formulations were sterilized before cell seeding by 1 hour long UV exposure to both sides (1.2 cm x 1.2 cm) and placed into well plates afterwards. Cells were seeded with concentration of 5×10^3 cells per well and incubated throughout 21 days.

In vitro cell interaction studies of UV cured samples are not presented in this thesis, because these results were prepared and presented as the master thesis of YUTEG lab member, Begüm Okutan.

4.10.1. MTS Assay of Thermal Cured Polymers

After (5000 cells/ well) cell seeding, cell proliferation was determined by applying CellTiter 96® AQueous One Solution Cell Proliferation Assay (MTS) to the samples and control groups at the time points of 1st 7th 14th and 21st days [59]. Results are illustrated on a graph that demonstrates the amount of alive cell as a function of time for the different PPF/VPA and PPF/VPES compositions (Figure 4.50.).

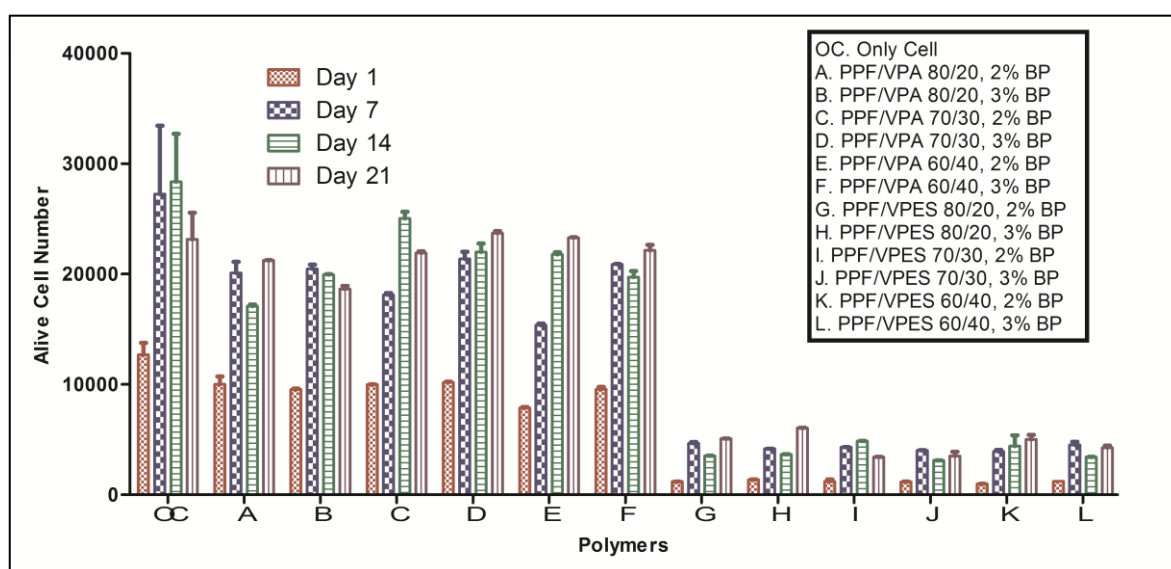


Figure 4.50. Cell proliferation on the thermal cured polymers

Cell number significantly increased throughout incubation time for all polymers. For the VPES containing samples less cell attachment was observed compare to the VPA containing ones at day one. While approximately 1000 cells attached on VPES containing samples, almost 10000 cells were found to attach on VPA containing ones. The main reason of this could be due to poreless, smooth and film-like surfaces of PPF/VPES samples. The majority of the seeded cells might be leaked under the polymer, before cell attachment. This dilemma can be eliminated by performing NaCl etching to VPES containing samples.

When PPF/VPA samples are compared between each other, the better cell proliferation results were obtained from PPF/VPA 70/30 compositions for both initiator amounts.

Although, there was no dramatic difference between these two compositions, it can be said that PPF/VPA 70/30 – 2% BP sample supported cell proliferation better than PPF/VPA 70/30 – 3% BP sample.

When PPF/VPES samples are compared between each other, it can roughly be generalized that PPF/VPES samples cured with 2 percent initiator supported cell proliferation better than 3 percent initiator containing samples but as discussed before, PPF/VPES 70/30 – 3% BP composition was an exception for this trait.

When 2 and 3 percent BP containing samples are compared between each other, in general, the better cell proliferation results were observed when 2 percent initiator was used for PPF/VPA samples and 3 percent initiator was used for PPF/VPES samples.

The decrease in cell number after day 14 which was observed for 2 percent BP containing PPF/VPA (70/30) samples was not a result of toxicity. It was due to overproliferation of cells. When cells can't find any blank space to attach on material, they start to detach and die [70].

4.10.2. Scanning Electron Microscopy of Thermal Cured Cell Seeded Polymers

Scanning electron microscopy images of all thermal cured polymers which were cultivated for determined time period are presented on Figure 4.51. Scanning electron microscopy was performed in order to observe morphological appearance, attachment and proliferation properties of HObs on designed polymers.

HObs are adherent cells that grow on a surface. It was observed that the cells liked to attach onto all polymers and proliferated rapidly. Observed morphologies of HObs cells were typical. Cell sheets that coated polymer surfaces were determined. Most of the cells produced extracellular matrix. Micrographs of day 7 and day 28 can be easily distinguished. All surfaces were confluent before day 28, while detachments were also observed. Seeded cells extensively proliferated and spreaded.

In summary, all compositions have characteristic features to support cell attachment and growth.

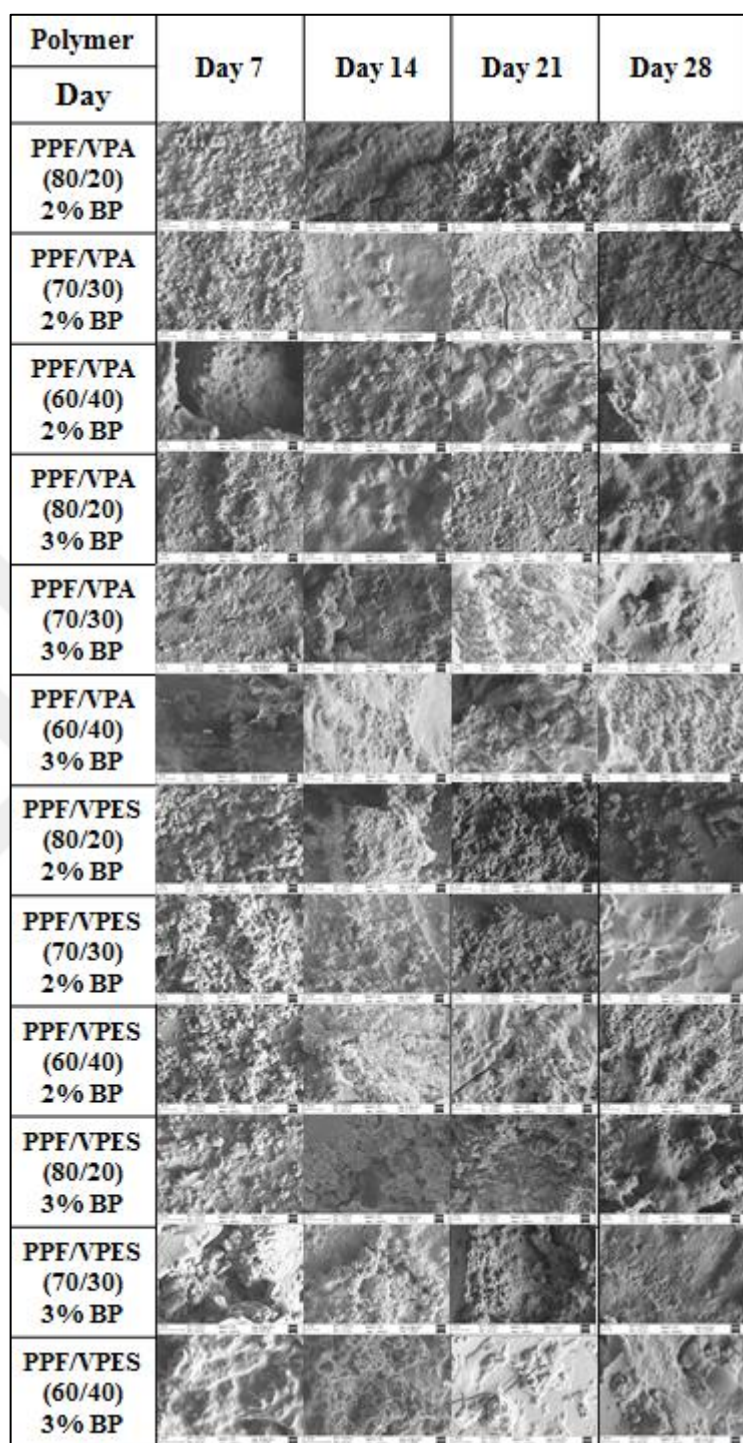


Figure 4.51. Scanning electron micrographs of cell seeded thermal cured polymers after 7, 14, 21 and 28 days of incubation

4.10.3. Determination of Mineralization by von Kossa Staining of Thermal Cured Polymers

Mineral depositions on the cured polymers were detected by von Kossa staining. Images of stained polymers at day 7, 14, 21 and 28 are presented in Figure 4.52. - 4.55. As the figures demonstrate, the materials in which the seeded cells were cultivated by the osteogenic differentiation medium, were stained darker than the materials in which the seeded cells were grown in the normal medium. The colour darkening is directly proportional to the amount of calcium deposits.

As it is obvious from figures, darkening of both samples cultivated with normal and osteogenic media increased throughout incubation time, which was an expected result. As mineral decomposition amount increases, stained minerals in other words staining amount increases.

When we compare the materials of osteogenic differentiation group, in terms of comonomer type, it is noticed that materials containing VPES were stained lighter than VPA-containing materials. This result was correlated with the MTS results. As a result of surface morphology, VPA-containing samples had a ten-fold cell attachment compared to VPES-containing samples.

Colour changes also occurred in the normal cell growth media group, because the cells used were already human osteoblast cells, but the mineralization on these samples were less than the samples in bone differentiation medium [15,16].

When results of first 14 days were considered, darkening of the PPF/VPA polymers cured with 3 percent of initiator were higher than 2 percent initiator containing ones, on the other hand, for PPF/VPES polymers just the opposite result was obtained. But after 14 days, colour density difference between samples in terms of initiator amount became impossible to notice by naked eye. Samples cured with two percent of initiator darkened as much as samples cured with three percent of initiator. This can be understood as changing initiator amount from two percent to three percent did not cause a significant difference in terms of mineral decomposition of the samples.

Among the samples cultivated in normal cell growth media, in first 14 days, PPF/VPA samples were darker than PPF/VPES samples, which was an expected result when MTS results were considered. But here again, after 14 days, there was no notable difference between PPF/VPA and PPF/VPES samples. This can be explained as both polymeric systems support extracellular matrix formation and mineralization nearly equally and good enough. When samples were cultivated in osteogenic media, colour difference was barely distinguishable from very first day. But still, for 14 days PPF/VPA polymers resulted in slightly darker colour when compared to PPF/VPES samples. This result was also in correlation with MTS results. But also here, after 14 days, there was no colour difference between samples since all of the samples were good at mineralization and cell proliferation and good candidates as bone tissue scaffolds.

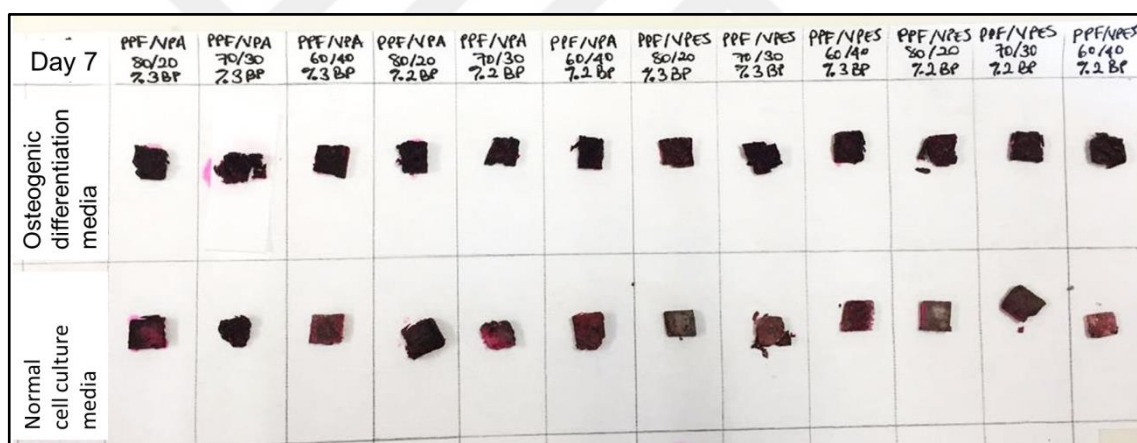


Figure 4.52. Von kossa staining of all thermal cured polymers at day 7

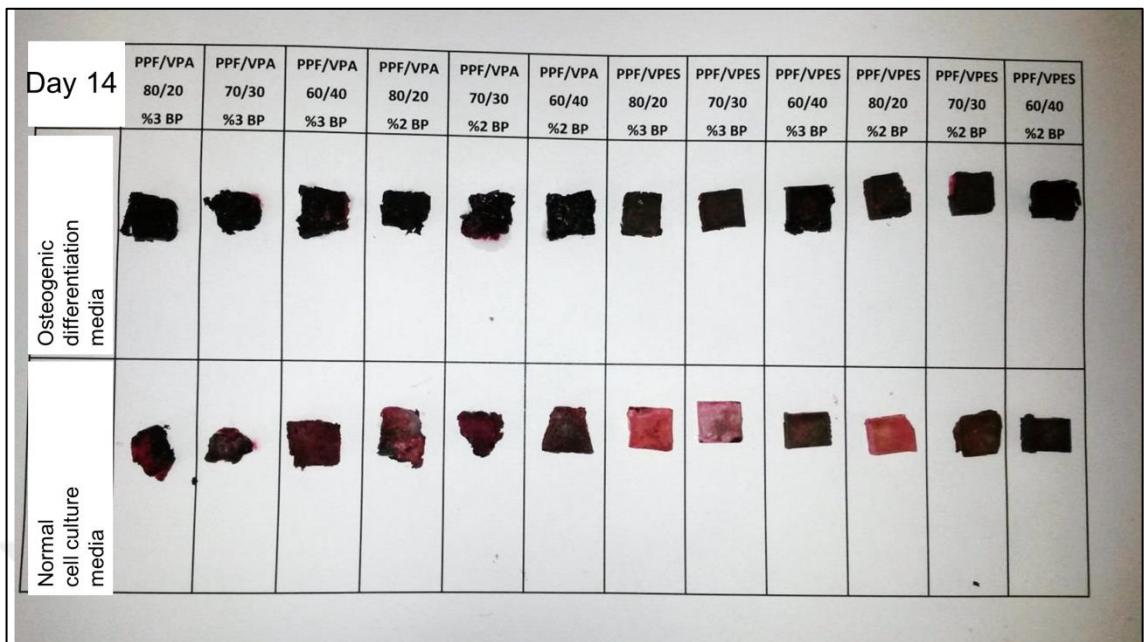
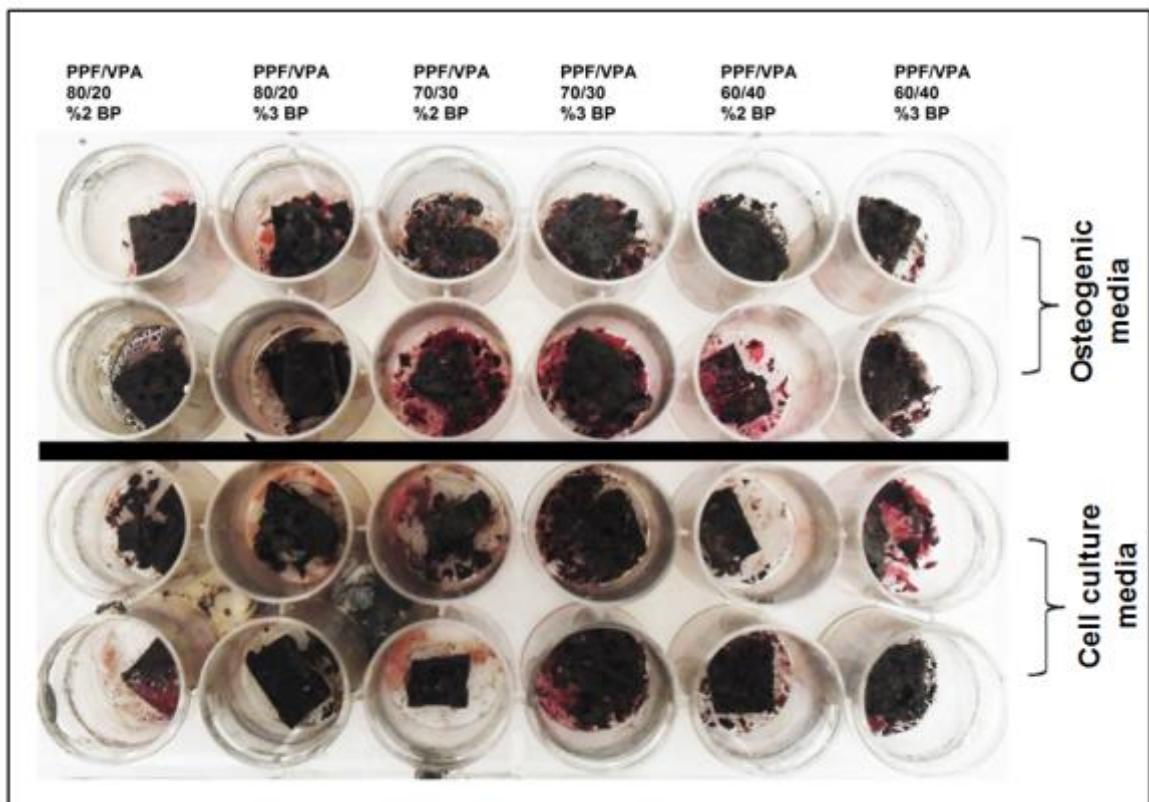
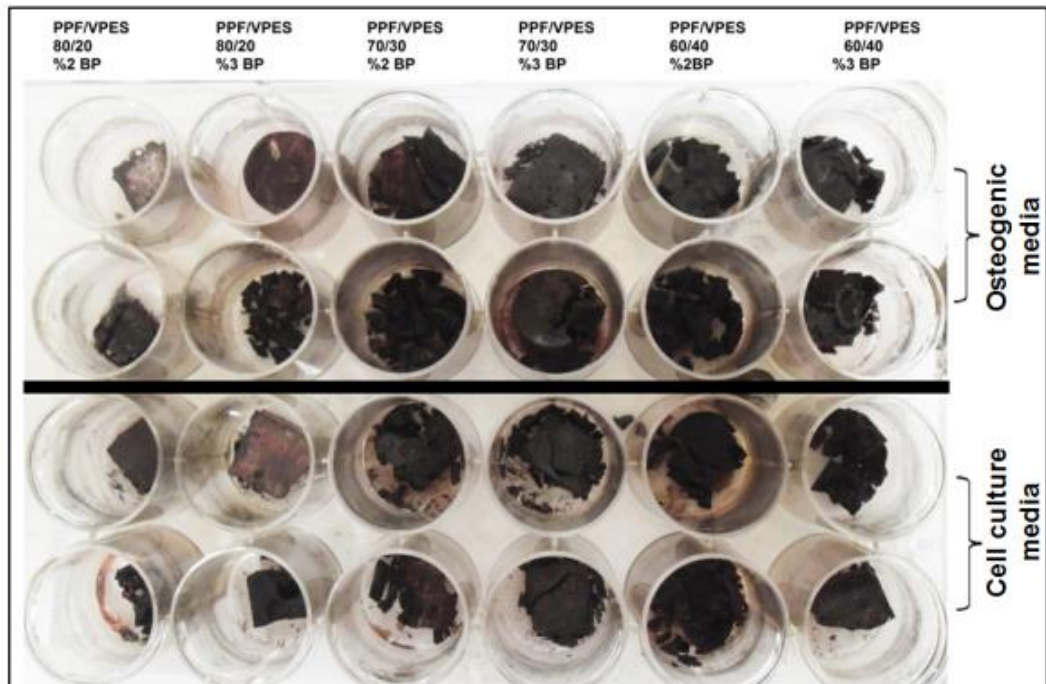


Figure 4.53. Von kossa staining of all thermal cured polymers at day 14

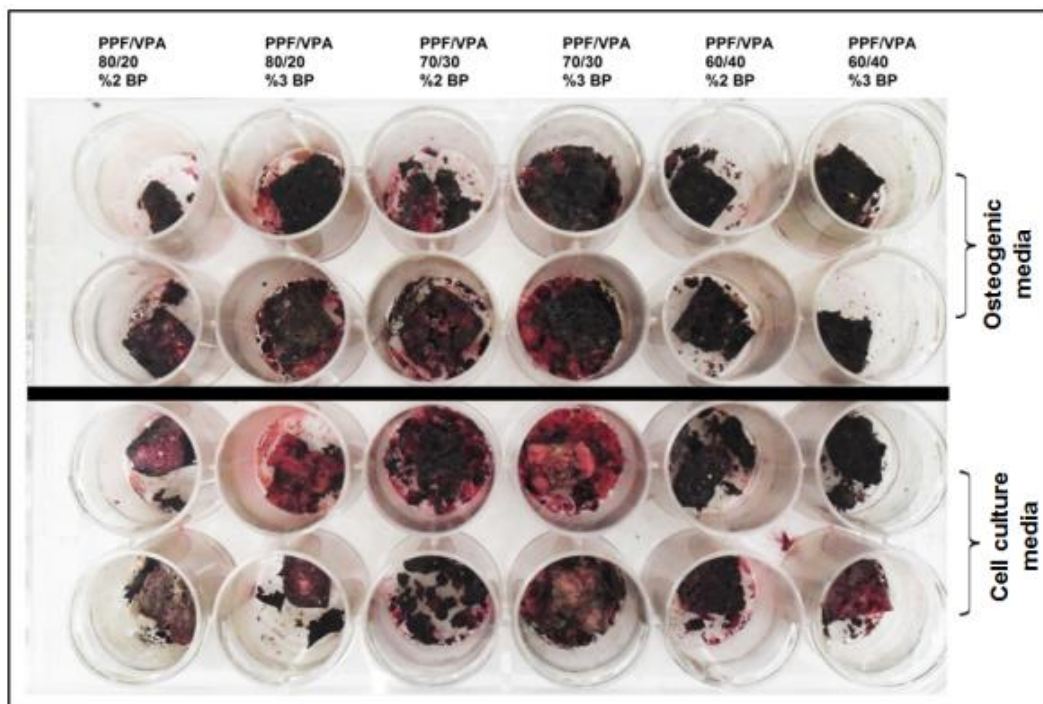


(a)

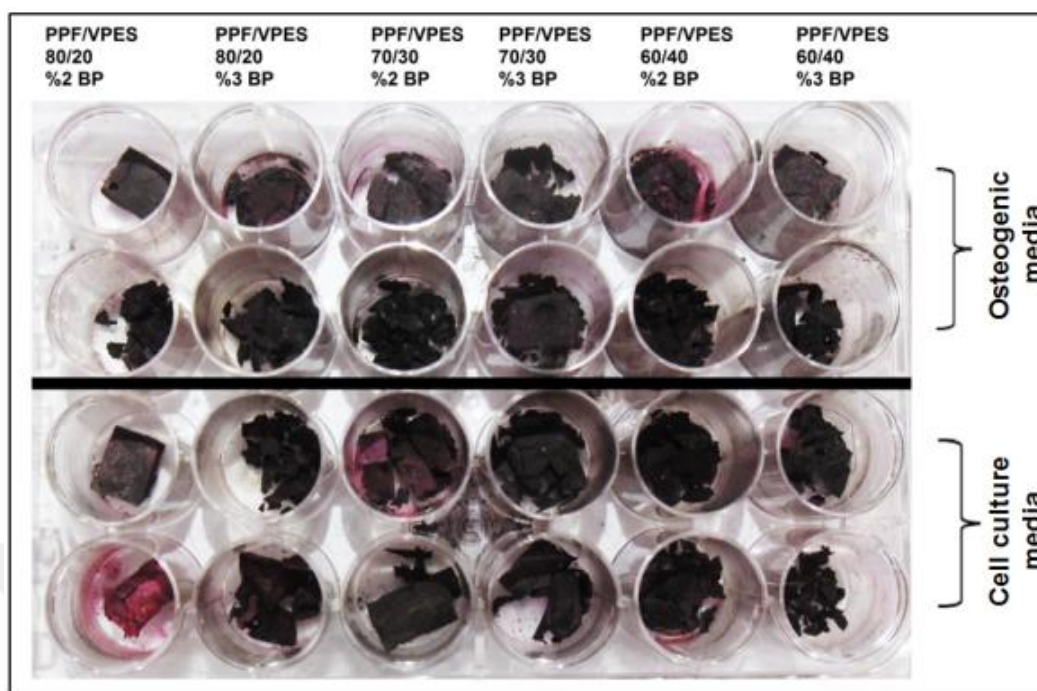


(b)

Figure 4.54. Von Kossa staining images of thermal cured (a) PPF/VPA and (b) PPF/VPES polymers at day 21



(a)



(b)

Figure 4.55. Von Kossa staining images of thermal cured (a) PPF/VPA and (b) PPF/VPES polymers at day 28

4.10.4. Determination of ALP Activity of Thermal Cured Polymers

Alkaline phosphatase activities of thermal cured polymers are illustrated in Figure 4.56. Alkaline phosphatase is an early marker in bone formation. For this reason, in general, a rapid increase in early periods and a decrease in concentration level as time progresses are observed. When collectively considered, it can be said that results were complied with this profile. A decrease from day 7 to 14, an increase from day 14 to 21, and another decrease until day 28 were observed, and this profile is related to the growth-division cycles of the cells. To sum up, concentration change in ALP activity is cyclic [59]

When PPF/VPA samples are considered, increase in ALP concentration was more in PPF/VPA 70/30 samples than that of in 80/20 and 60/40 samples for both initiator amounts from day 14 to day 21. Accordingly, PPF/VPA 70/30 samples supported osteogenesis more than PPF/VPA 60/40 samples. Additionally, among PPF/VPA samples, it can be said that 2

percent initiator containing samples expressed higher ALP activity than 3 percent initiator containing ones.

When results of PPF/VPES samples were examined, it was observed that generally ALP concentration is lower than PPF/VPA samples. This was related to cell number attached on polymer surfaces as discussed before with MTS results. Among PPF/VPES samples, 60/40 compositions exhibited better ALP activity for both initiator amounts.

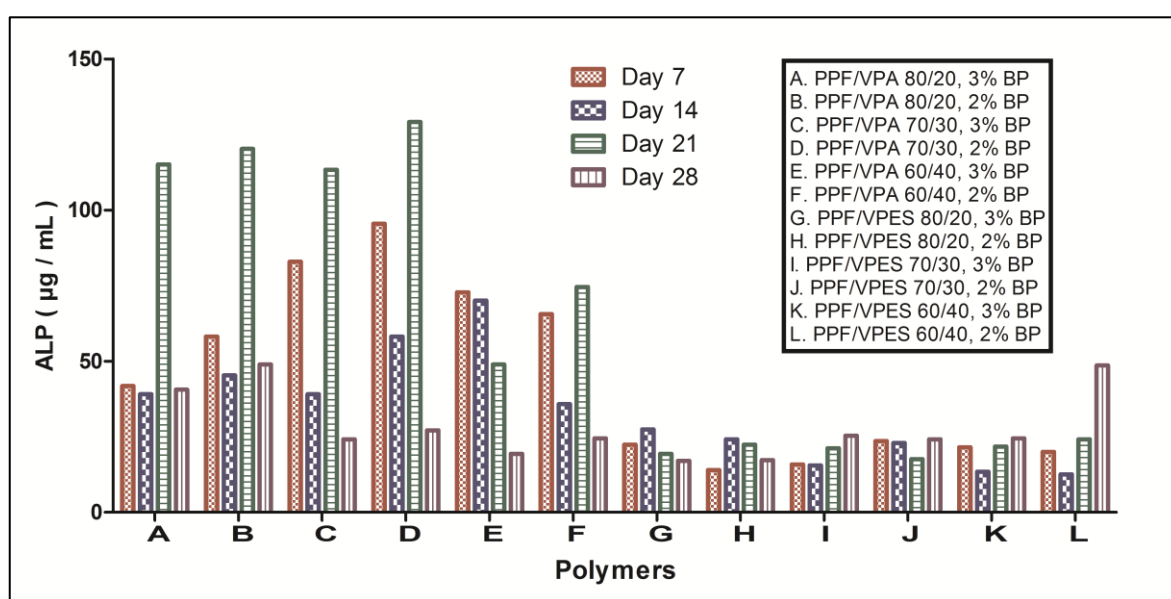


Figure 4.56. Alkaline phosphatase activity of HOB cells throughout 28 days of incubation on thermal cured samples

4.10.5. Determination of OST Activity of Thermal Cured Polymers

Osteocalcin activities of thermal cured polymers are illustrated in Figure 4.57. Osteocalcin is released by osteoblasts and is a bone marker. High osteocalcin levels are correlated with bone mineral density. Overall, in all samples, osteocalcin levels were increased on the days 7 and 14, and on the day 21 there was a slight decrease and on the day 28 there was an increase. This profile is related to the growth-division cycles of the cells. The increase in

day 28 was due to the introduction of osteocalcin released from newly dividing and proliferating cells.

The highest and preferred activities for samples containing both vinyl phosphonic acid (VPA) and vinyl phosphonic acid ester (VPES) were obtained in 70/30 compositions [64–68]. And among all the compositions, PPF/VPES 70/30 with 2 percent of initiator amount and PPF/VPA 70/30 with 3 percent of initiator amount samples showed significantly enhanced and preferable osteocalcin activity than all other samples.

Although there was a difference between PPF/VPA and PPF/VPES samples in terms of initial cell attachment and cell proliferation, osteocalcin activity results proved that PPF/VPES samples support osteogenesis as well as PPF/VPA samples and have potentials in terms of being bone tissue scaffolds.

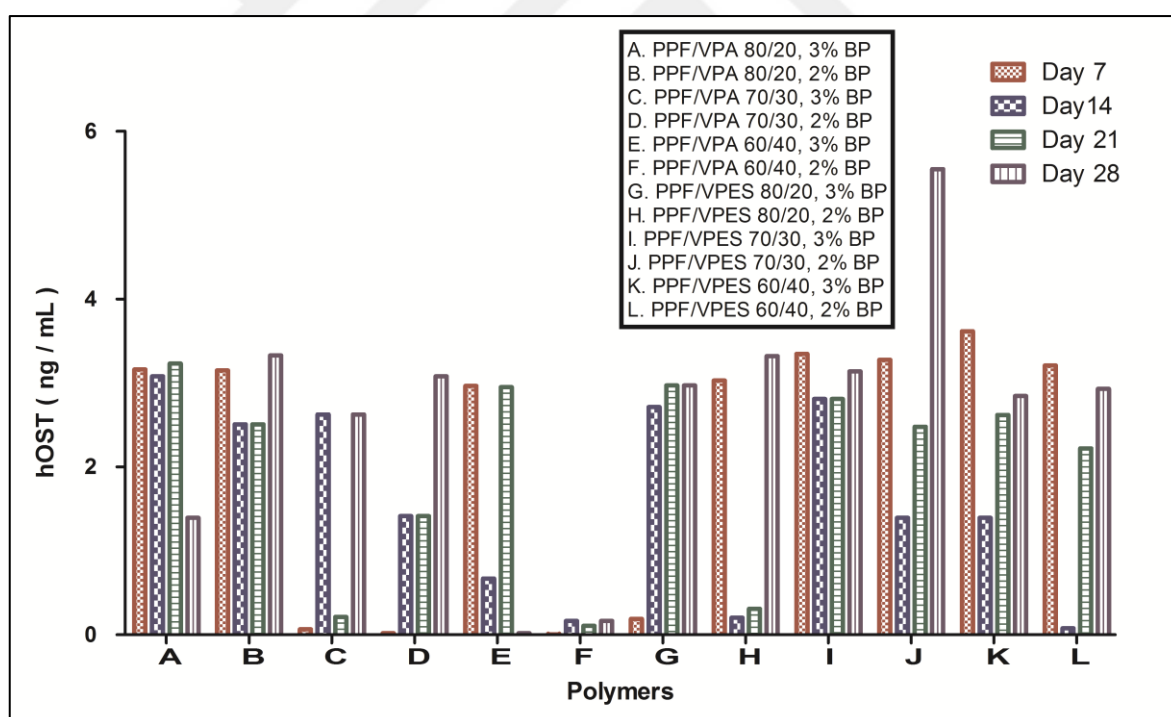


Figure 4.57. Osteocalcin activity of HOb cells throughout 28 days on thermal cured samples

5. CONCLUSIONS

The aim of the completed project was the development of poly(propylene fumarate) (PPF) and vinyl phosphonic acid (VPA) or vinyl phosphonic acid diethyl ester (VPES) based biodegradable and biocompatible polymer systems which were designed to be used as scaffolds for bone tissue defects and the investigation of their interactions with cells. To achieve this goal, in the first stage, poly(propylene fumarate) (PPF) polymer was synthesized via a polycondensation reaction of propylene glycol and fumaric acid using an excess of propylene glycol. In the second stage, the cross-linking of PPF with changing amounts of VPA and VPES was achieved via two methods: thermal cure at elevated temperature and UV cure at the room temperature. The structure of PPF pre-polymer was confirmed *via* FT-IR and $^1\text{H-NMR}$ spectroscopic techniques. The synthesized PPF pre-polymer had a number average molecular weight (M_n) of 1653 g/mol and a weight-average molecular weight (M_w) of 2880 g/mole as determined via GPC. The polydispersity index (PDI) was 1,74. Complete cure of PPF/VPA and PPF/VPES polymers was confirmed by DSC. Crosslink density of all samples was determined via swelling experiments and the effect of comonomer type and amount of comonomer and initiator on crosslink density was analyzed. Thermomechanical properties and thermal degradation profiles were characterized by DMA and TGA respectively. For different compositions of PPF/VPES polymers, storage modulus values at 37°C varied between 845-2430 MPa and for different compositions of PPF/VPA polymers they varied between 1134-6330 MPa. In general, T_g values as determined from DMA, increased with increasing VPA amount and decreased with increasing VPES amount. Thermal gravimetric analysis of the polymers generally indicated one step decomposition for the PPF/VPES and PPF/VPA copolymers showing the degradation of the network, however, a two-step decomposition was observed for the PPF/VPA (60/40) composition, at the highest VPA concentration. The first step degradation in this sample was attributed to the degradation of poly (vinyl phosphonic acid) which is believed to occur as a side product during the cure of PPF pre-polymer with VPA and the second step degradation was attributed to the degradation of the network. SEM analysis of the fracture surfaces of the copolymers showed micro and macro sized porous structure for the PPF/VPA copolymers and no porosity for the PPF/VPES copolymers. Different compositions of the PPF/VPES copolymers exhibited

compressive modulus values in the range of 169MPa - 836 MPa and compressive strength values in the range of 48-119 MPa, whereas different compositions of the PPF/VPA copolymers exhibited compressive modulus values between 10MPa and 256 MPa and compressive strength values between 14MPa and 73 MPa. The PPF/VPES copolymers generally showed higher compressive modulus and strength values than the PPF/VPA copolymers at the same comonomer and radical initiator (BP) concentrations. These results indicated that the PPF/VPA and PPF/VPES copolymers exhibit mechanical properties that are suitable to be used as a bone implant (substitute) either in the absence or presence of fillers such as calcium phosphates.

Surface hydrophilicity generally increased with increasing comonomer content for both PPF/VPA and PPF/VPES copolymers. Analysis of biodegradation via both weight loss and pH change measurements indicated that the PPF/VPA and PPF/VPES copolymers undergo a greater weight loss in the first 7 to 14 days and that the weight loss occurs at a lower rate after this period. The first stage degradation was attributed to the release of VPA or VPES comonomer or homopolymer that were not incorporated into the network structure and the second stage degradation was attributed to the network degradation

MTS studies showed that the PPF copolymers were biocompatible and von Kossa staining experiments indicated positive results for improving and increasing bone growth. Osteocalcin and ALP analyses indicated that the highest activities were achieved for the 70/30 compositions for PPF/VPA and PPF/VPES samples.

The results of the study indicated that when considering their properties, the thermal cured PPF/VPA and PPF/VPES copolymers can be used as a scaffold for trabecular bone tissue in preformed forms [76]. In *in vitro* studies, although PPF/VPA samples become prominent due to their porous structure, PPF/VPES samples can also be made porous via NaCl leaching and can also be used as potential scaffolds in tissue engineering applications either in their neat form or porous form. In addition the UV cured PPF/VPA and PPF/VPES copolymers show potential to be used as bone tissue substitutes in injectable form.

6. FUTURE PROSPECTS

Our construct showed promising results in terms of bone tissue engineering, however further experiments should be carried out to maximize the effectiveness of the future scaffolds of bone tissue engineering.

First of all, to enhance mechanical properties, composites of the PPF copolymers with inorganic additives such as calcium phosphates can be prepared and tested. Also the biodegradation profiles of these composites should be determined. Moreover, alkaline phosphatase and osteocalcin activities should be evaluated by real time PCR analysis.

In addition to osteogenic differentiation, chondrogenic differentiation analyses can be performed to ensure the possible chondrogenic capacities of the scaffolds.

Long term *in vivo* experiments can be performed on laboratory rats to observe the effects of these constructs on the site of implantation.

REFERENCES

1. Painter PC, Coleman MM. *Fundamentals of polymer science : an introductory text*. New York: Technomic Pub. Co; 1997.
2. Fried JR. *Polymer science and technology*. New Jersey: Prentice Hall; 2014.
3. Hermann Staudinger Foundation of Polymer Science - Landmark - American Chemical Society. [cited 2018 Nov 29]. Available from: <https://www.acs.org/content/acs/en/education/whatischemistry/landmarks/staudingerpolymerscience.html>
4. Akay M. Introduction to polymer science and technology. 2012 [cited 2018 Nov 29]. Available from: [http://www.iqytechnicalcollege.com/ME 209 Introduction-to-polymer-science-and-technology.pdf](http://www.iqytechnicalcollege.com/ME%209%20Introduction-to-polymer-science-and-technology.pdf)
5. Kaiser W. Crawford RJ., *Plastics engineering. 2nd edition*. Oxford: Pergamon Press; 1987.
6. Ebewele RO. *Polymer science and technology*. New York: CRC Press; 2000.
7. Krevelen DW. Nijenhuis K *Properties of polymers : their correlation with chemical structure ; their numerical estimation and prediction from additive group contributions*. Oxford: Elsevier; 2009.
8. Roberts JD, Caserio MC, Roberts JD. *A study guide to basic principles of organic chemistry*. California: W.A. Benjamin; 1977.
9. Fiocchi R. Study of the importance of the catalysis in organic synthesis and industrial applications in Thermoplastic Polyurethane (TPU) production. 2011 Mar 18 [cited 2018 Nov 29]; Available from: https://pubblicazioni.unicam.it/handle/11581/401856?mode=full.1041#.W__pddszaO4
10. Callister WD, Rethwisch DG. *Materials science and engineering : an introduction*. New Jersey: Wiley; 1997.

11. Defonseka C. *Practical guide to flexible polyurethane foams*. Shrewsbury, Shropshire, UK: Smithers Rapra; 2013.
12. Hasirci V, Huri PY, Tanir TE, Eke G, Hasirci N. *Polymer fundamentals: polymer synthesis*. Ankara: Elsevier; 2017
13. Bishop M. *An introduction to chemistry: atoms first*. Portsmouth: Chiral Publishing Company; 2009.
14. Peacock AJ, Calhoun AR. *Polymer chemistry: properties and applications*. Ohio: Hanser Gardner Publications; 2006.
15. Billiet L, Fournier D, Du Prez F. Step-growth polymerization and “click” chemistry: The oldest polymers rejuvenated. *Polymer (Guildf)*. 2009 [cited 2018 Nov 30]; 50:3877–86. Available from: <http://www.pcr.ugent.be/Publications/artikelsPCR/leen-featurearticle-2009.pdf>
16. Billmeyer FW. *Textbook of polymer science*. New York: Wiley; 1984.
17. Amin S, Amin M. Thermoplastic elastomeric (TPE) materials and their use in outdoor electrical insulation [cited 2018 Dec 2]. Available from: http://www.ipme.ru/e-journals/RAMS/no_12911/02_amin.pdf
18. Sorenson WR. *Unsolved problems in polymer science: a compilation of essays*. Washington: National Academy of Sciences-National Research Council; National Research Council. Publication; 1962
19. Lin YH. *Polymer viscoelasticity: basics, molecular theories, experiments and simulations*. New Jersey: World Scientific; 2011.
20. Brandrup J, Immergut EH, Grulke EA. *Polymer handbook*. Danvers: Wiley-Interscience; 1999.
21. Odian GG. *Principles of polymerization*. Staten Island: Wiley, 2004.
22. Hu W. *Polymer physics: a molecular approach*. Wien: Springer; 2012.
23. Baer E, Wada Y, Geil PH. The solid state of polymers: report of the *U.S.-Japan joint seminar on the polymer solid state, held in Cleveland, Oct. 9-13, 1972* New

York; 1974

24. Boyer RF. *Transition and relaxation in polymers* New York: John Wiley & Sons Inc; 1967
25. Ashby MF, Jones DRH *Engineering materials : an introduction to their properties and applications*. Cambridge: Pergamon Press; 1980.
26. Mechanical Properties of Metals [cited 2018 Dec 2]. Available from: <http://www.virginia.edu/bohr/mse209/chapter6.htm>
27. Thakur VK, Thakur MK. Handbook of polymers for pharmaceutical technologies. volume 3, biodegradable polymers [cited 2018 Dec 2]. Available from: <https://www.wiley.com/enus/Handbook+of+Polymers+for+Pharmaceutical+Technologies%2C+Volume+3%2C+Biodegradable+Polymers-p-9781119041429>
28. Fan M, Fu F. *Advanced high strength natural fibre composites in construction*. London: Woodhead Publishing; 2017.
29. Crompton TR. Plastics reinforcement and industrial applications [cited 2018 Dec 2]. Available from: <https://www.crcpress.com/Plastics-Reinforcement-and-Industrial-Applications/Crompton/p/book/9781482239331>
30. Seymour RB, Carraher CE. *Seymour/Carraher's polymer chemistry: an introduction*. Lancaster: M. Dekker; 1996.
31. Mechanical Properties. [cited 2018 Dec 2]. Available from: [http://faculty.uscupstate.edu/llever/Polymer Resources/Mechanical.htm#elongation](http://faculty.uscupstate.edu/llever/Polymer%20Resources/Mechanical.htm#elongation)
32. Koo JH. Fundamentals, properties, and applications of polymer nanocomposites [cited 2018 Dec 2]. Available from: https://books.google.com.tr/books/about/Fundamentals_Properties_and_Applications.html?id=57UtDQAAQBAJ&redir_esc=y
33. Black CRM, Goriainov V, Gibbs D, Kanczler J, Tare RS, Oreffo ROC. Bone tissue engineering. *Current Molecular Biology Reports*. 2015;1(3):132–40.
34. Amini AR, Laurencin CT, Nukavarapu SP. Bone tissue engineering: recent advances and challenges. *Journal of Critical Reviews in Biomedical Engineering*.

- 2012;40(5):363–408.
35. Chaikof EL, Matthew H, Kohn J, Mikos AG, Prestwich GD, Yip CM. Biomaterials and scaffolds in reparative medicine. *Annals of the New York Academy of Sciences* 2002;961:96–105.
 36. Stevens MM. Biomaterials for bone tissue engineering. *Materials Today* 2008;11(5):18–25.
 37. Liu X, Ma PX. Polymeric scaffolds for bone tissue engineering. *Annals of Biomedical Engineering*. 2004;32(3):477–86.
 38. Hutmacher DW. Scaffolds in tissue engineering bone and cartilage. *Biomaterials*. 2000;21(24):2529–43.
 39. Stratton S, Shelke NB, Hoshino K, Rudraiah S, Kumbar SG. Bioactive polymeric scaffolds for tissue engineering. *Bioactive Materials* 2016;1(2):93–108.
 40. Kumbar S, Laurencin C, Deng M. *Natural and synthetic biomedical polymers*. San Diego: Elsevier Science; 2014.
 41. Müller FA, Müller L, Hofmann I, Greil P, Wenzel MM, Staudenmaier R. Cellulose-based scaffold materials for cartilage tissue engineering. *Biomaterials* 2006;27(21):3955–63.
 42. Lee K-W, Wang S, Lu L, Jabbari E, Currier BL, Yaszemski MJ. Fabrication and characterization of poly(propylene fumarate) scaffolds with controlled pore structures using 3-dimensional printing and injection molding. *Tissue Engineering* 2006;12(10):2801–11.
 43. Kasper FK, Tanahashi K, Fisher JP, Mikos AG. Synthesis of poly(propylene fumarate). *Nature Protocols* 2009;4(4):518–25.
 44. Thi-Hiep N, Hoa D Van, Toi V Van. Injectable in situ crosslinkable hyaluronan-polyvinyl phosphonic acid hydrogels for bone engineering. *Journal of Biomedical Science and Engineering* 2013;6(8):854–62.
 45. Bassi AK, Gough JE, Zakikhani M, Downes S. The chemical and physical properties of poly(ϵ -caprolactone) scaffolds functionalised with poly(vinyl

- phosphonic acid-co-acrylic acid). *Journal of Tissue Engineering* 2011;2011:615328.
46. Bassi A, Gough J, Downes S. A novel phosphonate for the repair of critical size bone defects. *Journal of Tissue Engineering and Regenerative Medicine* 2012;6(10):833–40.
 47. Ghag AK, Gough JE, Downes S. The osteoblast and osteoclast responses to phosphonic acid containing poly(ϵ -caprolactone) electrospun scaffolds. *Biomaterials Science* 2014;2(2):233–41.
 48. Dey RE, Zhong X, Youle PJ, Guang Wang Q, Wimpenny I, Downes S, et al. Synthesis and characterization of poly(vinylphosphonic acid-co-acrylic acid) copolymers for application in bone tissue scaffolds. *Macromolecules* 2016 ;49(7)
 49. Gemeinhart RA, Bare CM, Haasch RT, Gemeinhart EJ. Osteoblast-like cell attachment to and calcification of novel phosphonate-containing polymeric substrates. *Journal of Biomedical Materials Research Part A* 2006 ;78A(3):433–40.
 50. Lee JW, Lan PX, Kim B, Lim G, Cho DW. Fabrication and characteristic analysis of a poly(propylene fumarate) scaffold using micro-stereolithography technology. *Journal of Biomedical Materials Research Part B: Applied Biomaterials* 2008;87B(1):1–9.
 51. Shalumon K, Jayabalan M. Studies on biodegradation of crosslinked hydroxy terminated-poly(propylene fumarate) and formation of scaffold for orthopedic applications. *Journal of Materials Science. Materials in Medicine*. 2008;20:161-171
 52. Mitha MK, Jayabalan M. Studies on biodegradable and crosslinkable poly(castor oil fumarate)/poly(propylene fumarate) composite adhesive as a potential injectable biomaterial. *Journal of Materials Science: Materials in Medicine* 2009;20(SUPPL. 1):203–11.
 53. Mark DT, Seongbong J , Chuanyue W , Catherine GA, Antonios GM. Characterization of the cross-linked structure of fumarate-based degradable polymer networks .*Macromolecules* 2002;35(11):4373-4379
 54. Jayabalan M, Shalumon KT, Mitha MK, Ganesan K, Epple M. The effect of radiation processing and filler morphology on the biomechanical stability of a

- thermoset polyester composite. *Biomedical Materials* 2010;5(2):25009.
55. He S, Yaszemski MJ, Yasko AW, Engel PS, Mikos AG. Injectable biodegradable polymer composites based on poly(propylene fumarate) crosslinked with poly(ethylene glycol)-dimethacrylate. *Biomaterials* 2000;21(23):2389–94.
 56. Zhu X, Liu N, Yaszemski MJ, Lu L. Effects of composite formulation on the mechanical properties of biodegradable poly(propylene fumarate)/bone fiber scaffolds. *International Journal of Polymer Science* 2010;5
 57. Mistry AS, Cheng SH, Yeh T, Christenson E, Jansen JA, Mikos AG. Fabrication and *in vitro* degradation of porous fumarate-based polymer/alumoxane nanocomposite scaffolds for bone tissue engineering. *Journal of Biomedical Materials Research Part A* 2009;89A(1):68–79.
 58. Wu CC, Yang KC, Yang SH, Lin MH, Kuo TF, Lin FH. In vitro studies of composite bone filler based on poly(propylene Fumarate) and biphasic α -tricalcium phosphate/hydroxyapatite ceramic powder. *Artificial Organs*. 2012;36(4):418–28.
 59. Köse GT, Korkusuz F, Korkusuz P, Hasirci V. In vivo tissue engineering of bone using poly(3-hydroxybutyric acid-co-3-hydroxyvaleric acid) and collagen scaffolds. *Tissue Engineering* 2004;10(7–8):1234–50.
 60. Lewandrowski KU, Bondre S, Gresser JD, Silva AE, Wise DL, Trantolo DJ. Augmentation of osteoinduction with a biodegradable poly(propylene glycol-co-fumaric acid) bone graft extender. A histologic and histomorphometric study in rats. *Bio-Medical Materials and Engineering* 1999;9(5–6):325–34.
 61. Calikoglu KAC, Gurel PG, Ramazanoglu M, Torun KG, Hasirci V. Cartilage tissue engineering on macroporous scaffolds using human tooth germ stem cells. *Journal of Tissue Engineering and Regenerative Medicine* 2017;11(3):765–77.
 62. Seibel MJ. Biochemical markers of bone turnover: part I: biochemistry and variability. *The Clinical Biochemist Reviews* 2005;26(4):97–122.
 63. Garnero P, Delmas PD. Biochemical markers of bone turnover: *Applications For Osteoporosis*. *Endocrinol Metab Clin North Am* 1998;27(2):303–23.

64. van Straalen JP, Sanders E, Prummel MF, Sanders GTB. Bone-alkaline phosphatase as indicator of bone formation. *Clinica Chimica Acta*. 1991 201(1–2):27–33.
65. Perrin R, Elomaa M, Jannasch P. Nanostructured proton conducting polystyrene–poly(vinylphosphonic acid) block copolymers prepared via sequential anionic polymerizations. *Macromolecules* 2009;42(14):5146–54.
66. Kenar H, Kose GT, Toner M, Kaplan DL, Hasirci V. A 3D aligned microfibrinous myocardial tissue construct cultured under transient perfusion. *Biomaterials* 2011;32(23):5320–9.
67. Can E, Wool RP, Küsefoğlu S. Soybean- and castor-oil-based thermosetting polymers: Mechanical properties. *Journal of Applied Polymer Science* 2006;102(2):1497–504.
68. Mow VC, Huiskes R. *Basic orthopaedic biomechanics and mechano-biology*. Philadelphia: Lippincott Williams & Wilkins; 2005.
69. Ber S, Torun Köse G, Hasırcı V. Bone tissue engineering on patterned collagen films: an in vitro study. *Biomaterials* 2005;26(14):1977–86.
70. Heller C, Schwentenwein M, Russmueller G, Varga F, Stampfl J, Liska R. Vinyl esters: Low cytotoxicity monomers for the fabrication of biocompatible 3D scaffolds by lithography based additive manufacturing. *Journal of Polymer Science Part A: Polymer Chemistry* 2009;47(24):6941–54.
71. Price PA. Vitamin K-dependent formation of bone Gla protein (osteocalcin) and its function. *Vitam Horm* 1985;42:65–108.
72. Minisola S, Scarnecchia L, Scarda A, Bigi F, Tabolli S, Valtorta C, et al. Serum osteocalcin in primary hyperparathyroidism: short-term effect of surgery. *Miner Electrolyte Metab* 1988 ;14(4):201–7.
73. Coleman RE, Mashiter G, Fogelman I, Whitaker KD, Caleffi M, Moss DW, et al. Osteocalcin: a potential marker of metastatic bone disease and response to treatment. *European Journal of Cancer and Clinical Oncology* 1988;24(7):1211–7.
74. Power MJ, Fottrell PF. Osteocalcin: diagnostic methods and clinical applications.

Critical Reviews in Clinical Laboratory Sciences 1991;28(4):287–335.

75. Demiaux B, Arlot ME, Chapuy MC, Meunier PJ, Delmas PD. Serum osteocalcin is increased in patients with osteomalacia: correlations with biochemical and histomorphometric findings. *The Journal of Clinical Endocrinology & Metabolism* 1992;74(5):1146–51.
76. Can E, Torun Köse G, Cemali G., Yeditepe University, assignee. A tissue scaffold production method. European patent EP3153187A1. 2018 Febr 14.



APPENDIX A: CALIBRATION CURVE OF ALP

Alkaline phosphatase activity at day 7, 14, 21 and 28 was measured by TaKaRa TRACP&ALP Assay kit, and quantified according to the manufacturer's instructions. Measurements were performed at 450 nm by Elisa Plate Reader. According to calibration curve, which is presented in Figure A.1, ALP concentration ($\mu\text{g/mL}$) graphs for each polymer were constructed.

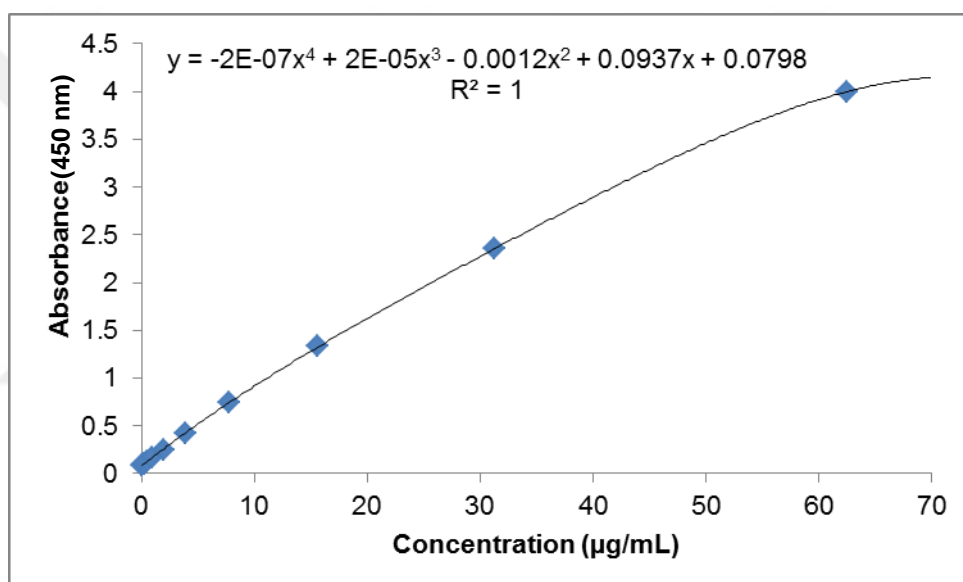


Figure A.1. Calibration curve for alkaline phosphatase activity

APPENDIX B: CALIBRATION CURVE OF OSTEOCALCIN

Osteocalcin activity at day 7, 14, 21 and 28 was measured by Invitrogen hOST human osteocalcin ELISA kit, and quantified according to the manufacturer's instructions. Measurements were performed at 450 nm by Elisa Plate Reader. According to calibration curve, which is presented in Figure B.1, OST concentration (ng/mL) graphs for each polymer were constructed.

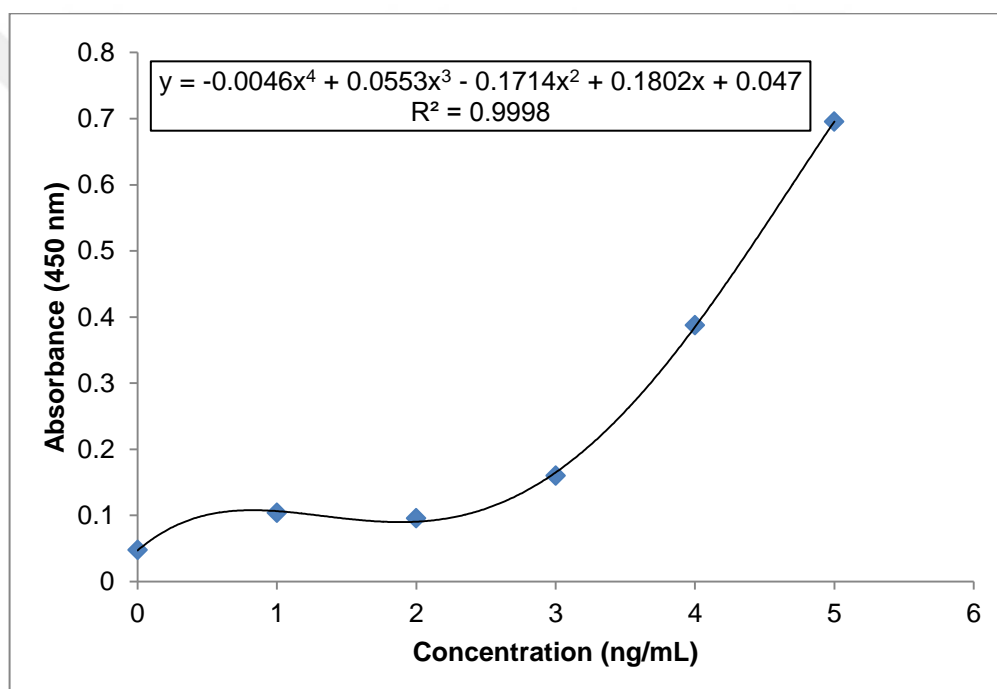


Figure B.1. Calibration curve for osteocalcin activity